



Eidgenössische Technische Hochschule Zürich
Swiss Federal Institute of Technology Zurich



HOST UNIVERSITY: ETH Zürich

FACULTY: Civil, Environmental and Geomatic Engineering

DEPARTMENT: Institute of Structural Engineering (IBK)

Academic Year 2019-2020

Performance-Based Design of an Industrial Hall with a Wooden Structure

Karannagodage Don Chamith Deemantha Kumara

Promoters:

Bart Merci, Ghent University

Andrea Frangi, ETH Zürich

Master thesis submitted in the Erasmus+ Study Programme

International Master of Science in Fire Safety Engineering

DISCLAIMER

This thesis is submitted in partial fulfilment of the requirements for the degree of *The International Master of Science in Fire Safety Engineering (IMFSE)*. This thesis has never been submitted for any degree or examination to any other University/programme. The author(s) declare(s) that this thesis is original work except where stated. This declaration constitutes an assertion that full and accurate references and citations have been included for all material, directly included and indirectly contributing to the thesis. The author(s) gives (give) permission to make this master thesis available for consultation and to copy parts of this master thesis for personal use. In the case of any other use, the limitations of the copyright have to be respected, in particular with regard to the obligation to state expressly the source when quoting results from this master thesis. The thesis supervisor must be informed when data or results are used.

Read and approved,



Chamith Karannagodage

April 30th, 2020

Abstract

The available standard and design fire curves used to analyse structural fire performance, do not reliably predict the exposure temperature for fires in large compartments. Also, these fire curves do not consider the effects of the extra fire load when combustible elements are a part of the structure.

A Performance-Based Designs (PBD) approach was required to analyse a large Industrial Hall, formed of a wooden structure, to understand the performance during a fire. This thesis presents a methodology that involves using advanced calculation techniques to generate real fire scenarios in timber buildings and to analyse structural performance due to those fires.

Fire Dynamic Simulator (FDS) was used to simulate a critical fire in the Industrial Hall accounting for the additional fire load from the combustion of timber elements. Key parameters and boundary conditions required to simulate the fire scenario and timber combustion have been discussed in detail. The FDS results were used to generate the parametric design fire curves, which were in turn used to study structural performance during the fire.

The thermo-mechanical analysis for timber columns was done using the commercial software package Abaqus. The temperature profiles inside the timber columns were predicted with temperature dependent material properties during an ISO standard fire exposure and parametric design fire exposure. Then the mechanical analysis was conducted using the predicted temperature values with the temperature dependent mechanical properties. The load bearing capacity and the buckling capacity of the timber element was checked during the 60 minutes of fire exposure for failure. The finite element model results were compared with the Eurocode 5 design calculations to see the difference between PBD method and the prescriptive code values. The results showed that the Eurocode 5 provides an over conservative solution to the structural performance of timber elements in the Industrial Hall compared to the PBD design.

සාරාංශය

ව්‍යුහාත්මක ගිනි ක්‍රියාකාරිත්වය විශ්ලේෂණය කිරීම සඳහා භාවිතා කළ හැකි ප්‍රමිතිය සහ සැලසුම් ගිනි වක්‍ර, විශාල මැදිරිවල ගින්න සඳහා නිරාවරණ උෂ්ණත්වය විශ්වාසදායක ලෙස පුරෝකථනය නොකරයි. එසේම, දහනය කළ හැකි මූලද්‍රව්‍යයන් ව්‍යුහයේ කොටසක් වන විට අමතර ගිනි බරෙහි බලපෑම මෙම ගිනි වක්‍රයන් නොසලකයි.

ගින්නක් අතරතුර සිදුවන ක්‍රියාකාරිත්වය අවබෝධ කර ගැනීම සඳහා ලී ව්‍යුහයකින් සාදන ලද විශාල කාර්මික ශාලාවක් විශ්ලේෂණය කිරීම සඳහා කාර්ය සාධනය මත පදනම් වූ සැලසුම් (පීබීඩී) ප්‍රවේශයක් අවශ්‍ය විය. මෙම නිබන්ධනය මගින් දැව ගොඩනැගිලිවල සැබෑ ගිනි නිවීමේ අවස්ථා උත්පාදනය කිරීම සහ එම ගින්න හේතුවෙන් ව්‍යුහාත්මක ක්‍රියාකාරිත්වය විශ්ලේෂණය කිරීම සඳහා උසස් ගණනය කිරීමේ ක්‍රමවේදයන් භාවිතා කරන ක්‍රමවේදයක් ඉදිරිපත් කරයි.

කාර්මික ශාලාවේ ඇති දැවැන්ත ගින්නක් දැවමය මූලද්‍රව්‍ය දහනය කිරීමෙන් අමතර ගිනි බරක් ගණනය කිරීම සඳහා ගිනි ගතික සිමියුලේෂන් (එෆ්.ඩී.එස්) භාවිතා කරන ලදී. ගිනි තත්වය සහ දැව දහනය අනුකරණය කිරීමට අවශ්‍ය ප්‍රධාන පරාමිතීන් සහ මායිම් කොන්දේසි විස්තරාත්මකව සාකච්ඡා කර ඇත. එෆ්ඩීඑස් පරාමිතික සැලසුම් ගිනි වක්‍ර ජනනය කිරීම සඳහා භාවිතා කරන ලද අතර ඒවා ගින්න අතරතුර ව්‍යුහාත්මක ක්‍රියාකාරිත්වය අධ්‍යයනය කිරීම සඳහා භාවිතා කරන ලදී.

දැව තීරු සඳහා තාප යාන්ත්‍රික විශ්ලේෂණය සිදු කරනු ලැබුවේ වාණිජ මෘදුකාංග පැකේජයක් වන අබාකස් භාවිතා කරමිනි. අයිඑස්ඒ සම්මත ගිනි නිරාවරණ සහ පරාමිතික සැලසුම් ගිනි නිරාවරණයේදී දැව තීරු තුළ ඇති උෂ්ණත්ව පැතිකඩයන් උෂ්ණත්වය මත රඳා පවතින ද්‍රව්‍යමය ගුණාංග සහිතව පුරෝකථනය කරන ලදී. එවිට උෂ්ණත්වය මත රඳා පවතින යාන්ත්‍රික ගුණාංග සමඟ පුරෝකථනය කරන ලද උෂ්ණත්ව අගයන් භාවිතා කරමින් යාන්ත්‍රික විශ්ලේෂණය සිදු කරන ලදී. මිනිත්තු 60 ක ගිනි නිරාවරණයක් අසාර්ථක වීම සඳහා බර දරණ ධාරිතාව සහ දැව මූලද්‍රව්‍යයේ ගාංවු ධාරිතාව පරීක්ෂා කරන ලදී. පී.බී.ඩී ක්‍රමය සහ නියම කරන ලද කේත අගයන් අතර වෙනස බැලීමට සීමිත මූලද්‍රව්‍ය ආකෘති යුරෝ කේත 5 සැලසුම් ගණනය කිරීම් සමඟ සංසන්දනය කරන ලදී. පී.බී.ඩී සැලසුමට සාපේක්ෂව කාර්මික ශාලාවේ දැවමය මූලද්‍රව්‍යයන්ගේ ව්‍යුහාත්මක ක්‍රියාකාරිත්වයට යුරෝකෝඩ් 5 සම්ප්‍රදායික විසඳුමක් සපයන බව ප්‍රතිපල වලින් පෙනී ගියේය.

IMFSE Master Thesis Declaration

This form has been developed in the context of the unforeseen circumstances due to Covid-19, necessitating a reduction of practical project work (whether it be laboratory based, computational, or fieldwork) during the master thesis semester. It acts as a record of the impact on the master thesis. The form has been completed by the student and verified by the supervisor. **A copy of the signed form is included behind the abstract in the dissertation.**

Name: Chamith Karannagodage

Work completed

All items of wholly, or partially completed work must be listed, indicating the percentage completion for each task. **Please take care to provide a full detailed list of all work done.**

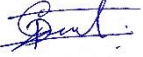
All the expected work have been carried out

Work not commenced

Any items of outstanding work that have not been started should be listed here.

Declaration

To the best of our knowledge, this form is an accurate record of the project status on 28th April 2020

Student: _____ 

Supervisor: _____ 

Table of Contents

DISCLAIMER	ii
Abstract	iii
සාරාංශය	iv
IMFSE Master Thesis Declaration	v
Table of Contents	vi
List of Tables	xii
Nomenclature	xiii
List of Abbreviations.....	xiii
1. Introduction	1
1.1. Timber as Construction Material.....	1
1.2. Fire Resistance	2
1.3. Objective	2
1.4. Introduction to Building.....	3
1.5. Scope and Methodology	4
2. Literature Review	6
2.1. Prescriptive Based Design versus Performance-Based Design Approach in Fire.....	6
2.2. Post-Flashover Fire.....	7
2.3. Fire Temperatures.....	9
2.3.1. The standard fire curve	10
2.3.2. The parametric fire curves	11
2.4. Structural Fire Resistance	13
2.4.1. Time equivalence	13
2.5. Performance of Timber Structures Exposed to Fire	15
2.6. Adiabatic Surface Temperature.....	17
3. Timber Section Calculation	19
3.1. Actions	19
3.1.1. Ultimate Limit Sate (ULS).....	20
3.1.2. Fire Limit Sate (FLS)	21
3.2. Design of Timber Section at Ambient Conditions	21
3.2.1. Calculation process for compression and buckling capacity	23

3.2.2.	Flow chart for the calculation process of compressive capacity	24
3.2.3.	Flow chart for the calculation process of buckling capacity	25
3.3.	Timber Section Resistance for Fire Conditions	26
3.3.1.	Charring depth	26
3.3.2.	Effective cross section	27
4.	Fire Modelling Techniques for Large Enclosures	29
4.1.	Fire Dynamics Simulator (FDS)	29
4.2.	Numerical Fire Model	30
4.2.1.	Heat release rate of the wood crib fire	32
4.3.	Properties of Timber Columns	34
4.3.1.	Combustion of wood and ignition temperature	35
4.3.2.	Heat release rate of timber columns	36
4.4.	Mesh Sensitivity	39
4.5.	Sensitivity to Number of Radiant Angles	43
4.6.	Results and Discussion	44
4.6.1.	Ignition of Columns and Heat Release Rate	44
4.6.2.	Exposed Heat flux and Surface Temperatures	46
4.6.3.	Design Fire Curve	51
5.	Thermal Analysis	55
5.1.	Abaqus/Standard	55
5.2.	Abaqus Thermal Model	55
5.3.	Results and Discussion	57
6.	Thermo-Mechanical Analysis	61
6.1.	Mechanical Model	61
6.2.	Load Bearing Capacity	62
6.3.	Eigenvalue Buckling Analysis	62
6.3.1.	Buckling Model	63
7.	Conclusion	68
7.1.	Limitations and the potential future work	70
	Acknowledgement	72
	References	73
	Appendices	80
	Appendix A - Drawings of Industrial Hall	80

Appendix B- FDS Results	81
Appendix C - Temperature dependent material properties for softwood timber (EN 1995-1-2)	83
Appendix D - Thermal Analysis Results.....	85
7.2. Appendix E – FDS Input File.....	87

List of Figures

Figure 1: Plan view of the industrial building (Basler & Hofmann, 2017)	3
Figure 2: Potential fire scenarios in the Industrial Hall (Basler & Hofmann, 2017)....	4
Figure 3: Performance-based design framework (Hurley et al., 2015)	8
Figure 4: Energy balance for a fully developed enclosure fire (Andrew H. Buchanan et al., 2017).....	9
Figure 5: Comparison of standard fire curves for fully developed fires in enclosures (Andrew H. Buchanan et al., 2017)	10
Figure 6: Comparison of parametric fire curves according to EN 1991-1-2 for different fuel loads, materials and ventilation factors (Andrew H. Buchanan et al., 2017).....	12
Figure 7: Temperature-time curves from experimental study by Magnusson, et al. (1970).....	12
Figure 8: Equal areas concept for time equivalence (Ingberg, 1928).....	14
Figure 9: Time equivalence base on maximum temperature of element (Andrew H. Buchanan et al., 2017)	15
Figure 10: Methods to calculate structural response of timber elements subjected to parametric design fires taken from Brandon (2018)	17
Figure 11: Spacing of the typical column grid in the building.....	20
Figure 12: Effective timber cross section	27
Figure 13: Side view of the FDS model.....	31
Figure 14: Top view of the FDS model	32
Figure 15: Plan view of area near the wood cribs and timber columns.....	32
Figure 16: Heat release rate with time for one wood crib.....	33
Figure 17: Different stages of pyrolysis process in burning timber section (Di Ha Le et al., 2019).....	36
Figure 18: Variation of heat release rate with heat flux for different wood material (Tran et al., 1992)	37
Figure 19: Heat release rate versus time for different heat fluxes in Red Oak (Tran et al., 1992)	38
Figure 20: Total heat release rate with time for various grid sizes with 1000 radiation angles	41

Figure 21: (a) - (f): Fire plume and smoke temperature distribution with height above the wood crib 1 for different mesh sizes with 1000 radiation angles	42
Figure 22: Incident heat flux vs. time for column 1 face 1 at H = 2 m	43
Figure 23: Incident heat flux vs. time for column 1 face 1 at H = 2 m	44
Figure 24: Heat release rate comparison for the simulation	45
Figure 25: Ignition point of Column 1 (T = 190s).....	45
Figure 26: Fire development in columns (T = 600s)	46
Figure 27: Steady burning of columns after burnout of wood cribs (T = 2500 s)	46
Figure 28: Incident heat flux change with height in Column1 face 1	47
Figure 29: Surface temperature change with height in Column1 face 1	48
Figure 30: Smoke layer temperature change with height above the wood crib 1	49
Figure 31: Smoke layer temperature change with horizontal distance from the column 1 surface 1 at 10.75 m height	50
Figure 32: Adiabatic temperature change with time at different heights in column 1 face 1	52
Figure 33: Adiabatic temperature change with time at different heights in column 1 face 4.....	52
Figure 34: Adiabatic surface temperature comparison for inert and timber columns	53
Figure 35: Heat Flux comparison for inert and timber columns	54
Figure 36: cross section of the thermal finite element model	56
Figure 37: 300°C isotherm after 60 minutes standard fire exposure (From 2.5 mm mesh).....	58
Figure 38: Maximum char layer observed at 2 m height after 900 seconds	59
Figure 39: Temperature profile change with time in timber cross section at 2 m height during parametric fire exposure	60
Figure 40: Mechanical finite element model	61
Figure 41: Compressive stress profile along the vertical direction in timber section exposed to ISO standard fire	64
Figure 42: Compressive stress profile along the vertical direction in timber section exposed design fire	65
Figure 43: Bending deformation of the timber column exposed to design fire	65

Figure 44: (a)-(b): Critical buckling mode and loads for different fire exposure in the timber column.....	67
Figure 45: Side view of the Industrial hall.....	80
Figure 46: Existing column grid of the Industrial hall	80
Figure 47: Ignition point of Column 1 face 4 (T=310s)	81
Figure 48: Ignition point of Column 2 face 2 (T=490s)	81
Figure 49: Adiabatic temperature change with time at different heights in column 1 face 2.....	82
Figure 50: Adiabatic temperature change with time at different heights in column 1 face 3.....	82
Figure 51: Temperature dependent material properties for softwood timber (EN 1995-1-2).....	84
Figure 52: Char layer development with time for standard fire exposure	85
Figure 53: Thermal finite element model	86

List of Tables

Table 1: Dead load action	20
Table 2: Parameters and values used for section calculation at ambient condition ..	22
Table 3: Comparison $D^*/\delta x$ for different grid cell sizes	41

Nomenclature

List of Abbreviations

PBD	Performance-Based Design
ULS	Ultimate Limit State
FLS	Fire Limit State
FDS	Fire Dynamic Simulator
CFD	Computational Fluid Dynamics

CHAPTER I

1. Introduction

Fire safety engineering has become a rapidly growing industry during last two decades with constant research and development. More focus was given to the fire safety field with tragic events like 9/11 World Trade Centre attack, Grenfell Tower fire, Lakanal House fire, Dubai Torch Tower fire and many more which shook the entire world (Rein, 2013) (Rehm et al., 2003). Furthermore, the U.S. Fire Department statistics shows that there are an average of 14,500 fires per year in high rise buildings within the USA, causing 40 fatal cases, 520 fire injuries and \$154 million direct property losses per year (Marty Ahrens, 2007).

These disasters changed the perceptions of fire safety engineering with new innovative design methodologies and approaches by changing old regulations. Construction industry wanted to utilize multi-disciplinary research procedures like non-combustible facades, structural fire protective materials and fire compartmentations into new projects (Mohamed et al., 2019).

1.1. Timber as Construction Material

Timber is considered as a most aesthetically pleasing, environmental-friendly and sustainable material which has a high demand in building industry for different type of structures. With the production of high performance timber materials like glue laminated timber (Glulam), cross laminated timber (CLT) and laminated veneer lumber (LVL), interest for high-rise timber structures have developed once again as an alternative to steel and concrete designs (O'Neill et al., 2014).

Glued laminated timber, which is also known as Glulam, is an engineered timber material product made out of two or more lumber laminations glued together with structural adhesive in the parallel grain direction (Kuzman et al., 2010). Glulam technology produces a generally uniform material which is less disturbed by natural physical characteristics like knots in wood (Anshari et al., 2012). Glulam has enhanced elastic and mechanical properties compared to common wood and considered as one of the lightest building materials. Therefore, it gives the flexibility to use as load bearing elements. From smaller elements such as columns and beams it is possible to use glulam for large constructions like houses, bridges (Kuzman et al., 2010) (Anshari et al., 2012).

However, due to the combustibility of timber, it can create or contribute to massive fires leading to loss of lives and damages to property (Lowden et al., 2013). Therefore, there are many limitations in regulations for timber structures and thorough study should be done when using as a construction material.

1.2. Fire Resistance

The most important property in structural fire safety engineering is the fire resistance (Yang et al., 2009). For glulam or any other wood-based engineering timber materials, it is important to understand the fire behaviour in many aspects of fire engineering. During fire exposure, timber loses its cross section due to charring. Char layer acts as a protective layer to uncharred wood, while the remaining unburnt timber carries the structural loading (Yang et al., 2009).

Standard fire testing has been used to assess the fire resistance of timber for structural fire design work for decades. However, there is a question among fire safety community, whether standard fire testing such as ISO 834, ASTM E119, EN 13501-2 can represent the real fire scenario or not. On the other hand, recent developments in performance-based designs tries to answer this issue by using rational advance calculation design models, which also provides an alternative to the expensive, labour intensive and time consuming testing (Werther et al., 2012). These validated design models require a sufficient knowledge and experience of numerical modelling with understanding of underlying principals and mechanism to accurately represent real fires and the thermo-mechanical structural behaviour under the fire (Gillie, 2009).

1.3. Objective

The broad aim of this thesis is to propose a performance-based design for an industrial hall with a wooden structure. The design is required to replace the existing steel structure by engineering timber. The design will lead to better understanding of the complex thermal and mechanical response of timber structure during a real fire with a performance-based approach. The study is limited to structural performance of timber columns in Industrial Hall, which are directly exposed and considered as critical elements in a fire.

1.4. Introduction to Building

A performance-based design was required to be carried out for a large industrial building which is used to manufacture and store steel components for automobiles. The building is mainly divided into two separate halls with a firewall at the middle. Each part acts as a separate fire compartment with an area around 3500 m². Figure 1 shows the plan view of the structure (Refer Appendix 1 for side view and column grid of the industrial hall). The building is 153 m long, 44.5 m wide and has a height around 11 m (Basler & Hofmann, 2017).

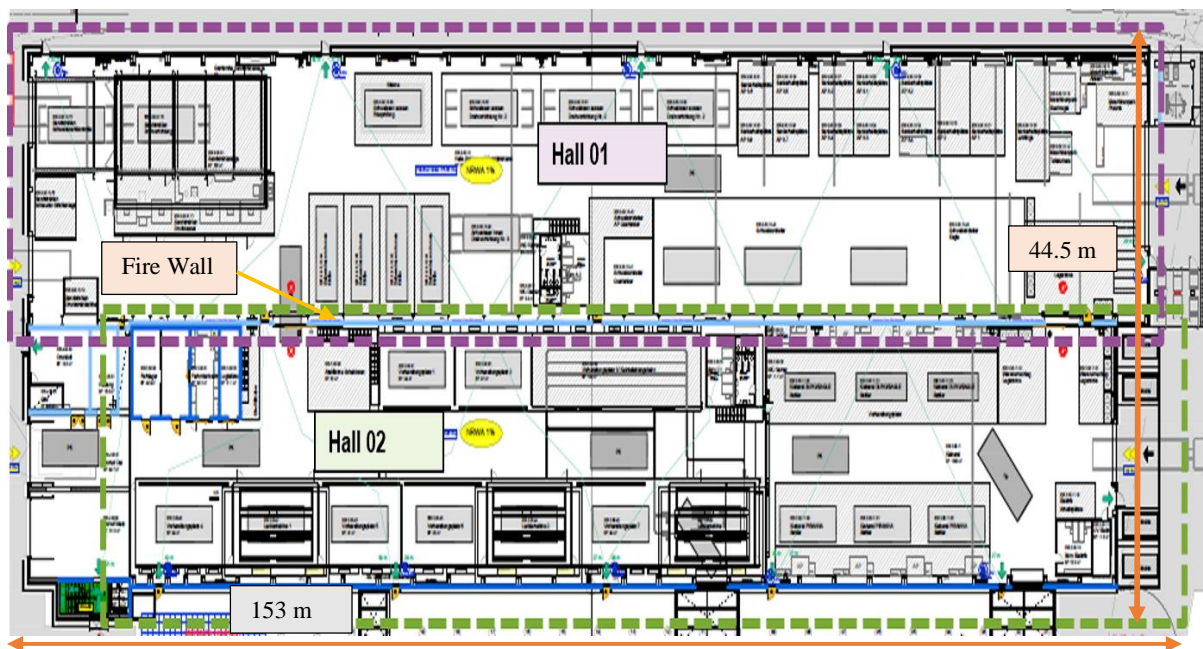


Figure 1: Plan view of the industrial building (Basler & Hofmann, 2017)

The main building structure has already been built with steel elements. According to the Swiss design codes, these type of buildings doesn't need to fulfil any special structural or fire safety requirements (Basler & Hofmann, 2017). But in this case, a 60-minutes stability for the structure was required to ensure safety of fire-fighters during a fire brigade intervention. Considering this requirement Basler & Hofmann (2017) has developed a fire safety strategy for existing unprotected steel structure as mentioned in next section.

The manufacturers have used “just on time” storage and delivery business concept for the factory-made automobile components. Therefore, the number of stored goods is limited. Mainly raw materials used for manufacturing process are stored and most of these steel goods are non-combustible. However, other combustible materials and their storage areas in the building has been identified to develop a parametric study. The result of this study is a set of fire scenarios used to generate real temperature curves and challenge the unprotected steel

elements considering the actual fire loads rather than using the ISO 834 temperature curve from the standard fire test.

Three potential fire scenarios have been considered in the building according to the risk of fire as shown in Figure 2. The same number of computer simulations with FDS software has been carried out to find out critical temperature values for different scenarios. The results show that only few critical points near the storage areas are really threatened in a fire event and therefore, it is not necessary to protect the entire structure to achieve the required fire performance goals. Partial protection at the places where the critical temperatures are expected is enough considering the building's current use.

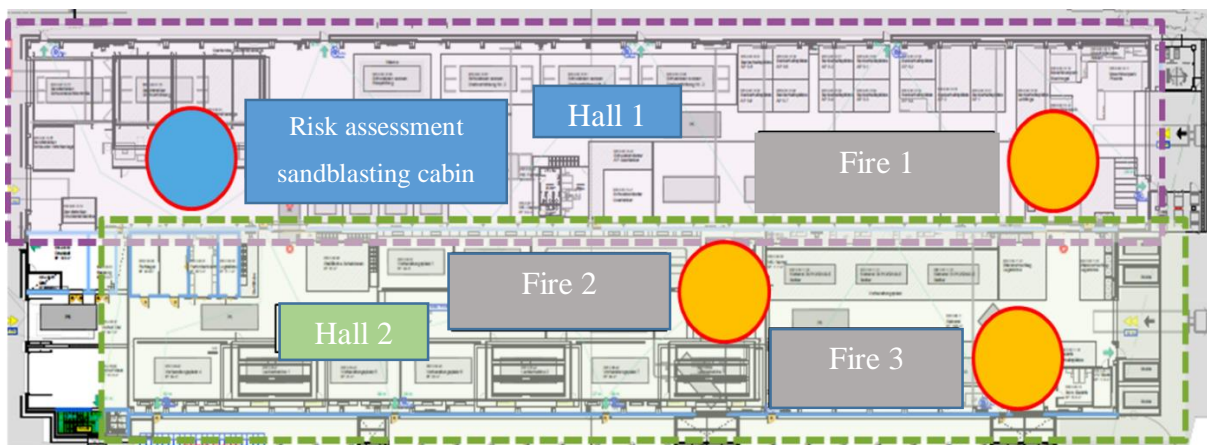


Figure 2: Potential fire scenarios in the Industrial Hall (Basler & Hofmann, 2017)

The research problem discussed in this thesis is, how to approach the fire safety requirements if the industrial hall was built with combustible structural timber elements and what is the performance-based approach to consider design fire and extra fire load added by timber elements.

1.5. Scope and Methodology

Glued-laminated timber is considered as a wooden material, and Eurocode 5 EN 1995-1-2 (2004) is followed for designing the initial nominal section sizes of column elements under the ultimate limit state loads at ambient temperature. The failure criteria are identified, and the section is determined for the most critical condition. Then the load bearing capacity of the section is determined using Eurocode 5 (EN 1995-1-2, 2004) for a 60-minute fire, which is the necessary fire resistance requirement to satisfy the national code.

Available code-prescribed design approaches are based on ISO 834 standard fire exposure and do not take into account the temperature changes with height in burning timber. Furthermore, the existing parametric fire curves for example according to Eurocode 1 (EN 1995-1-2, 2004) cannot be used since the parametric curves in codes are based on fully developed fires in compartments and do not represent large enclosures. On the other hand, the wooden structure is combustible and the burning of timber is adding additional fire load. The parametric curves in prescribed codes have not considered the effect of this additional fire load.

Fire testing is time-consuming and costly. Simulations provide flexibility to optimise the design or to develop simplified design models for structural fire engineers. A new design strategy is identified to simulate fire in the commercial computational fluid dynamics (CFD) package Fire Dynamic Simulator (FDS). The most critical fire scenario is selected to generate new parametric design fire curves. The generated parametric fire curves are used to analyse the thermal and mechanical performance of the timber column elements during real fire exposure. This analysis is carried out using the commercial finite element analysis software Abaqus/Standard.

Initial thermal finite element model is used to simulate ISO standard fire exposure for 60 minutes (ISO 834-1:1999, 1999), and results are validated with the Eurocode 5 (EN 1995-1-2, 2004) design. The validated finite model is used to analyse the response when exposed to the parametric design fire curve which includes temperature variation with the height of the element.

The design model developed in this thesis can be used to simulate real fire scenarios in a timber structure and to analyse structural timber elements which are exposed during the fire. In the post-fire investigation, the reduction factor of fire resistance after the burnout is checked to determine the reusability of structural elements. Comparison between the numerical model and the Eurocode method is done to check if the results in the prescribed design method are conservative or non-conservative.

CHAPTER II

2. Literature Review

2.1. Prescriptive Based Design versus Performance-Based Design Approach in Fire

The main goal of fire safety in any structural design is to provide sufficient protection for life, property and the environment (Bailey, 2004). There are two accepted methods to achieve the adequate safety requirements in legislation, namely, Prescriptive Design approach and Performance-Based Design (PBD) approach.

The prescriptive design approach is based on rules and guidelines prescribed to be followed systematically with an implicit safety level to build each component according to a certain standard. For long time, this approach was used all over the world for fire safety engineering using well recognized codes to build a safe design by fulfilling minimum requirements (Arora, 2014). Prescriptive based approach is a relatively straightforward and easily accessible approach to follow to meet defined goals. It gives flexibility to engineers to follow and defend selection criteria, with less regard for underlying scientific principles. Furthermore, the prescriptive codes are mainly empirically driven and updated with the experience in past incidents (Nour, 2018).

However, novel concepts in architectural designs have led to more complex structures with different shapes. Even though building legislations for prescriptive approach specify the requirements to achieve in high-rise building designs, those innovative building design concepts are not fully covered with the codes and regulations which are created for conventional designs with low uncertainty. Therefore, applying similar codes to new projects and processes can result in being under conservative or over conservative. Furthermore, blindly applying the prescriptive method may not provide an adequate safety protection if the building has a higher fire risk than specified in the codes. Thus, additional fire safety features are needed to protect life and to mitigate problems in firefighting and rescue operations (Ronchi et al., 2013). On the other hand, if the solution from a prescriptive approach is over conservative, it can lead to an inefficient and costly output to build and maintain. To conclude, prescriptive design method is an easy approach to implement and offers an adequate level of safety for conventional buildings. However, this method does not encourage novel designs, and following

the rules and regulations for innovative unique designs in the prescriptive approach may not be very cost effective.

On the other hand, performance-based design (PBD) method, which is based on meeting explicitly stated fire protection requirements and goals using engineering tools and performance criteria, allows for unique novel designs and innovative features in the buildings. It helps to understand the behaviour of the structure during a fire with the newest fire safety techniques. The fire safety engineer can perform the modelling and calculations with higher flexibility to identify problem specific hazards and fire scenarios resulting in cost effective solutions (Nour, 2018).

The performance-based design approaches provide a complete solution. The solution being sustainable is one of the most important aspects. Also, it questions the real requirement of active fire protection methods like sprinkler systems and smoke detectors. This approach has clearly changed the thinking of fire safety community. Instead of arguing about words in prescriptive codes and where to apply them, now fire engineers are able to focus on problem specific questions like, where is the fire going to occur, how big the fire can be, how to evacuate occupant safely and special requirements to provide enough safety for fire team intervene (A. H. Buchanan, 1999). Figure 3 shows the process for Performance-based design approach, described in SFPE Handbook of Fire Protection Engineering (Hurley et al., 2015). However, the PBD method needs more expertise to design and to evaluate whether the required objectives are met. Also, PBD design can take longer time for the verification and validation process compared to the straightforward prescriptive design approach.

2.2. Post-Flashover Fire

Temperature in hot smoke layer increase with the time during a compartment fire resulting on a high level of heat flux irradiance to objects below the hot smoke. After reaching a critical heat flux, all combustibles may instantly ignite, increasing total heat release and temperature in the compartment. This phenomena is referred as flashover (Drysdale, 2011). After the flashover occurs, fire is commonly called post-flashover fire or fully developed fire and the behaviour of the fire changes significantly. The plume and smoke becomes very turbulent and high radiation heat fluxes make all combustible material to burn if there is enough oxygen after pyrolysing. Most important factor in a fully developed fire for structural design is the high room temperatures, which can be more than 1000°C at some situations. Most of the post-flash over fires are under-ventilated and the burning rate depends on the geometry of the openings.

The burning rate in this type of fire is controlled by the volume of ambient air entering the room and the volume of smoke flowing out of the room (Andrew H. Buchanan et al., 2017).

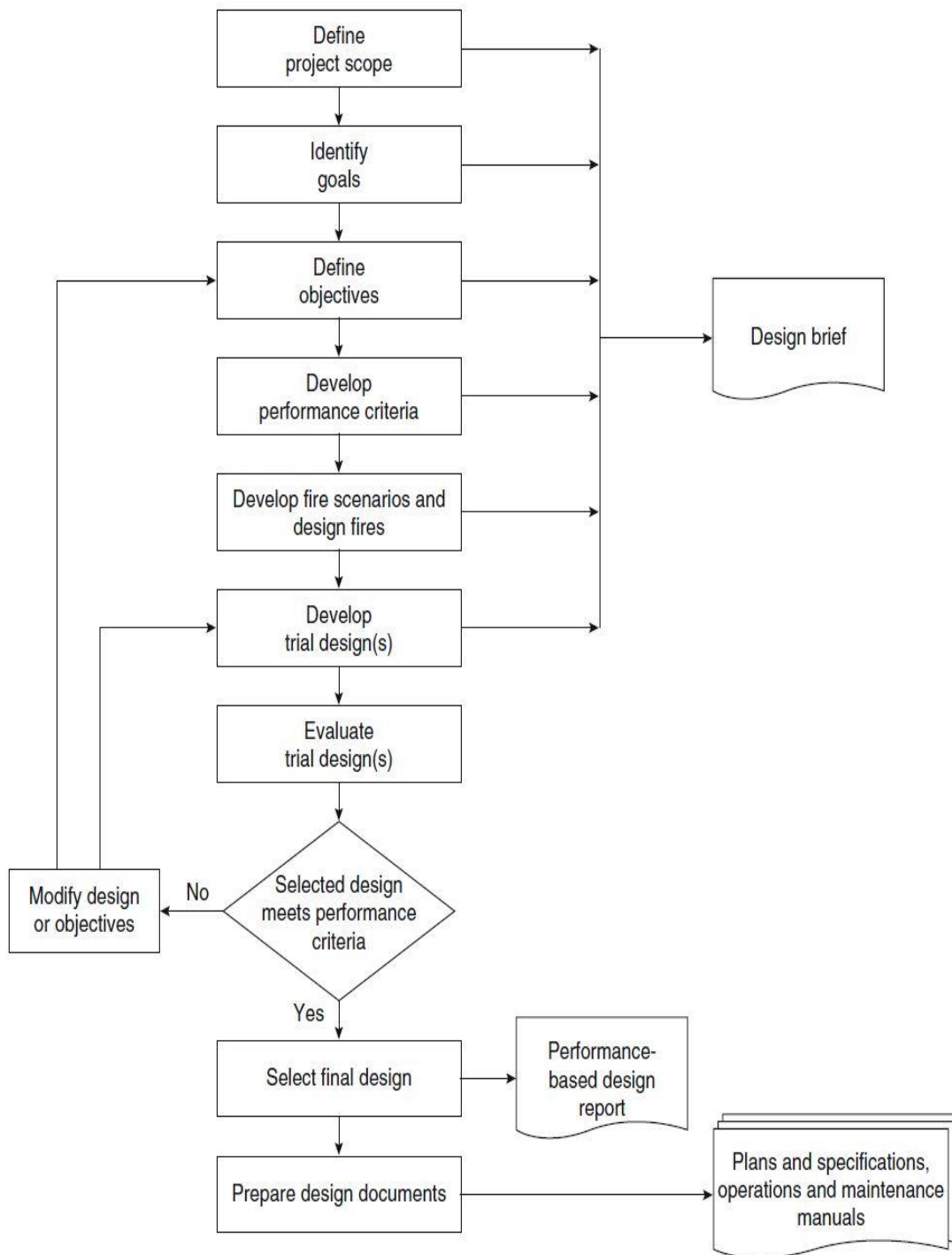


Figure 3: Performance-based design framework (Hurley et al., 2015)

However, not all the well-developed fires are under-ventilated. The heat release rate of fires in large rooms, like storage areas with limited fire load, will be controlled by the available combustible material. The rate of burning can be expected to be similar to fuel burning in the open air with the additional radiant heat feedback from hot smoke and other hot surfaces in the structure. In addition, Law (1983) has shown from results of fire experiments that the heat release rate for a well-ventilated fire in a large enclosure can be determined by dividing total combustible fuel load by expected duration of free burning.

2.3. Fire Temperatures

Determining temperature values and temperature variation with the time for a fire scenario is a very important part in structural fire safety designs. The temperature inside a room is solely related to the balance between the amount of heat released by fuel burning and the heat losses to the outside through openings, walls, ceiling and floors by different heat transfer mechanisms as shown in Figure 4. However, it is not a straight forward task to precisely calculate temperatures with the unpredictable behaviour of fire. There have been many studies on this and several methods have been introduced for design purposes.

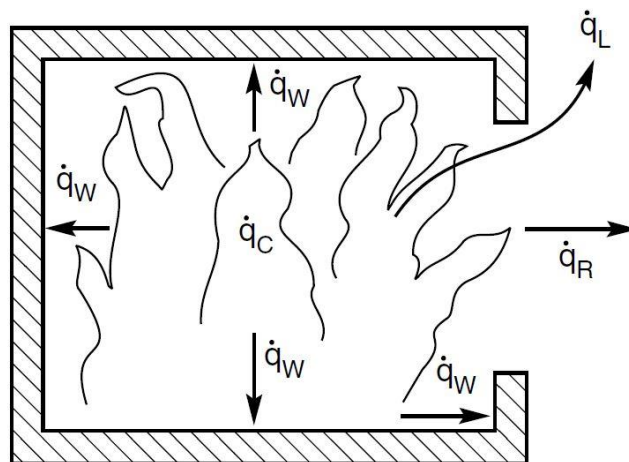


Figure 4: Energy balance for a fully developed enclosure fire (Andrew H. Buchanan et al., 2017)

Most commonly used method to calculate temperature-time curve is based on the full-scale fire resistance tests, which is named as Standard Fire Test. The standards define the heating of ambient air inside a furnace where the structure is exposed. Some of the widely used standards are ISO 834, ASTM E119, BS EN 13501 and AS 1530 (A. H. Buchanan, 1999). It is important to note that most of the standards in different countries are created based on ISO 834 or ASTM

E119. There are other different fire curves like hydrocarbon curve based of burning of different fuel types in an enclosure. Figure 5 shows a comparison of some standard fire curves.

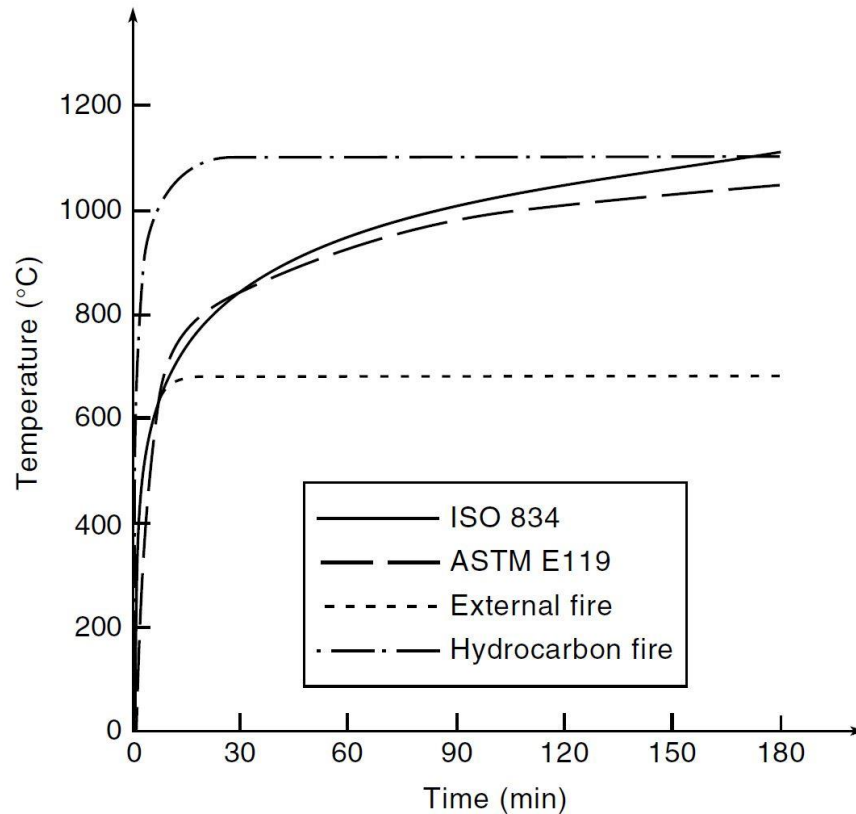


Figure 5: Comparison of standard fire curves for fully developed fires in enclosures (Andrew H. Buchanan et al., 2017)

2.3.1. The standard fire curve

The ISO standard is generated for fully developed fires in enclosed compartments by considering burning of cellulosic material (ISO 834-1:1999, 1999). Equation 1 shows the temperature time relationship for the standard ISO curve. Moreover, The ISO standard fire curve is used in Structural fire design for timber structures Eurocode 5 (EN 1995-1-2, 2004), which will be followed for the design calculations and simulations in next chapters.

$$T_g = 20 + 345 \log_{10}(8t + 1) \quad (1)$$

where, t is in minutes.

However, it is important to note that this curve is a more generalized one and does not consider parameters like fire size, geometry, construction material properties, size and shape of

openings, which can significantly vary for different fire scenarios and buildings. Also, ISO curve only has a heating phase and does not provide a decay phase, whereas real fires can show steady and descending trend of temperature with time.

2.3.2. The parametric fire curves

A parametric temperature-time curve is a more realistic representation of post-flashover fire, which is determined based on situation-specific fire models and specific physical parameters of the compartment. It is also based on burning on cellulose fuel and has both the growth and decay phases. Parametric time-temperature curve takes into account the fuel load, ventilation openings, floor area and properties of the boundary lining materials. The Eurocode EN 1995-1-2 (2004) provides a method for calculation of parametric fires. The growth phase in this curve has a good agreement with ISO 834 standard curve. On the other hand, Eurocode parametric curve equations give high room temperatures for highly insulated enclosures with large openings and low temperatures for poorly insulated compartments with small vent openings. Figure 6 shows a comparison of parametric temperature-time curves for different wall lining materials, fire loads and floor areas with respect to ISO 834 standard fire curve.

In addition, there are many experimental research that has been done considering real fire exposures to measure temperatures change with the time in fully developed fires (Butcher et al., 1966) (Thomas et al., 1972). One of the widely used experiment-based temperature curves for real fire scenarios have been introduced by Magnusson, et al. (1970). Figure 7 shows the temperature time curves from their study with different fuel loads and ventilation factors. Furthermore, it is visible that the curve with 0.04 ventilation factor shows similar growth to the ISO 834 temperature-time curve (Andrew H. Buchanan et al., 2017). Also, the parametric curves from Eurocode discussed in previous section has a good approximation to Magnusson et al. (1970) temperature curves and can be considered as a further improved version from the experiments.

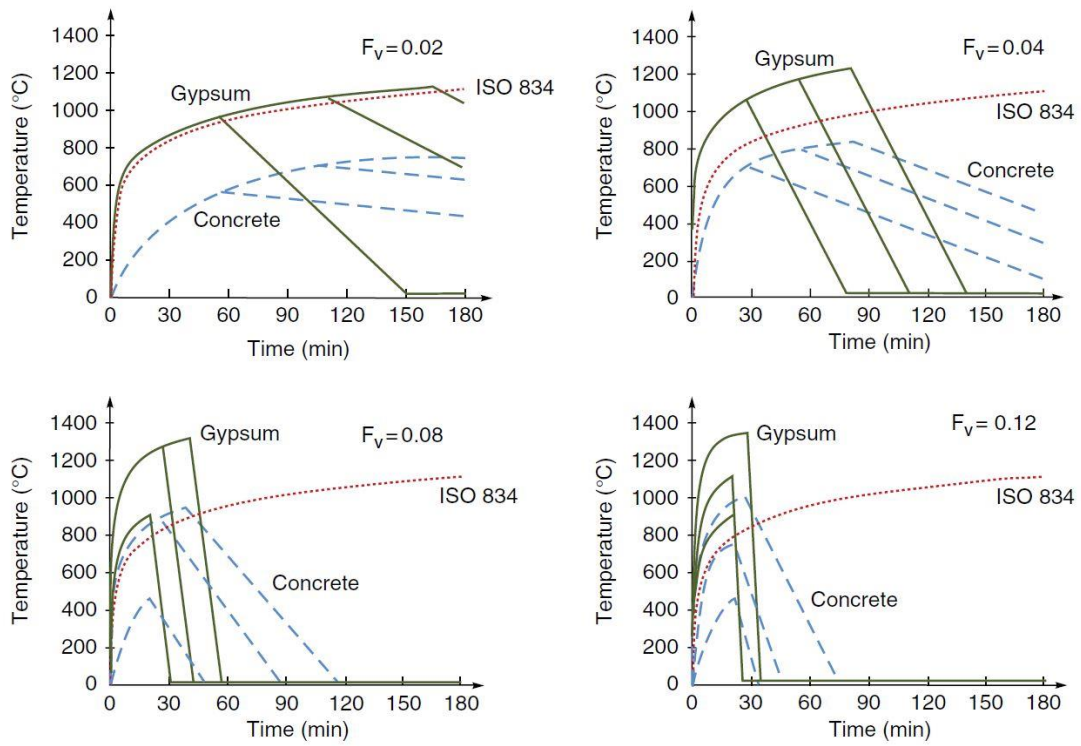


Figure 6: Comparison of parametric fire curves according to EN 1991-1-2 for different fuel loads, materials and ventilation factors (Andrew H. Buchanan et al., 2017)

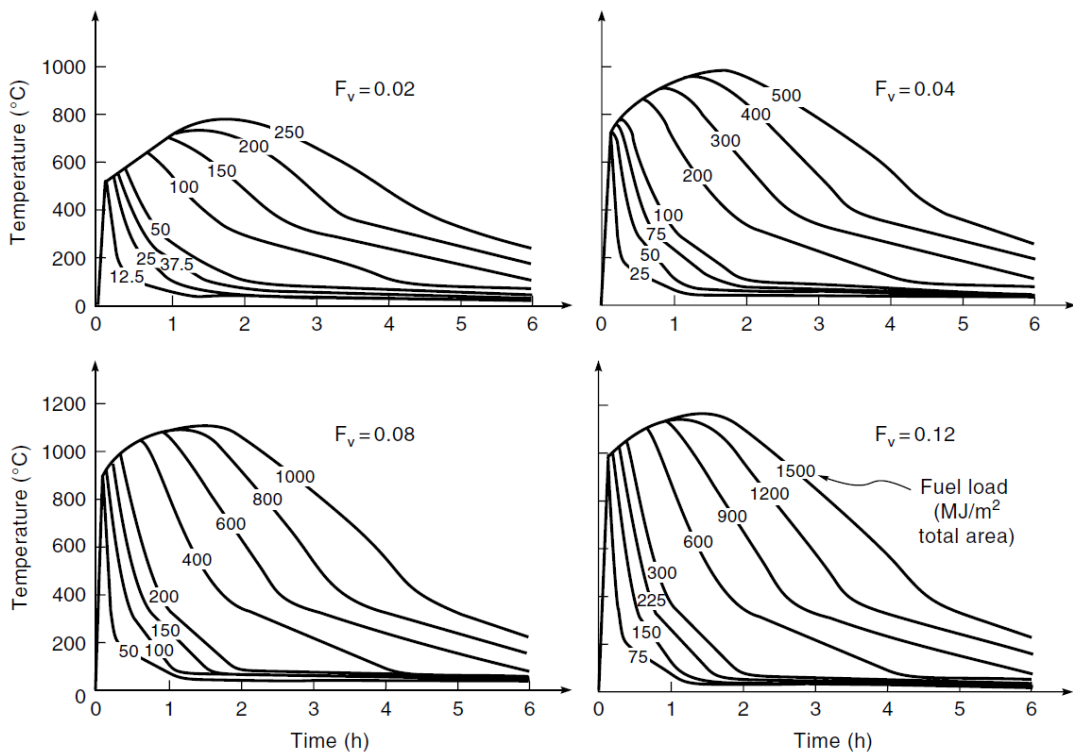


Figure 7: Temperature-time curves from experimental study by Magnusson, et al. (1970)

However, even though most of the published curves from the experiments provide data points, they do not contain simple formulas to use as in standard or parametric fire curves. In large scale enclosures-like industrial buildings, storages and large compartments, uniform fully developed fires cannot be expected at the same time for the entire space. It may be visible more localized flashover and post-flashover fires due to that. Since the methods mentioned above are to calculate temperature-time curves for small compartments, they are not applicable for the enclosures with large floor areas. (Kirby et al., 1999). Furthermore, there are not many studies on post-flashover fires in large scale compartments. Therefore, it is necessary to carry out an experiment or computer simulation to determine the valid design fire curves for these kinds of large rooms.

2.4. Structural Fire Resistance

The most important reason in structural fire engineering for taking into account the real fire scenario is that different fire types can lead to different structural responses. This can be further explained using an example with reinforced concrete element. When the element is exposed to high temperature in a short duration, concrete spalling occurs exposing steel reinforcement. On the other hand, exposure to low temperatures throughout a longer time, leads to higher overall temperature, reducing the strength of material (Bailey, 2004).

Understanding the structural behaviour during a fire has a huge impact on calculating the fire resistance of the structure. Fire resistance is the ability of the structure to withstand the specified fire load without collapsing (Bailey, 2004). The fundamental designing step in structural fire engineering is the fire resistance of structure being greater than the fire severity according to the selected method. Adequacy of fire resistance is compared with the severity of the fire using time to failure, maximum temperature to failure or load capacity at elevated temperature. Most commonly used approach to describe the fire resistance is the time to failure of a building element. This is presented as a fire resisting rating using standard fire test or by time equivalence from a real fire as explained in the next section.

2.4.1. Time equivalence

Fire resistance of structural elements is widely defined in design codes using the resistance against the standard fire. This gives a common platform for the designers, regulating bodies, researchers, contractors and others to discuss. However, as explained before, the behaviour of a structure to a real fire is not similar to a standard furnace test. Therefore, to equate the real

fire severity with the standard fire exposure whenever it is necessary, the concept of equivalent fire severity has been introduced by Ingberg (1928). He proposed the “equal areas” approach by comparing area under the temperature-time curves of real fire and standard fire as shown in Figure 8. The time where the two areas are equal was named as the “time equivalence”.

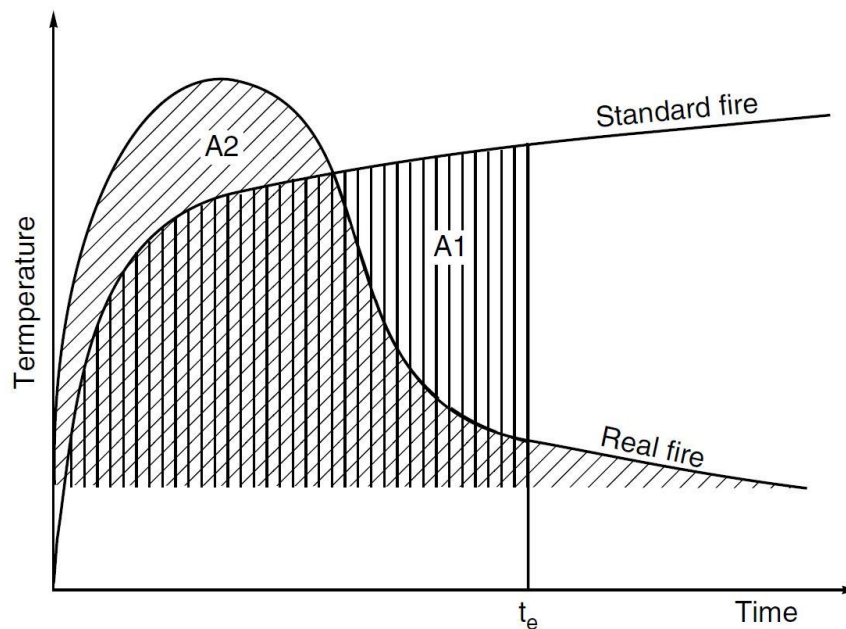


Figure 8: Equal areas concept for time equivalence (Ingberg, 1928)

There are major shortcomings in the equal area basis, because the dominant heat transfer mechanism to structure is by radiation and it depends on the fourth power of the temperature. Ingberg (1928) also knew this method is scientifically inadequate when he proposed it. However, there is no better approach yet to compare fires and fire resistance in most of modern design codes are based on time equivalence method.

Law (1971) and others suggested another time equivalence concept for standard fire curve with the same maximum temperature in covered steel elements exposed to a real fire. As shown in Figure 9, this method compares temperatures in steel element for real fire to reach similar maximum temperature in standard fire. This method can be useful for timber members where the charring process starts at 300°C. However, the maximum temperature approach can provide inaccurate results, if the maximum temperature for standard fire and real fire has a huge variation which is used to determine time equivalence.

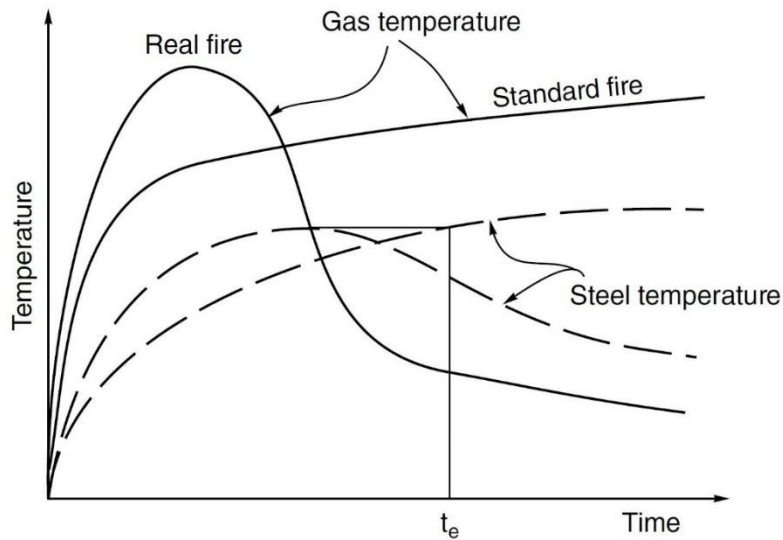


Figure 9: Time equivalence base on maximum temperature of element (Andrew H. Buchanan et al., 2017)

2.5. Performance of Timber Structures Exposed to Fire

Many researches have been conducted to study the fire performance of structural timber, either using experiments or computer modelling or both, depending on the area of interest and the available resources and expertise.

Frangi et al. (2009) presented an experimental study of cross laminated timber (CLT) panels exposed to ISO standard fire to understand the reduction of cross section in elevated temperatures due to charring. The study shows that the fire behaviour of CLT is mainly controlled by the type of the adhesive used. If there is no falling off of the charred CLT layers then it shows a similar fire behaviour as in uniform timber members. Furthermore, Klippel and Frangi (2017) have studied the influence of different types of adhesives for load capacity behaviour in glued laminated timber in bending under standard fire.

Laplanche et al. (2006) carried out a thermo-mechanical finite element analysis for structural timber connections exposed to fire. This 3D numerical model investigates the performance of timber dowelled joints under fire by taking into account the variation of timber properties with temperature. The thermal analysis was based on standard fire condition ISO 834. The thermo-mechanical model has been validated using an experimental fire test under 10% of difference between predicted and measured fire resistance time. The temperature values in the thermal model has been compared with the thermocouple measurements and the non-linear finite

element mechanical model. The local plastic behaviour of the numerical model has been tested with failure modes and stress distribution in the experiment.

O'Neill et al. (2014) have conducted a study for timber concrete composite floors with three-sided exposure to the standard ISO fire curve. The aim of the study was to develop a simplified design method to test the fire performance of composite timber floors using a numerical Abaqus model and experimental data from the furnace tests.

Similar kind of work has been proposed by various researchers to understand the fire performance of timber elements exposed to fires with advanced computer modelling and experiments (Thi et al., 2017), (Fragiacomo et al., 2013) (Schmid et al., 2018) (Werther et al., 2012). All of those studies are based on standard fire curves and mechanical behaviour in fire is analysed using that. Very few studies are available based on parametric design fires or real fires to evaluate timber structures behaviour in fire

Brandon et al. (2018) presented a performance-based design for a mass timber structure in a fire. The design calculations were expected to achieve a predefined goal of structure withstanding without failing for the full duration of an uncontrolled fire. The temperature-time curve has been determined using the parametric fire equations in EN 1991-1-2 for a fire tested small compartment with a floor area of less than 500 m². The results show that the temperatures in parametric design method are more conservative than the measured temperatures in fire tests.

Another study done by Brandon and his research team (2018) discusses a design approach for high-rise timber buildings to reduce risk of structural collapse during fires . It discusses the importance of the timber fuel load contribution for the fire development. The study suggests an iterative method to account for the additional fire load from the exposed wood to the parametric fire design in Eurocode EN 1995-1-2 (2004) by using the Equation 2. Here, the char depth in first iteration is used to calculate the fuel load density in the second iteration.

$$q_{td}^{i+1} = q_{mfl} + \frac{A_{tim}\alpha_1(d_{char,end}^i - 0.7\beta_{par}t_{max}^1)}{A_c} \quad (2)$$

where q_{td}^{i+1} is the total fuel load in MJ/m², q_{mfl} is the movable fuel load per total surface area in MJ/m² and for non-combustible material $q_{td}^{i+1} = q_{mfl}$. A_{tim} is the exposed area of the timber in m². $d_{char,end}^i$ is the final char depth in mm. β_{par} is the charring rate in mm/min and t_{max}^1 is the exposure time in min. A_c is the total surface area of the compartment. The subscript 1 denote

the number of iterations. However, this equation is only valid for small compartments and only if the moveable fuel load can reach the post-flashover fire without the contribution of additional fire load in structure. Furthermore, ignition and burning of timber will depend on the exposed irradiance heat flux and ventilation conditions. Also, the entire structure may not be involved as additional fire load in a large compartment and it is difficult to predict the exposed area due to the uncertainty of fire.

In addition, Brandon (2018) has presented three methods as shown in Figure 10 to evaluate the mechanical performance of Glulam and CLT, after the design fire is calculated. Two methods are based on the reducing the cross section of timber elements at elevated temperature to calculate the reduced resulting load bearing capacity. The third method is based on the reducing mechanical properties of timber elements at high temperatures to reduce the resulting resistance capacity.

Name	Reference	Description	Glued laminated timber	Cross laminated timber
Method 1	Lange et al. (2015)	Reducing the load bearing cross section of structural elements by subtracting a non-linear char layer and a constant zero-strength-layer.	Suitable	Not suitable
Method 2	Brandon et al. (2017)	Reducing the load bearing cross section of structural elements by subtracting a non-linear char layer and a non-linear zero-strength layer.	Suitable	Not suitable
Method 3	Brandon et al. (2018)	Reducing local mechanical properties throughout structural elements based on calculated temperatures	Suitable	Suitable

Figure 10: Methods to calculate structural response of timber elements subjected to parametric design fires taken from Brandon (2018)

2.6. Adiabatic Surface Temperature

The temperature profiles inside the solid material are critical to calculate the structural performance of elements when exposed to a fire. Therefore, an accurate model representing heat transfer to solids by convective and radiative heat flux is necessary. FDS allows to apply temperature or heat flux boundary conditions to solids for heat conduction and to measure temperatures and other properties inside the solid. Even though FDS is considered as leading validated software package to simulate real fires and smoke, the usefulness of solid heat transfer results is limited. The reason is that FDS only solves the one-dimensional heat transfer

equation inside the solids. Furthermore, if the solid geometry is greater than one cell thick, the heat conduction by every surface is done separately without communicating to other solid surfaces (McGrattan et al., 2016). Therefore, a more advanced software package is required to account for lateral heat transfer inside solids according to exposed thermal boundary conditions.

Wickström et al. (2007) have presented a concept of “adiabatic surface temperature” to express the thermal boundary condition of a solid, when the exposure temperatures are obtained from a fire model or experiment and later use to calculate temperature profile in fire exposed solid elements. The adiabatic surface temperature (AST) is the temperature of a surface, considering it as a perfect insulator, when heated from fire flame and hot gasses via radiation and convection. By definition the net heat flux of the ideal surface is zero as shown in Equation 3 (Wickström et al., 2007).

$$\epsilon(\dot{q}_{inc}'' - \sigma T_{AST}^4) + h(T_g - T_{AST}) = 0 \quad (3)$$

Here, \dot{q}_{inc}'' is the incident heat flux, ϵ is the emissivity, σ is the Stefan-Boltzmann constant, T_g is the gas temperature.

The AST can be predicted using a fire model for real fire scenarios, and it is similar to the measurement in plate thermometer value in an experiment. Furthermore, the study has presented AST as gas-solid interphase between the fire and the structural model to use for more detailed thermal calculations inside a solid. The net total heat flux to the structural model ($\dot{q}_{tot,SM}''$) can be expressed using AST from the fire model and surface temperature in the solid model ($T_{s,SM}$) as shown in Equation 4 (Wickström et al., 2007).

$$\dot{q}_{tot,SM}'' = \epsilon\sigma(T_{AST}^4 - T_{s,SM}^4) + h(T_{AST} - T_{s,SM}) \quad (4)$$

Since there are almost no studies that have been done to calculate the temperature-time relationship for real fires considering combustibility of timber elements in large enclosures, it was decided to create a parametric design fire to the studied Industrial Hall. The thermal and mechanical analysis using the calculated design fire curves based on adiabatic temperatures are presented in subsequent chapters. Additionally, more literature is discussed in the next chapters, which are used for numerical modelling.

CHAPTER III

3. Timber Section Calculation

3.1. Actions

The applied loads on the building must be known to carry out the structural building analyses. There are many actions that can act on a structure, like dead loads, imposed load, accidental dynamic actions from impact and explosions, snow loads, wind loads and etc. (Pluto, 2018). It is important to understand the possibility of which loads that can induce a structural response, according to the situation. In this thesis, the design loads used for the steel structural design in Industrial Hall (Dead Loads and Imposed Loads) were considered to calculate the equivalent new timber cross section of columns to withstand those loads. Timber section capacity was designed to resist applied loads at ambient conditions. Resistance of the section to 60 minutes of standard fire was also checked.

The Figure 11 shows a part of the typical column grid in the Industrial Hall. Internal columns are expected to bear a higher load compared to the outer columns. Coloured area in Figure 11 shows load distribution to a critical column at the centre. The codes instruct to consider One-Way slab load distribution when the longer span in a slab bay is greater than twice the shorter span of the slab bay (Lantsoght et al., 2014) (Shoukry et al., 2018). Therefore, the load distribution in the slab was assumed to be one-way. The coloured area with one-way slab load distribution was used to calculate the total dead load and imposed load acting on a critical column.

Table 1 shows the summarized dead loads acting on a column. The total dead load was found to be 169.1 kN. The imposed load value of 0.4 kN/m² for the structure was taken from Eurocode 1 EN 1991-1-1 (2002) considering the roof which is not easily accessible except for normal maintenance and repair. Using that value total live load on a column was determined to be 44.5 kN.

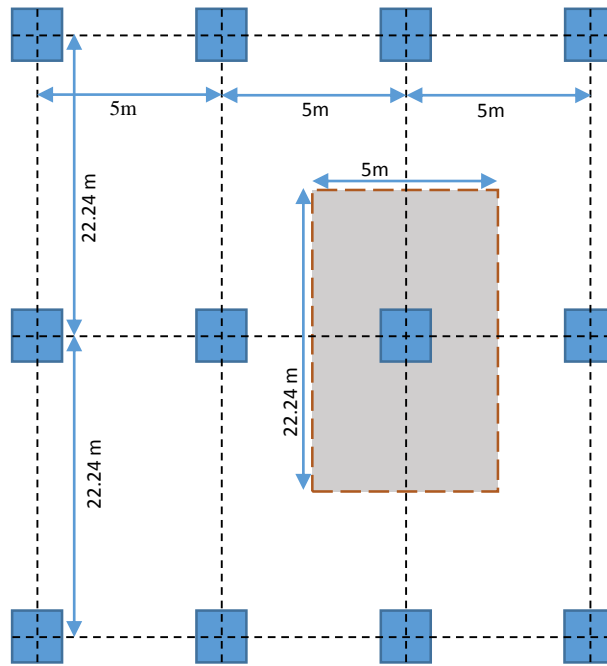


Figure 11: Spacing of the typical column grid in the building

Table 1: Dead load action

<i>Dead Load Type</i>	<i>Value (kg/m)</i>	<i>Value (kN/m)</i>
<i>Self-Weight</i>	200	1962
<i>Super Dead Load</i>	500	4905
<i>Solar Panel</i>	75	735.75
<i>Total dead load on a column</i>	$(1962 + 4905 + 735.75) \times 22.24 = 169.1 \text{ kN}$	

3.1.1. Ultimate Limit State (ULS)

The maximum design load that a structure must resist without collapsing is named the ultimate limit state (ULS). The column cross section at ambient temperature was designed to withstand the ULS load. Equation 5 shows the simplified form to calculate ULS design load from Eurocode EN 1990:2002+A1 (2005) and the ultimate limit design load was calculated as 296 kN. However, it is noteworthy that in some design cases like deflections and vibrations, the serviceability limit state can govern the section size of the structural element.

$$q_{ULS} = \gamma_{DL}q_{DL} + \gamma_{IL}q_{IL} \quad (5)$$

where,

q_{ULS} is the ultimate limit design load,

γ is the partial safety factors, 1.35 for dead loads and 1.5 for imposed loads (EN 1990:2002+A1, 2005)

q_{DL} is the dead load

q_{IL} is the imposed load

3.1.2. Fire Limit State (FLS)

Fire limit state (FLS) loading is also determined in a similar approach to the ULS by adjusting the partial safety factors. Safety factors in FLS tends to be smaller than the ULS because the likelihood of the accidental fire load can be considered low. Equation 6 shows the simplified form to calculate FLS design load from Eurocode EN 1990:2002+A1 (2005) and the fire limit design load was calculated as 209.2 kN.

$$q_{FLS} = \gamma_{DL,FL}q_{DL} + \gamma_{IL,FL}q_{IL} + A_d \quad (6)$$

Where,

q_{FLS} is the FLS design load,

γ are the partial safety factors, 1.0 for dead loads and 0.9 for imposed loads in a storage (EN 1990:2002+A1, 2005)

q_{DL} is the dead load

q_{IL} is the imposed load

A_d is the load induced due to thermal expansion

3.2. Design of Timber Section at Ambient Conditions

The design calculations of the section at ambient temperature was carried out following the guidelines in Eurocode 5 EN 1995-1-1 (2004), Design of Timber Structures – General Common Rules and Rules for Buildings code. Homogeneous Glulam (GL24h) material and its properties was used for the calculations.

Glulam columns are built with wood grains along the axis of height due to the higher strength along grains compared to the strength perpendicular to the grains. Therefore, compressive strength of the section parallel to grain was checked to select adequate dimensions. The column is 11 m high and there is a high possibility to fail in buckling before reaching its axial capacity. To ensure that this does not happen, the stability of the member was checked for buckling. On a side note, loads acting on the column were considered to be axial loads without any eccentricity. This helps to neglect bending moments in the calculations, even though sometimes it is possible for the columns to undergo bending. It is a reasonable assumption to make with the given data on the Industrial Hall, since the study focuses more on fire performance and structural calculations were only carried out to find a reasonable cross section.

Table 2 shows the parameters and their values used to determine the column cross section in the next subsection. Here, the loads were considered as long term and less than 20% moisture for softwood. Characteristic strength and stiffness properties were taken from EN 1194:1999 (1999).

Table 2: Parameters and values used for section calculation at ambient condition

Parameter	Value used	Standard
Load Duration class	Long-term load class for a storage	EN 1995-1-1
Service class	Service class 2 for moisture content not exceeding 20%	EN 1995-1-1
The partial factor for material property (γ_m)	1.25 for glued laminated timber	EN 1995-1-1
Modification factor accounting for duration of load and moisture content (k_{mod})	0.7 for long term load, service class 2	EN 1995-1-1
Creep deformation factor (k_{def})	0.8 for service class 2	EN 14080
Characteristic compression strength ($f_{c,0,k}$)	24 N/mm ²	EN 1194:1999
The fifth percentile value of modulus of elasticity parallel to the grain ($E_{0,g,05}$)	9400 N/mm ²	EN 1194:1999

Characteristic density ($\rho_{g,k}$)	380 kg/m ³	EN 1194:1999
β_c	0.1 for glued laminated timber	EN 1995-1-1

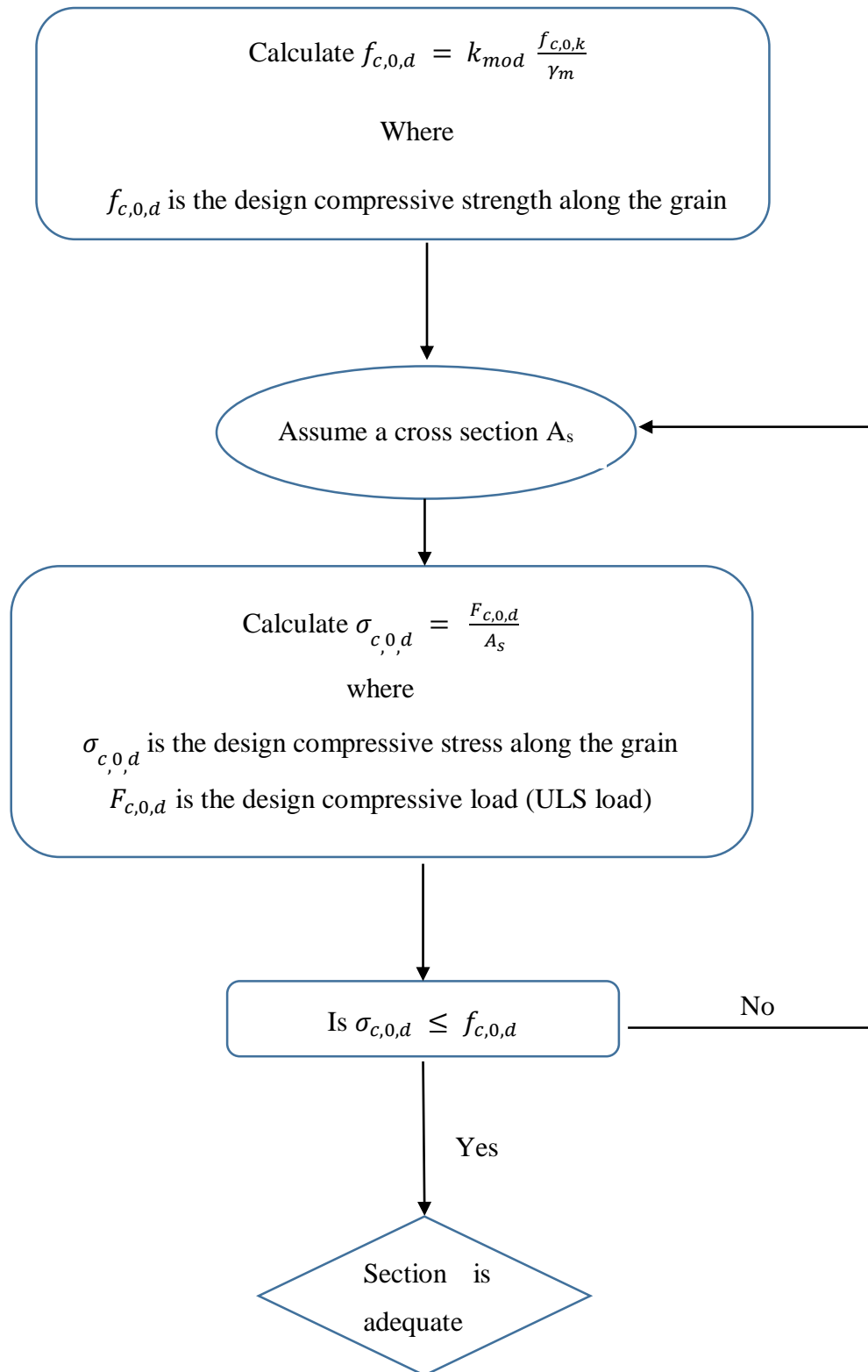
3.2.1. Calculation process for compression and buckling capacity

Initial cross section of 480 mm x 220 mm was selected for the calculation and the flowchart in Section 3.2.2 demonstrates the steps to determine the adequacy of compressive capacity for the selected dimensions. The cross section was adequate since the design compressive strength of the section is higher than the applied design compressive stress.

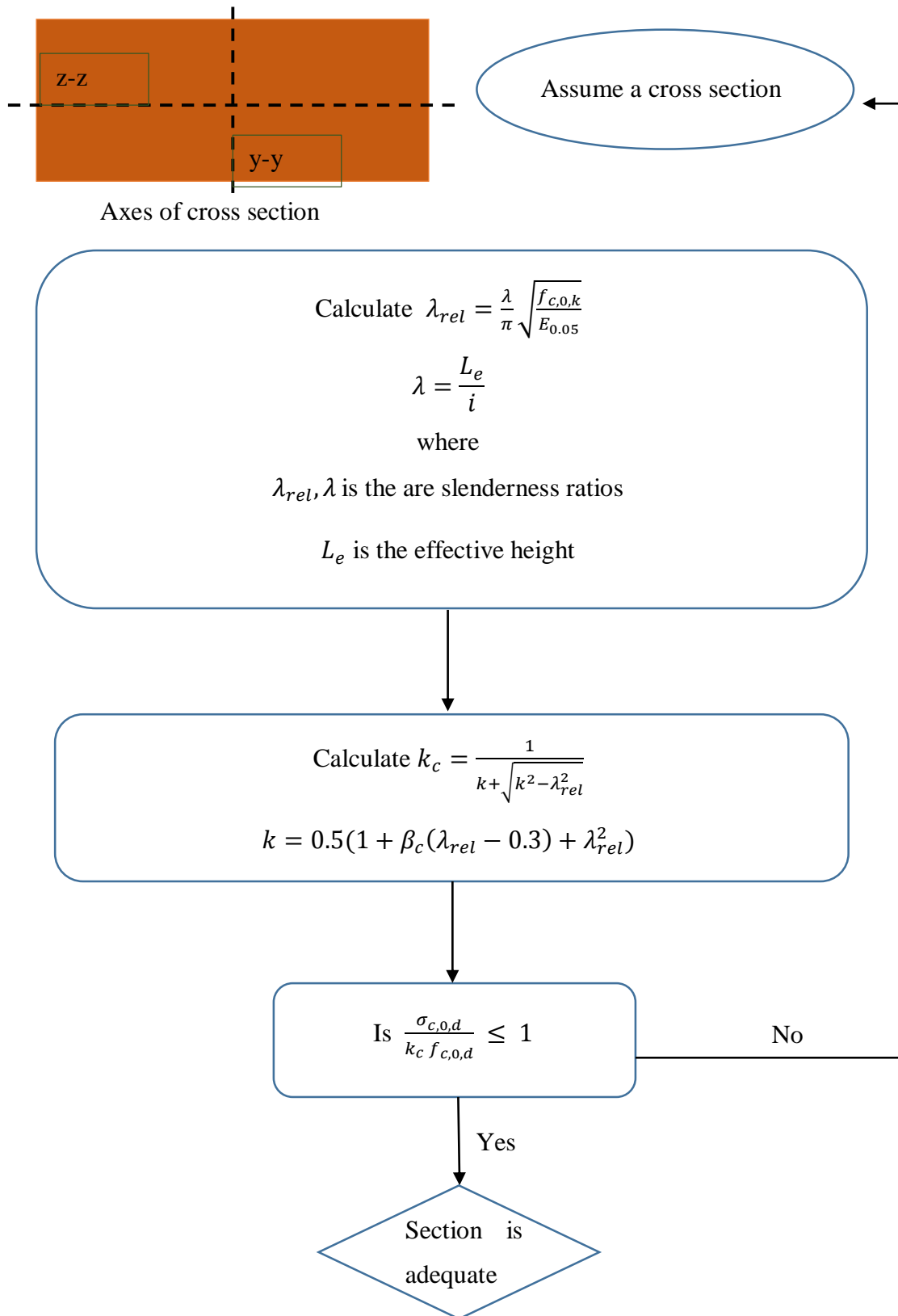
Stability of the member was checked using the buckling formula for columns subjected to compression. The flowchart in section 3.2.3 shows the process to calculate buckling capacity of the column. As mentioned earlier, a similar cross section of 480 mm x 220mm was used initially. However, for the buckling it is important to consider the direction where the deflection going to occur. For the Industrial Hall it was assumed that the columns were braced for out of plane (Z) direction. Therefore, buckling would only occur in plane about the stronger (Y) axis (Refer section 3.2.3). For Y axis, effective height was taken as 11 m with pinned-pinned boundary condition. Fifth percentile value was used for the modulus of elasticity.

Calculations showed that the initial section has enough buckling capacity at ambient condition to withstand the applied loads. However, selecting a large cross section for a safe design is not a good engineering practice because it can be very costly. Therefore, backward calculation was done to find out a more reasonable section using the initial section and similar formulas. Afterwards, the final dimension was determined as 300 mm x 220 mm to satisfy both compressive and buckling capacity requirements.

3.2.2. Flow chart for the calculation process of compressive capacity



3.2.3. Flow chart for the calculation process of buckling capacity



3.3. Timber Section Resistance for Fire Conditions

During an event of fire, properties of materials change significantly due to thermal reactions. This leads to reduce the structural performance and resistance of elements. Thus, it is important to check whether a structure can bear the fire limit state loading during a fire with degraded material properties. Therefore, the axial and buckling capacity of the cross section which was calculated for ambient condition was checked after 60 minutes nominal (standard) fire exposure using guideline EN 1995-1-2 (2004), Design of timber Structures – Structural Fire Design code.

3.3.1. Charring depth

Charring is taken into account for all wood surfaces directly exposed to fire. Charring depth, which is the distance between original out position of the section and char-line, is used to find the effective cross section using fire exposure time and the charring rate of wood material. Here, char-line is considered as the 300 °C isotherm position. In addition, charring rate can be different depending on the type of wood surface protection. Therefore, for the calculations, unprotected timber columns were considered throughout the duration of fire exposure. Furthermore, in two-dimensional heat transfer, corner rounding and fissures should be taken in to account for the charring depth, with a constant charring rate as shown in Equation 7.

$$d_{char,n} = \beta_n t \quad (7)$$

Here,

$d_{char,n}$ is the design charring depth considering the effect of corner rounding

β_n is the design charring rate including corner rounding, cracks and fissures

t is the fire exposure time

The design charring depth was calculated as 42 mm for 60 minutes fire using β_n value of 0.7 mm/min for softwood Glued laminated timber with density greater than 290 kg/m³. This value was then used to calculate the effective charring depth (d_{ef}) using Equation 8, so that the reduced cross section can be determined .

$$d_{ef} = d_{char,n} + k_0 d_0 \quad (8)$$

Here, d_0 is given as 7 mm and k_0 is taken to be 1.0 for unprotected surfaces with exposure time greater than 20 min. Using those values, the effective charring depth was determined to be 49 mm.

3.3.2. Effective cross section

The effective cross section was calculated as 202 mm x 122 mm by reducing the effective charring depth from initial cross section of 300 mm x 220 mm. Figure 12 illustrates the effective cross section after 60 minutes of standard fire exposure. It is worthwhile to note that the above method assumes timber material to have zero strength and stiffness close to the char line, while unchanged properties for remaining unburnt material section.

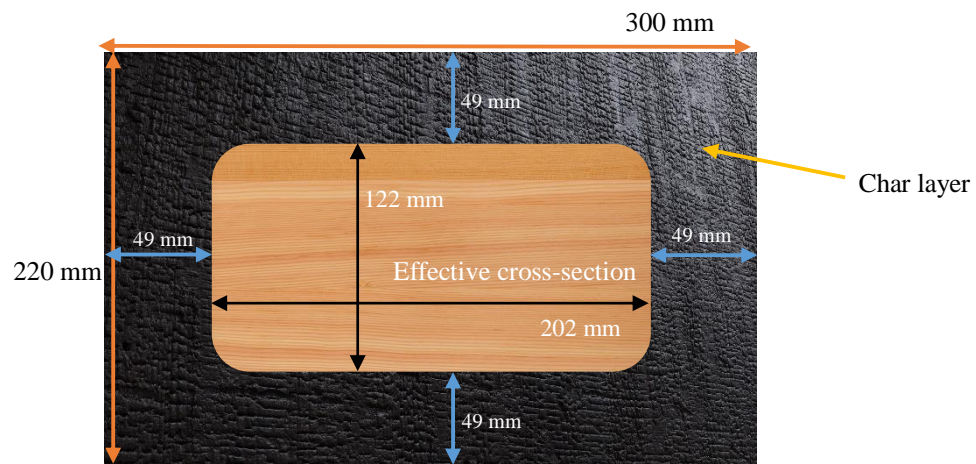


Figure 12: Effective timber cross section

Next, the mechanical capacity of the effective cross section after the fire was calculated and compared with the fire limit state (FLS) loading. The compressive strength and buckling capacity checks were carried out using flowcharts in section 3.2.2 and section 3.2.3, following a similar way as discussed earlier. However, design strength and stiffness values considered to be higher in fire design calculation compared to ambient temperature conditions. The reason being that the fire load is considered to be an accidental load with low likelihood to occur simultaneously with other events like a hurricane, a snowstorm and therefore, magnitude of safety factors have changed to account for this in fire design codes. Equations 9 and 10 give the design values for strength and stiffness in fire. In addition, $k_{mod,fi}$ and γ_m were taken to be 1.0 in this method as recommended in EN 1995-1-2 (2004). The 20 % fractile values were calculated using Equations 11 and 12 with the characteristic values stated in Table 2.

$$f_{d,0,fi} = k_{mod,fi} \frac{f_{20}}{\gamma_m} \quad (9)$$

$$E_{d,0,fi} = k_{mod,fi} \frac{E_{20}}{\gamma_m} \quad (10)$$

$f_{d,0,fi}$ is the compressive design strength parallel to grain in fire

$E_{d,0,fi}$ is the design modulus of elasticity parallel to grain in fire

f_{20} is the 20% fractile value of compressive strength parallel to grain at normal temperature

E_{20} is the 20% fractile value of modulus of elasticity parallel to the grain at normal temperature

$$f_{20} = k_{fi} f_{c,0,k} \quad (11)$$

$$E_{20} = k_{fi} E_{0,g,05} \quad (12)$$

where k_{fi} is 1.15 for Glued-laminated timber

The calculations showed that the effective cross section has enough compressive capacity to withstand compression FLS loading parallel to grain. However, member stability calculation showed that the column does not have enough buckling capacity and may fail if exposed to 60 minutes of fire. These findings were later used to compare with the finite element model results for mechanical analysis.

CHAPTER IV

4. Fire Modelling Techniques for Large Enclosures

4.1. Fire Dynamics Simulator (FDS)

Fire Dynamics Simulator (FDS) developed by National Institute of Standards and Technology (NIST) was used to simulate the fire inside the industrial hall. FDS is a Computational Fluid Dynamics (CFD) software package which solves simplified forms of Navier-Stokes equations numerically. FDS can be used to simulate low speed thermally driven fluid flow with smoke plume in fire safety engineering. FDS is a powerful tool to predict heat generation and transfer from a fire (Ryder et al., 2004).

Navier-Stokes equations govern the conservation of momentum of a fluid flow and are applicable for fluids which are Continuum, Newtonian, Thermally Isotropic and Ideal Gasses. To describe the flow field in a fire the Navier-Stokes equations can be applied. These partial differential equations describe the motion of fluids. Simplification can be made by assuming the above criteria (ideal gas, low Mach number flow etc.) (Luketa-Hanlin, 2006). The Navier-Stokes equations can be solved numerically depending on the different approaches adopted by CFD packages as described below:

- Direct numerical simulation (DNS): Provides exact solution for the Navier-Stokes equations by resolving all scales without any simplifications. The discretized grid has characteristic dimension smaller than the Kolmogorov Microscale which represents the eddy size where the viscous dissipation occurs in turbulence. (Busini, 1895). Still there is no general analytical solution for DNS and even if a solution exists, practically not possible to utilise it. Grid sizes around 1 mm required to numerically solve the governing equations (SFPE Handbook, 2016) and thus too computationally expensive for standard engineering problems
- Large eddy simulation (LES): Solves for the turbulence energy diffuse in the largest scale in time and space. Discretization of the grid is done allowing the turbulent motion of large eddies to be resolved. According to the Pope criterion, for an accurate simulation 80% of dynamic kinetic energy must be resolved. Remaining energy dissipation at smallest scale motion is represented with a sub-grid model. LES

simulation uses filtering in governing equations and it is computationally demanding compared to RANS simulation (Busini, 1895).

- Reynolds-averaged Navier–Stokes (RANS): Transport equations are averaged over time. Instantaneous variables represent with an averaged value and fluctuating component. RANS do not have close-set equations for Navier-Stokes solution and therefore, requires introduction of new equations (sub models). An empirical model is introduced to compute the turbulent diffusion and the turbulent fluctuations. The accuracy of the simulation vastly depends on the empirical model used. RANS provides a balance between computational efficiency and reliability. However, it unable to identify complex turbulence flows (Luketa-Hanlin, 2006) (Busini, 1895)

Fire dynamic simulator (FDS) version 6.7.0 was used for the numerical simulation. FDS is an LES simulator where the algorithm used in the software approximates the Navier-Stokes equations by applying a Favre filter and modelling the sub grid scale turbulent viscosity. The default turbulence model in FDS is the Deardorff model. The core explicit predictor-corrector solver in FDS provides a second order accuracy in space and time (Anderson et al., 2019). On the other hand, it should be noted that the accuracy of a CFD solution in fire depends on many factors like grid resolution, turbulence sub model, complex chemical and physical parameters of fire and accurate representation of boundary conditions related to fire. Thus, it is required to have a good understanding on these parameters to get adequate results for a fire scenario (Ryder et al., 2004). Furthermore, FDS use a rectilinear meshes and converts all the geometric obstructions to fit the rectilinear grid. As an example, triangular or circular objects will approximate as a series of rectangles. Therefore, the thickness and shape of the obstructions should be handled carefully when creating the model.

4.2. Numerical Fire Model

FDS is a CFD solver, which does not contain a graphical user interface (GUI). The input file with all the necessary details can be created using a text editor or a third-party prepossessing software like PyroSim. Furthermore, the post-processing can be done using Smokeview or PyroSim software to visualize the fire behaviour and other fire related parameters. In this study, PyroSim 2020 commercial software package developed by Thunderhead Engineering was used for the pre-processing and post-processing of the FDS model.

Figures 13 and 14 show the top view and side view of the FDS model geometry with the modelled dimensions. The roof in the top view and a smoke collector obstruction in the side

view has been hidden in Figures 13 and 14 to provide a better visibility in the model. The walls, roof and floor obstructions were assumed to have inert surface conditions. The columns were modelled using the timber properties discussed later in this chapter.

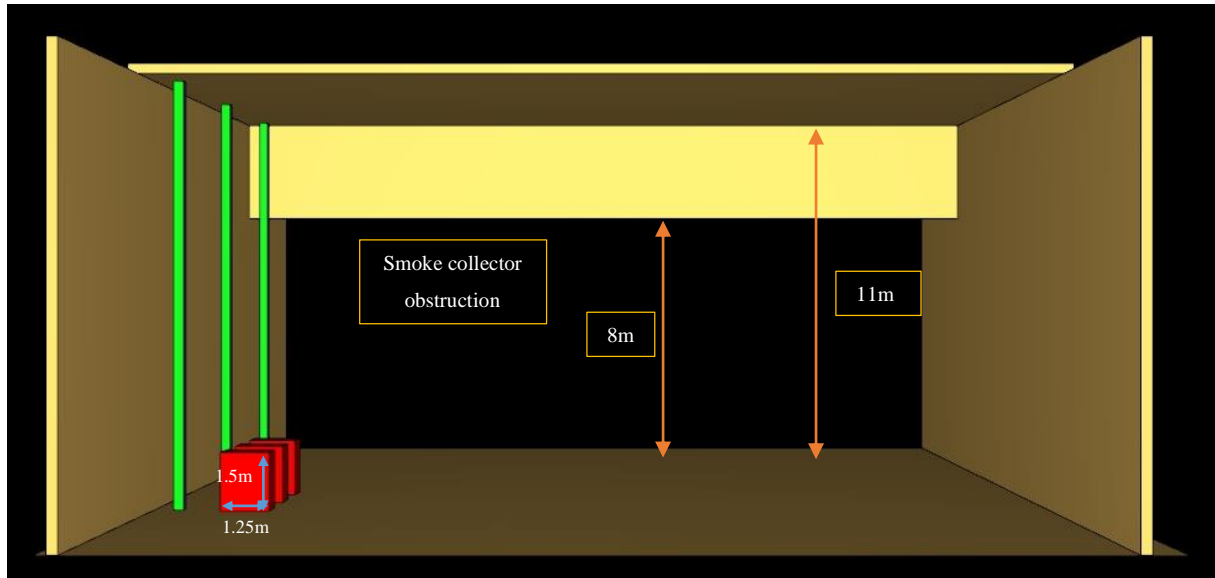


Figure 13: Side view of the FDS model

Three critical timber columns near to the critical fire scenario was selected for the simulation. The column obstructions were created with 250 mm x 250 mm geometry due to the rectilinear mesh limitation in FDS. However, the actual columns section of 300 mm x 220 mm was used to define the thermal thickness and the actual dimensions were used to solve the conduction of heat through the solid. Figure 15 shows a zoomed-in section near to the fire with a grid of 250 mm. Three wood cribs with 1.25 m x 0.75 m x 1.5 m dimensions were used to generate heat release rate from fire. Each of the columns, column surfaces and wood cribs were named as shown in Figure 15 to easily identify and describe in the discussion.

In addition, two obstructions with a height of 3 m were created descending from the roof to represent the smoke layer in the analysis to observe the smoke layer affect to temperatures and other critical parameters. Furthermore, different solid and gas phase devices in FDS were installed to measure the critical fire related parameters such as, surface temperature, heat flux, heat release rate, gas temperature and adiabatic temperature in column surfaces, above the wood cribs and in the smoke layer. The properties and the values used for the FDS analysis is discussed thoroughly in the next section.

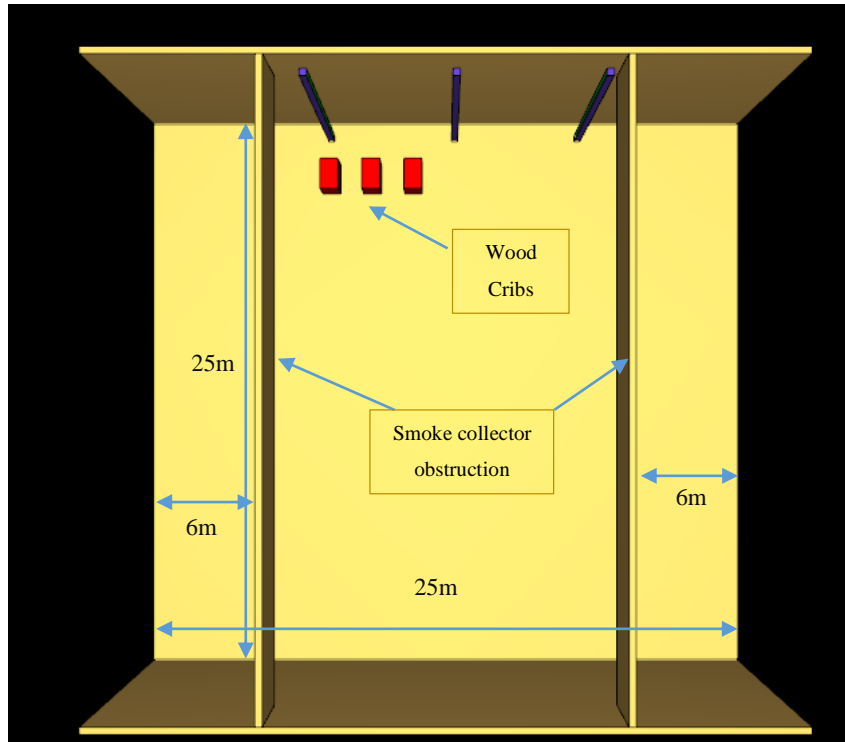


Figure 14: Top view of the FDS model

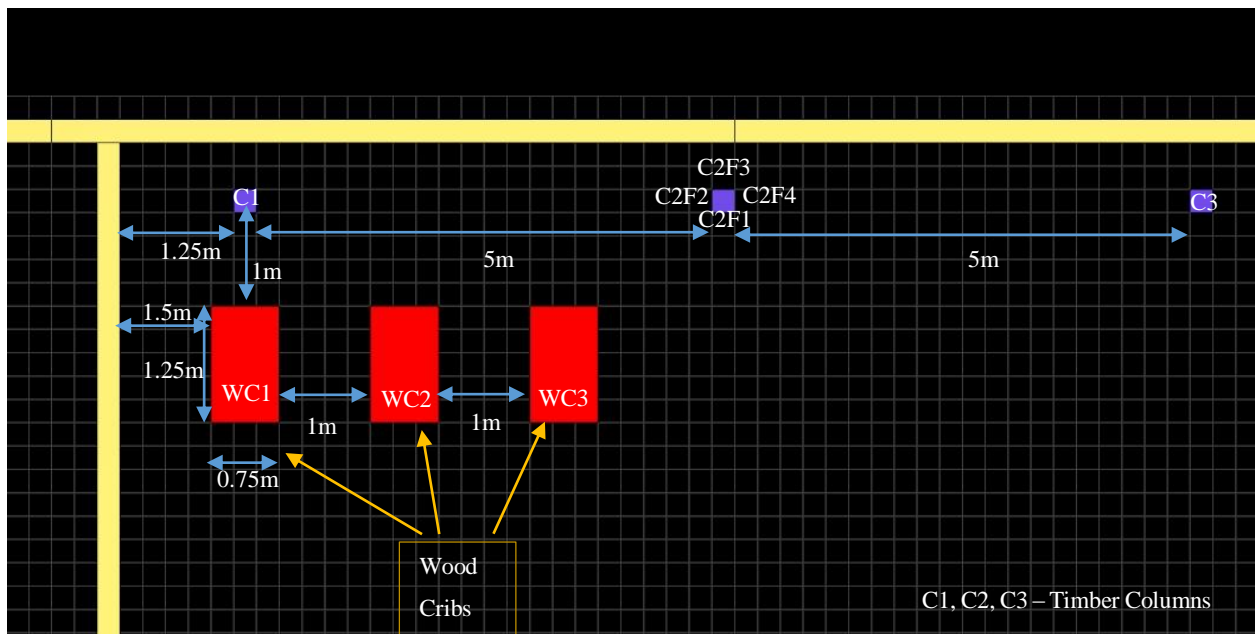


Figure 15: Plan view of area near the wood cribs and timber columns

4.2.1. Heat release rate of the wood crib fire

Considering the current storage and use concept in the Industrial Hall, the critical fire load was assumed to be burning of three wood cribs, the wood cribs consist of 100 wood pallets placed together. Each wood crib has 10 pallet stacks, each stack having 10 pallets.

The wood crib has a size of 1.25 m x 0.75 m and 1.5 m height. Basler & Hofmann (2017) specified the fire performance of wood cribs shown below which was used to determine the heat release rate which will be modelled.

One wood crib has a peak HRR of 4 MW during free burning test. For a single wood crib, a fire load of 400 MJ/m² and mass of 200 kg has been taken by Basler & Hofmann (2017). The time for the peak HRR to be reached from the beginning of the simulation and decay from peak HRR to burnout was determined using Equation 13. A t² fire with a fast growth and decay rate was assumed.

$$q = \alpha t^2 \tag{13}$$

Where,

q is the heat release rate (kW)

α is the growth and decay rate (0.047 kW/s² for fast growth fire)

t is the time in seconds

The total time for the growth and decay phase considering the 10 cribs was calculated as 583 seconds. However, this time is not enough to burn all the fuel material. Therefore, a constant burning period with peak HRR was assumed in between the growth and decay phase to create HRR curve as shown in Figure 16. The time duration of the steady burning period was determined by dividing the remaining fuel load from the peak HRR. The fuel area was taken as 7 m², considering burning of 5 surfaces in a wood crib.

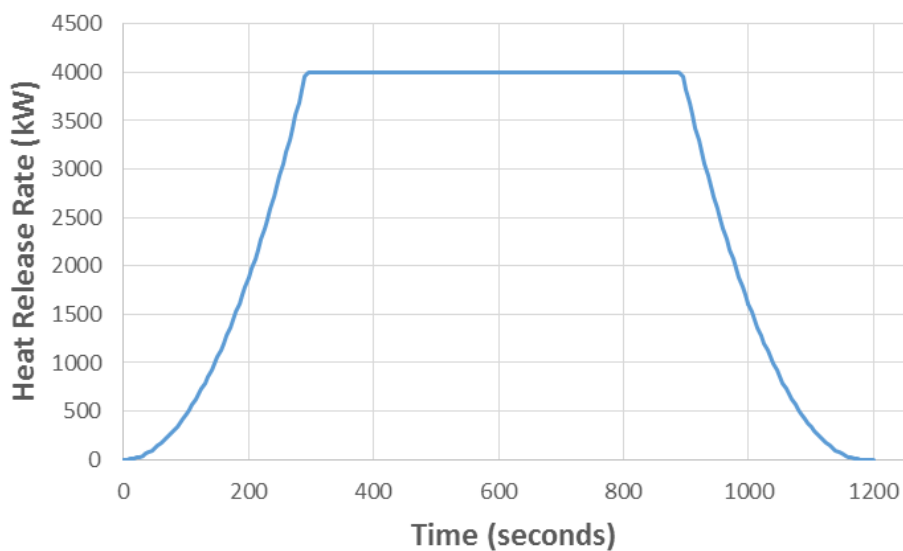


Figure 16: Heat release rate with time for one wood crib

The real fire scenario was considered as burning of three wood cribs at the same time. Since the fire was assumed as fuel dependent and there is enough oxygen for combustion in the Industrial Hall, a combination of three HRR curves as shown in Figure 16 with peak HRR of 1200 kW was considered for the fire scenario. Then, considering the study by Degler et al. (2015), the HRR of wood cribs in FDS was modelled by adding vents to obstruction in FDS.

Simple chemistry combustion model with single mixing controlled step was used to model the combustion reaction for wood in FDS. In this approach, the mixing of the fuel and oxygen is considered to be infinitely fast (McGrattan et al., 2016). The reaction parameters were specified in *REAC* line in FDS code, based on the values in SFPE Handbook (2016) as shown below. Here, the letters of C, H, O and N symbolise Carbon, Hydrogen, Oxygen and Nitrogen respectively. Furthermore, radiative fraction of 0.35 was used to represent radiation loss from fire.

```
&REAC ID='WOOD'          C=1.0          H=1.7,  
O=0.72          N=1.0E-3,          CO YIELD=4.0E-3,  
SOOT YIELD=0.015
```

4.3. Properties of Timber Columns

Temperature dependent thermal properties for the conductivity and the specific heat of the Glulam (GL24h) timber as mentioned in Eurocode EN 1992-1-2 were defined using *RAMP* convection in FDS. It is reasonable to use values from Eurocode since the timber properties are found in a wide range of well-documented experiments and experiences. On the other hand, since the FDS does not allow to specify temperature varying density, a constant value of 380 kg/m³ for GL24h was used based on the recommendations in EN 1194:1999.

Furthermore, the heat of combustion value of 14240 kJ/kg was defined for timber, which will be used to calculate the mass loss rate according to the heat release rate after the columns ignite (SFPE Handbook, 2016). The penetration, absorption and emission of radiation in solid material were expressed using the emissivity value of 0.9 and the absorption coefficient value of 5x10⁴ (1/m) (López et al., 2013). In addition, the default convective heat transfer model in FDS was used for the analysis.

4.3.1. Combustion of wood and ignition temperature

The surface temperature of a combustible material at the point it starts to ignite is defined as the ignition temperature (Babrauskas, 2002). When the wood is exposed to heat, at high temperatures it begins to change its cellular structure and start the pyrolysis process. Pyrolysis is the thermal decomposition of a material (Lowden et al., 2013). At elevated temperatures, lumber degrades the constituent natural polymers producing volatile gasses, tar and char. When the pyrolysis volatile gases mix with ambient air it makes a combustible mixture which can lead to a flaming combustion (Bartlett et al., 2019). Further oxidation of char creates smouldering or glowing combustion.

Wood shows different stages in pyrolysis process due to its material properties as shown in Figure 17. After temperature reaches around 100°C moisture in timber starts to evaporate and below 200°C, very slow pyrolysis starts. Onset pyrolysis continues till around 300°C and production of volatile gases increases above 300°C (Bartlett et al., 2019). Different wood types show ignition point at different temperatures. Previous studies show that pilot ignition temperature of timber can be varied from 220°C-500°C (Fangrat et al., 1996) (Babrauskas, 2002) (Li, 1992) (Atreya, 1983). Furthermore, Atreya (1983) and Li (1992) show that surface temperature at ignition changes with the exposed irradiance. Surface temperature at the ignition tends to rapidly increase with the decreasing irradiance heat fluxes below 24 kW/m². This is due to the char layer occurring at the low irradiance flux during a longer exposure. Char layer gives protection for the unburnt wood and additional energy is needed to generate enough volatile gasses for flaming combustion. On the other hand, above the 24 kW/m², the ignition temperature decreases at a slower rate with respect to increasing heat flux (Li, 1992).

In addition, for high heat fluxes more than 35 kW/m² ignition temperature can be assumed to be between 300°C-350°C for all kinds of wood (Babrauskas, 2002) (Li, 1992) (Atreya, 1983). Timber columns in the FDS model are expected to expose more than 24 kW/m² heat flux and therefore ignition temperature was taken as 300°C considering simple pyrolysis model. Later, in the results and discussion section, exposed heat flux values are discussed and justified with the initial assumptions. This temperature accounts for the completion of wood pyrolysis mechanism and flaming combustion with the assumption of wood material as non-combustible until reach the ignition point.

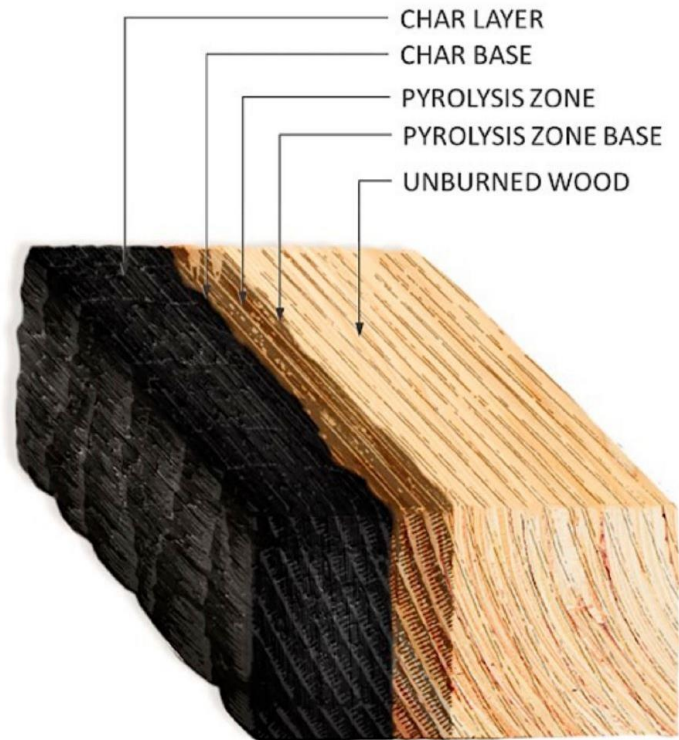


Figure 17: Different stages of pyrolysis process in burning timber section (Di Ha Le et al., 2019)

4.3.2. Heat release rate of timber columns

Additional fire load added by the wooden elements can play a major role for the total heat release in a fire. The burning rate is very important in modelling fire growth and fire spread in a wooden structure. The heat release rate or the mass loss rate of wood can be used in FDS to represent the pyrolysis model of wood. When one of the parameters is defined, the other parameter is calculated using the heat of combustion of the material. The FDS model in this research uses the heat release rate to describe the burning behaviour of Glulam timber using values from the previous studies. Tran et al. (1992) highlight that the burning rate is directly related to the exposed heat flux. Figure 18 shows variation of HRR with heat flux for different wood types. Hard wood like Red Oak and softwood like Southern Pine tend to show similar patterns along with most of the wood types. The heat release rate increases linearly with heat flux. Furthermore, the study shows that the heat release rate is almost constant for long time exposures independent of the incident heat flux as shown in Figure 19 (Tran et al., 1992). Considering a conservative approach, 100 kW/m^2 was selected as a representative HRR for Glulam timber in FDS, since the heat fluxes higher than 40 kW/m^2 are expected. This value was compared with another study to check the reliability as described next.

Equation 14 can be used to calculate the HRR in fuel controlled fire based on charring rate of timber (Schmid et al., 2019). Charring rate strongly depends on the original wood density and exposure temperature condition. Bartlett et al. (2019) suggests general values for charring rate as 0.8 mm/min soft wood and 0.4 to 0.5 mm/min hard wood. At the same time, other researches show that 0.65-0.7 mm/min charring rate as a good average value for Gulam made out of softwood (EN1995-1-2) (Tran et al., 1992) (Fonseca et al., 2009) (Bartlett et al., 2019). Considering charring rate of 0.7 mm/min, Equation 14 gives 91 kW/m² for HRR and it is close to the selected value of 100 kW/m².

$$HRR_{timber} = s\beta \tag{14}$$

Where,

s is the specific heat release rate ($0.13 \frac{MW}{m^2} / \frac{mm}{min}$)

β is the charring rate

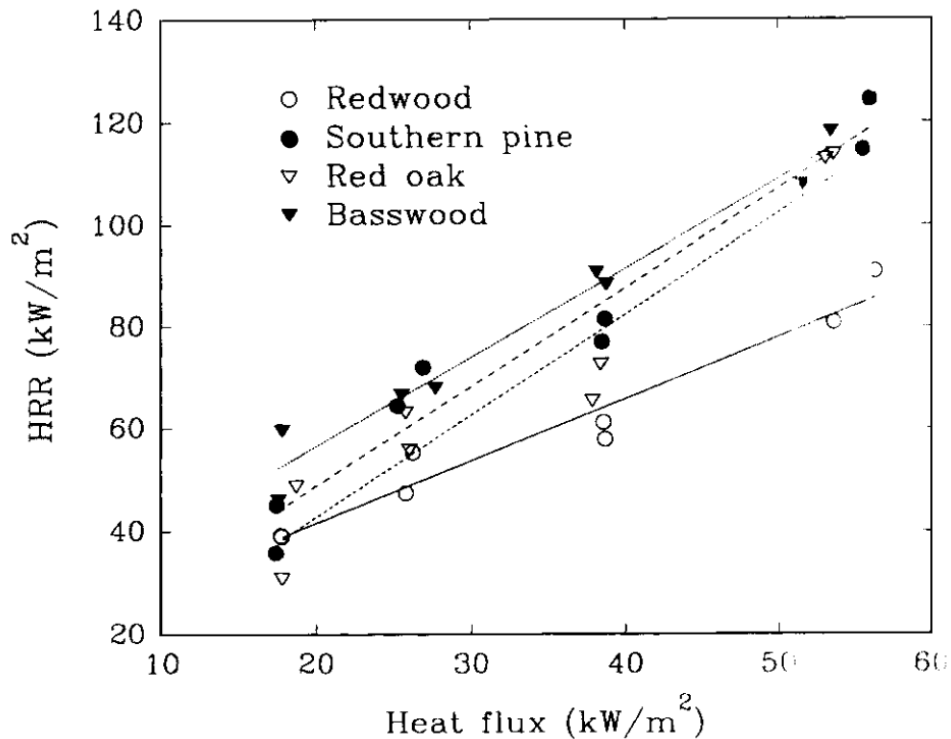


Figure 18: Variation of heat release rate with heat flux for different wood material (Tran et al., 1992)

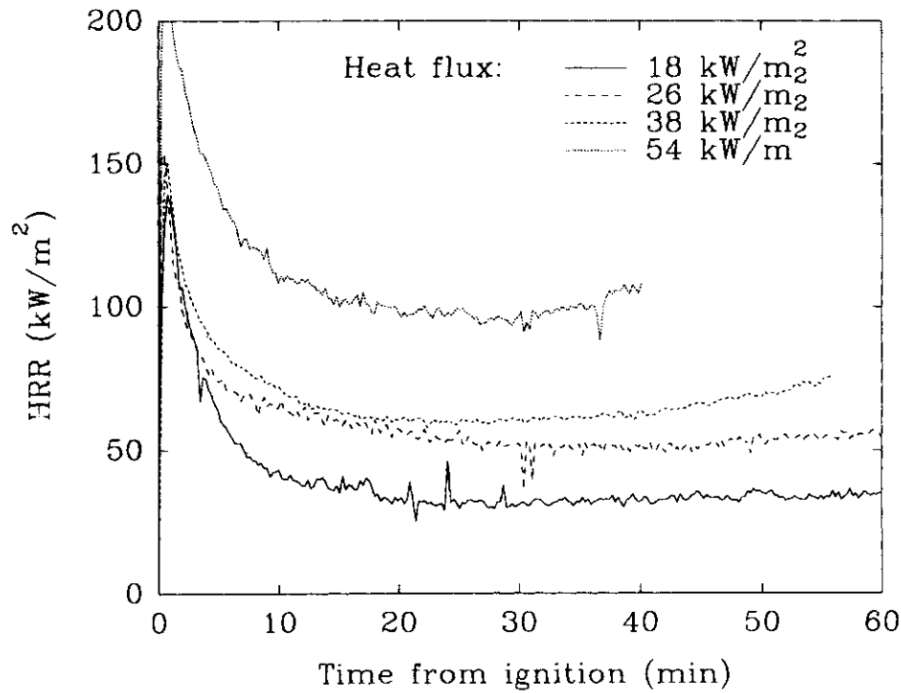


Figure 19: Heat release rate verses time for different heat fluxes in Red Oak (Tran et al.,1992)

Domain Size

Among the many factors affecting the accuracy of the CFD models which are used to numerically simulate the physical and chemical development of fires, the computational domain size has a huge impact on the predicting parameters governing the fluid flow at the boundary (Zadeh et al., 2015). Studies show that there is a huge variation in results between with a domain extension and without a domain extension (He et al., 2008) (X. Zhang et al., 2010). Adequate domain extension beyond the openings yield consistent results within the enclosure. Therefore, similar to studying the importance of grid size dependency, it is important to understand the required domain size for verification and validation of the model.

The required computational domain can be varied with the heat release rate of the fire and the size of the vertical vent openings (He et al., 2008). The Domain has to extend beyond the walls and openings according to the relationship with the two above mentioned factors. Previous research has identified the minimum extension of the computational domain for a fuel controlled fire to be half of the hydraulic diameter of the largest opening and one hydraulic diameter for an under-ventilated fire to have a good computational accuracy in FDS results (He et al., 2008) (X. Zhang et al., 2010).

The hydraulic diameter for the FDS model was calculated as 12 m using Equation 15 for the largest vent opening with the dimensions of 23m x 8m (He et al., 2008). The industrial storage has a large volume and a good ventilation system. Therefore, it is a fair assumption to consider a well-ventilated (fuel controlled) fire. Considering that, half of hydraulic diameter in biggest opening which is 6 m was extended beyond the all vent openings in the FDS model. Furthermore, the domain was extended to at least one cell thick beyond the exterior blind walls, where there is no opening or any connection to the fire and plume.

$$D_H = \frac{4A}{P} \quad (15)$$

Where,

D_H is the hydraulic diameter of vent opening (m)

A is the area of the vent (m)

P is the perimeter of the vent (m)

4.4. Mesh Sensitivity

Buoyant driven plumes have a wide range of different length scales. For example, the domain size of a fire can be 10 m and the diameter of the fire can be 1 m. Meanwhile, the flame can have large scale eddies in the range of 10 cm with small scale eddies in flame with dimensions as small as 1cm. Therefore, the resolution of the mesh depends on which scale is predominant for the analysis (Yuen et al., 2016) (W. Zhang et al., 2002).

A sensitivity analysis was conducted to investigate the grid dependence and the number of radiation angles on the FDS results. The mesh sensitivity analysis was conducted with three mesh resolutions sizes ranging from coarser to finer at 500 mm, 250 mm, and 125 mm respectively. For grid spacing 500 mm and 250 mm, the entire mesh had a similar resolution in all directions. However, for the finer mesh with spacing of 125 mm it was not practical to model the entire domain with a uniform resolution since it will take more than 3 million cells in model. Therefore, only the areas of interest with critical phenomena like combustion or plume dynamics, were prescribed fine mesh with 125 mm cells in the near-field region. For the other regions a 250 mm grid spacing was applied.

The computational domain was divided into multiple connected meshes. The main reason for that is to reduce computational wall clock time by running FDS simulation using MPI (Message Passing Interface) with a High-performance computer, which has the capability for parallel

processing. When dividing the mesh, guideline given by FDS user's guide was followed (McGrattan et al., 2016). Mesh division was carried out in a way, where a single mesh was used to cover the fire and buoyant plume. Boundaries between the meshes were avoided at the places where the critical fire behaviours occur to align meshes correctly to yield accurate results.

The selected grid sizes were cross checked to compare the extent to which the flow field with buoyant plume is resolved in simulation using the non-dimensional parameter $D^*/\delta x$ given in FDS manual (McGrattan et al., 2016). The characteristic diameter of the fire, D^* was evaluated using the Equation 16 given in McGrattan et al. (2016). The nominal grid spacing is stated by δx .

$$D^* = \left(\frac{\dot{Q}}{\rho_{\infty} c_p T_{\infty} \sqrt{g}} \right)^{2/5} \quad (16)$$

Here,

D^* is the characteristic fire diameter

\dot{Q} is the total heat release rate in kW

ρ_{∞} is the density of ambient air (1.2 kg/m³)

c_p is the specific heat capacity of air (1.0 kJ/m³)

T_{∞} is the ambient air temperature (293 K)

g is the gravity (9.81 m/s²)

Table 3 shows the calculated $D^*/\delta x$ and number of elements within each mesh for the FDS model. This non-dimensional parameter is an indicator of how many cells are spanning over the characteristic diameter of the fire. The higher the $D^*/\delta x$ ratio, more cells are available to resolve the fire dynamics directly resulting in a higher accuracy in the results. In addition, past studies suggest that $D^*/\delta x$ ratio values between 5 and 10 generates an acceptable solution at a reasonable computational cost (McGrattan et al., 2015) (Salley et al., 2007). Therefore, from all the mesh sizes in this study it is possible to expect accurate results. However, computational cost for finest mesh can be very high. Furthermore, FDS uses Fast Fourier Transformation (FFT) for the pressure solver in “y” and “z” and computational cost was reduced by defining

number of cells in “y” and “z” direction as factors of low prime numbers like 2, 3 and 5 making the solver efficient.

Table 3: Comparison $D^*/\delta x$ for different grid cell sizes

Q (kW)	D^*	dx (m)	D^*/dx	Number of Elements
12000	2.59	0.5	5.2	73,500
		0.25	10.4	588,000
		0.125	20.8	1,673,280

The grid independence is discussed using simulation results for three mesh sizes with 1000 radiation angles. Figure 20 shows the total heat release results from the FDS simulations with different mesh sizes. It is observed that all the grids follow an almost similar shape for HRR curve with the 500 mm mesh showing the lowest correlation. Maximum HRR and the HRR after the burnout of wood cribs have similar values for the simulations with grid cells of 125 mm and 250 mm.

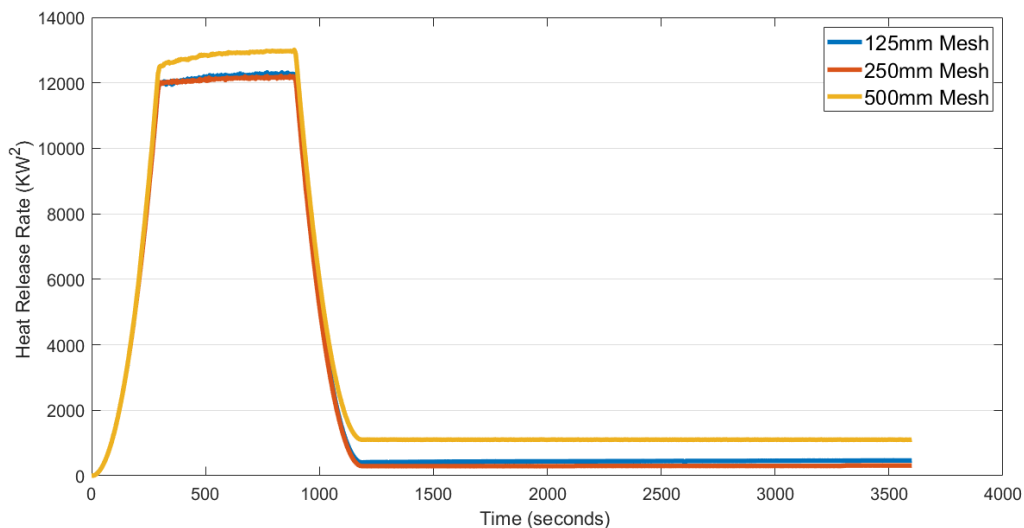


Figure 20: Total heat release rate with time for various grid sizes with 1000 radiation angles

The temperature profiles from the fire plume and smoke above the wood crib 1 was compared at different heights for the three grid resolutions. As shown in Figure 21, the 500 mm mesh has the lowest correlation with other two meshes. It shows lower values than other meshes except for 10.75 m. On the other hand, temperature curves for 250 mm and 125 mm cell sizes generates

similar values till half of the height. At upper heights where the graphs show the temperature of smoke, grid size 250 mm vary from 125 mm cell and closer to values of 500 mm cell size.

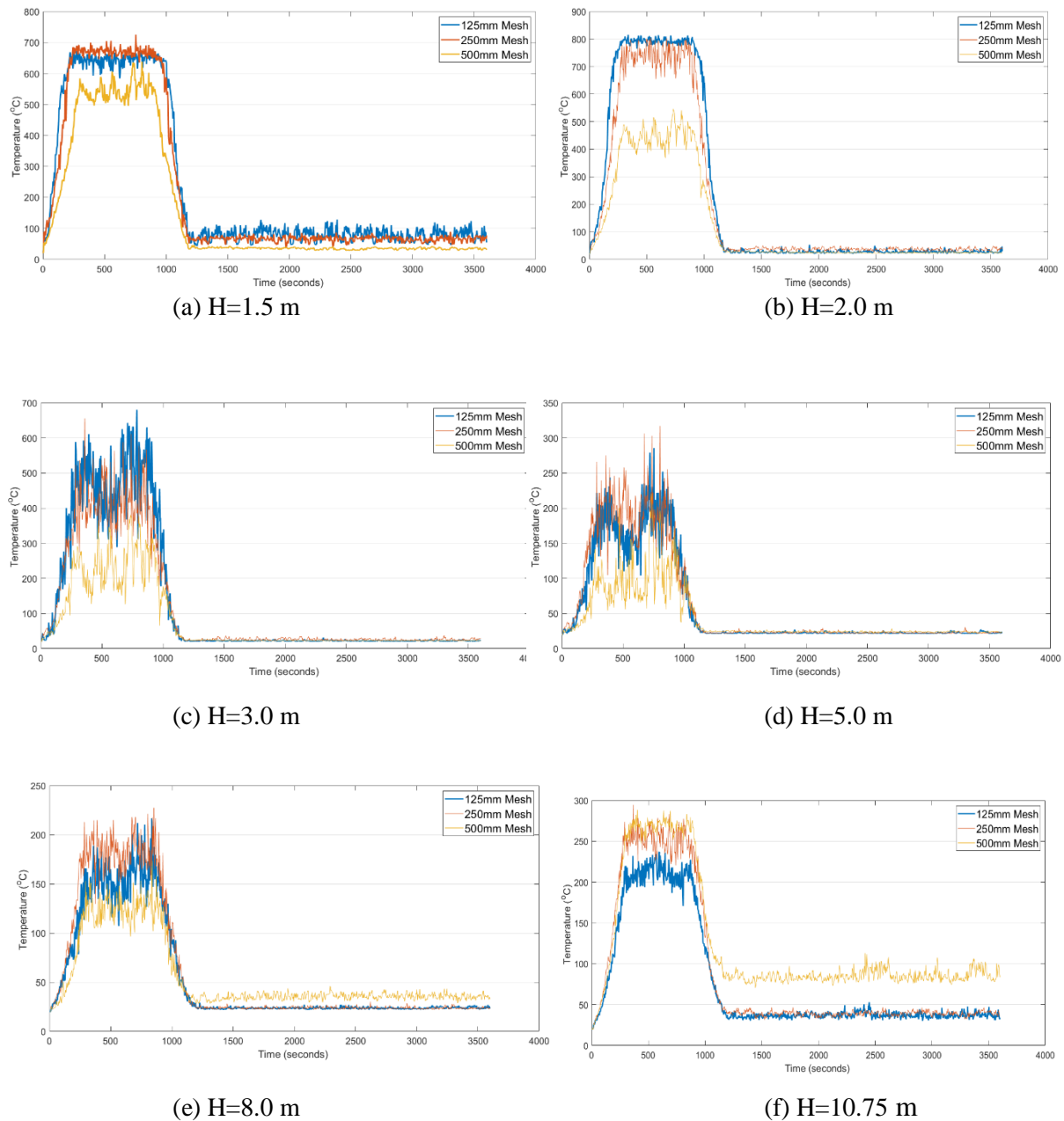


Figure 21: (a) - (f): Fire plume and smoke temperature distribution with height above the wood crib 1 for different mesh sizes with 1000 radiation angles

In summary, 500 mm cell size have significant deviations and 250 mm grid size and 125 mm grid cells resolve the fire adequately. It is shown that for the two finer meshes there is a minimal difference in smoke temperatures at high elevations. Therefore, considering the computational cost and adequacy, the grid resolution of 250 mm was selected for simulations. The mesh

boundaries at sides were opened to represent the ventilation conditions similar to the large Industrial Hall.

It should be noted however, that FDS results also depend on the number of radiation angles and temperature values used for comparison can have an effect on that. Therefore, the sensitivity analysis for the number of radiant angles was done next for the chosen mesh size of 250 mm.

4.5. Sensitivity to Number of Radiant Angles

Fire Dynamic Simulator solves the radiation transport equation for a non-scattering grey gas to include the radiative heat transfer in FDS model (Ryder et al., 2004). The equation is solved using finite volume method. When using approximately hundred discrete angles, the solver uses around 20% of the total CPU time of a calculation (Anderson et al., 2019).

Sensitivity analysis for number of radiation angles was done with 100, 1000 and 5000 radiation angles with 250 mm mesh size. FDS result of adiabatic surface temperature and heat flux for column 1 face 1 at 2 m height, which is dependent on radiative heat transfer, were used for comparison. As shown in Figure 22 and Figure 23, results are very similar and have good correlation with each other to different number of radiation angles. On the other hand, when the number of angles is lower, results show some oscillations compared to values with higher radiation angles. Thus, 100 radiation angles were used for simulation considering both accuracy and computational time.

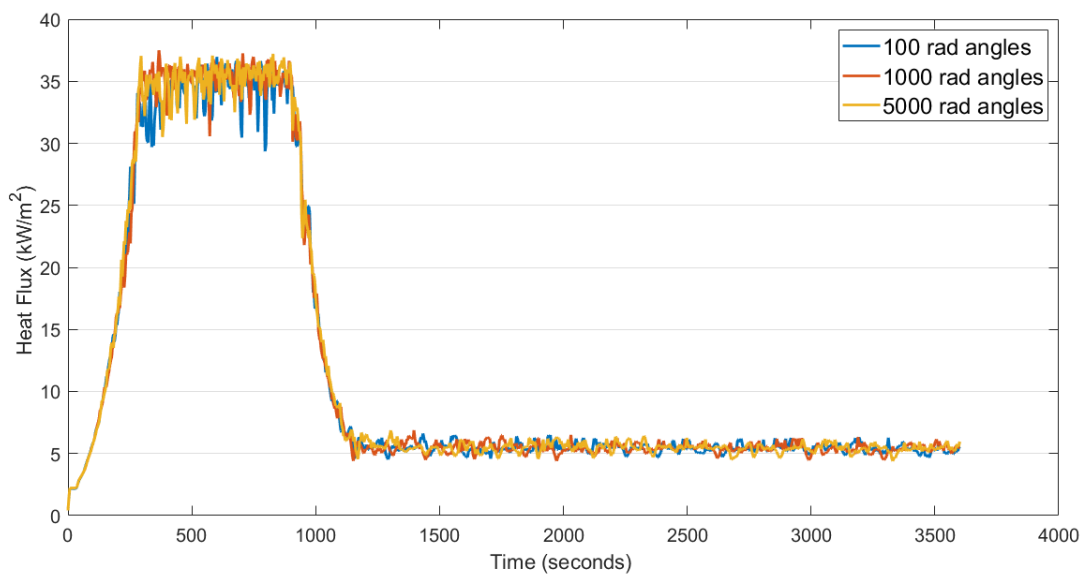


Figure 22: Incident heat flux vs. time for column 1 face 1 at H = 2 m

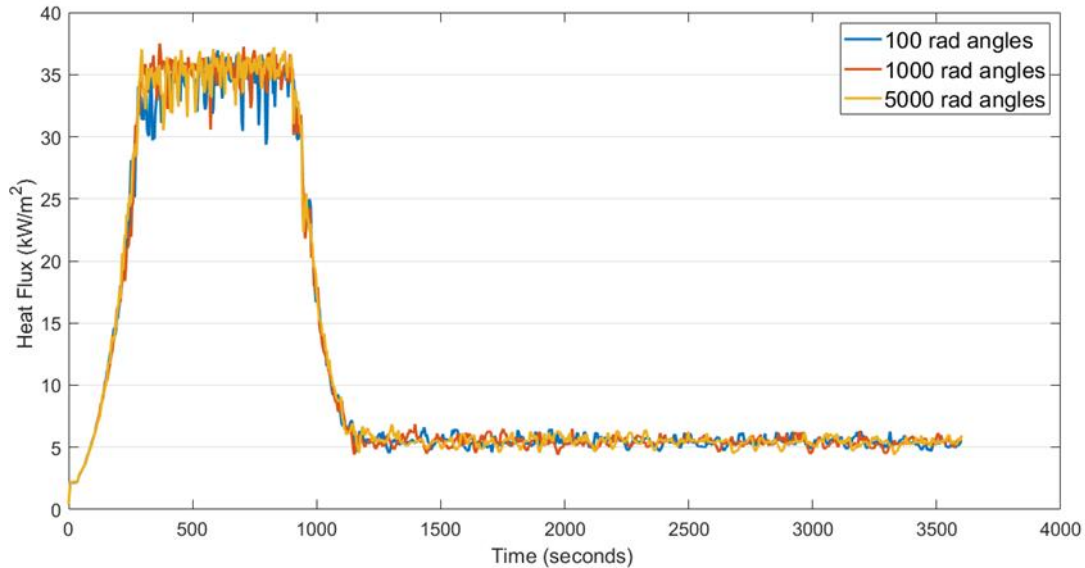


Figure 23: Incident heat flux vs. time for column 1 face 1 at H = 2 m

4.6. Results and Discussion

4.6.1. Ignition of Columns and Heat Release Rate

The maximum total heat release rate value, which was recorded as 12217 kW has been greater than the peak HRR of 12000 kW from the burning of fuel wood cribs, indicating that there has been additional heat generated from the combustion of timber columns, as shown in Figure 24. The total HRR follows a growth similar to heat release from fuel wood cribs and goes to the maximum HRR at the end of steady burning period of wood cribs. Furthermore, the total HRR shows a similar decay with HRR reducing for the wood cribs. However, after the wood cribs burn out at 1200s, total heat release rate continues at an almost steady burning rate of 310 kW.

FDS simulation visual results confirm the ignition and burning of the timber columns. The first ignition point is at face 1 in column 1, shown in Figure 25. The flaming ignition starts after 190 seconds when the surface temperature reaches 300°C as expected and it can be seen in the legend of Figure 25. After that, the fire spreads with time in column 1 to around 4.5 - 5 m height as shown in Figure 26. Furthermore, ignition of face 4 in column 1 and face 2 of column 2 was observed at 310 second and 490 second respectively as presented in Appendix B. The three faces which were ignited burned until the end of simulation at 3600 seconds. The steady burning period after the burnout of the wood cribs at 2500 second is shown in Figure 27 and it is visible that the fire in column 1 is more intensive when compared to column 2. This is well explained because the column 1 is closer to the fire and receives a higher radiative heat flux.

The view factors of ignited surfaces can be considered to be large considering their orientation to the fire. However, the fire spread after the burnout of wood cribs was observed to be very slow. Next, a detailed analysis and interpretation of the observed findings is discussed.

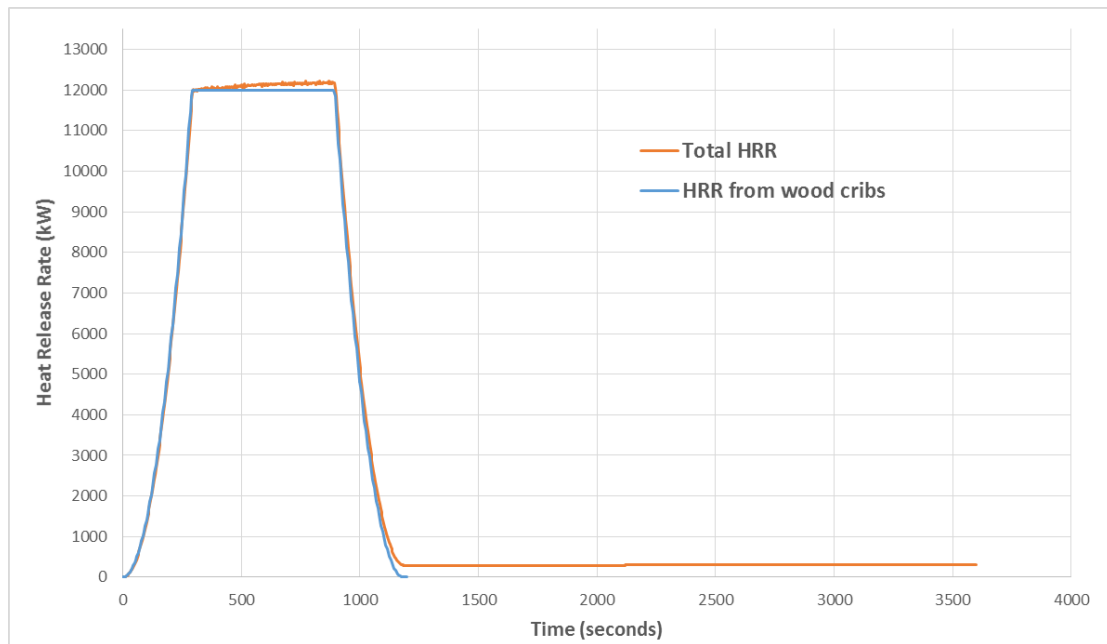


Figure 24: Heat release rate comparison for the simulation

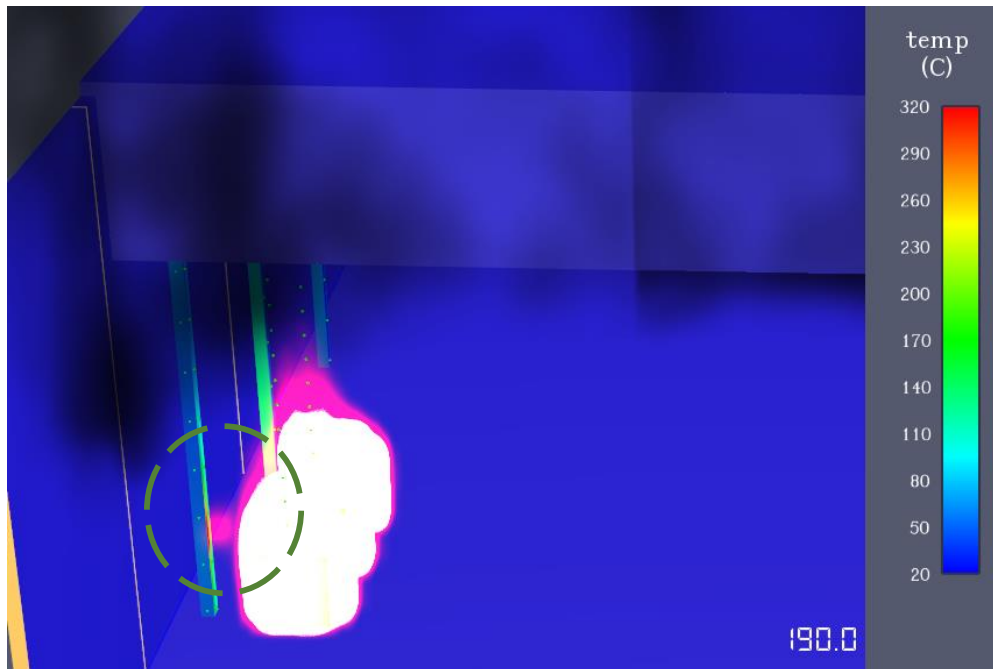


Figure 25: Ignition point of Column 1 (T = 190s)

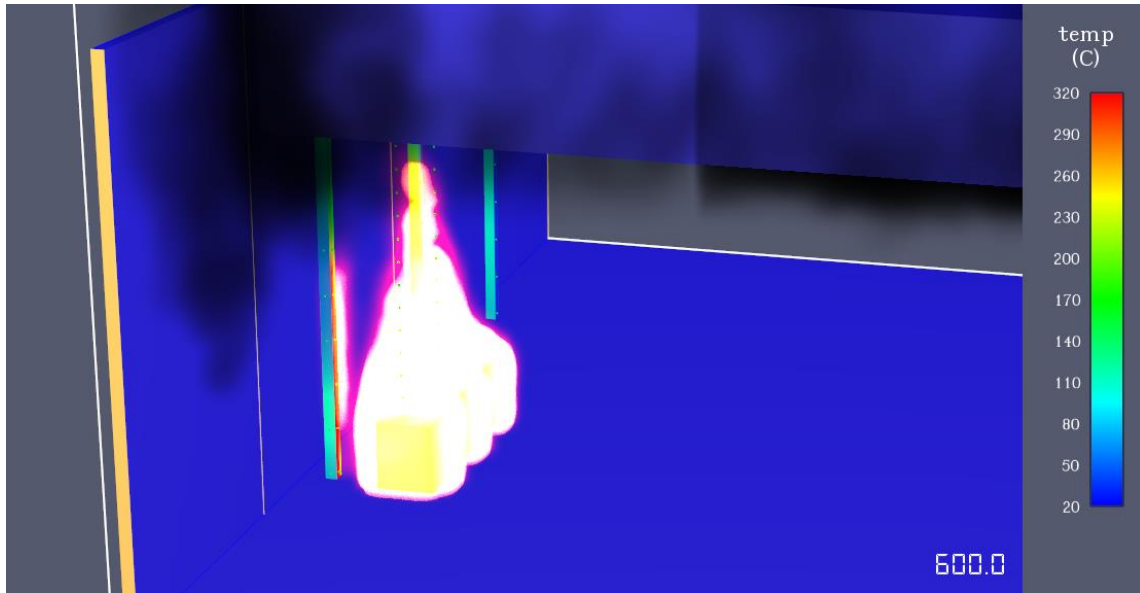


Figure 26: Fire development in columns (T = 600s)

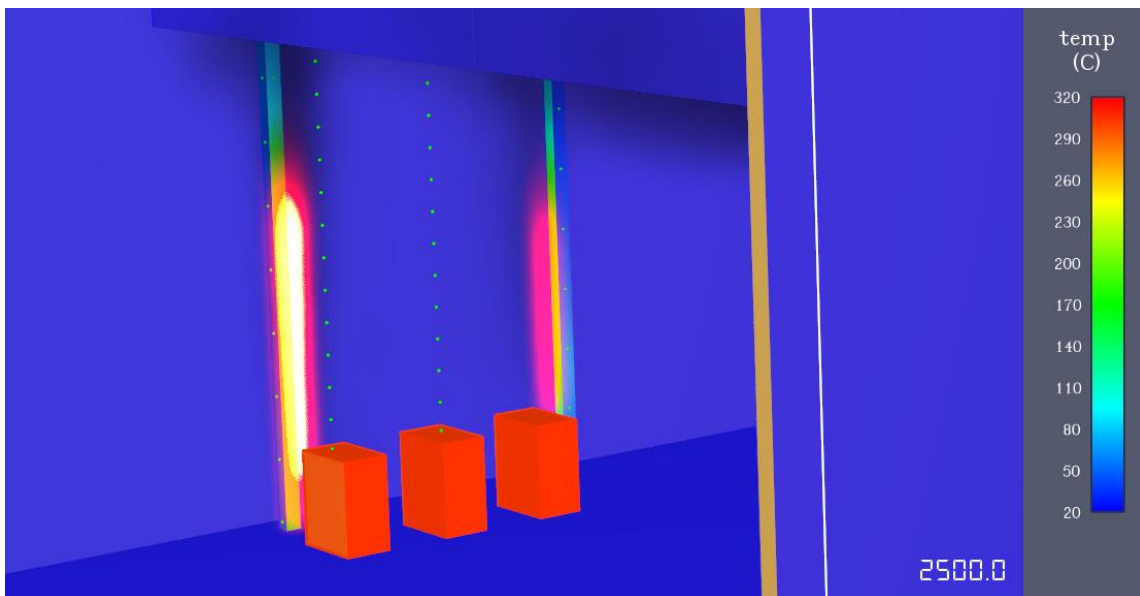


Figure 27: Steady burning of columns after burnout of wood cribs (T = 2500 s)

4.6.2. Exposed Heat flux and Surface Temperatures

The predicted parameters in column 1 surface 1, which is directly exposed to the fire was used to understand the fire behaviour of columns in the Industrial Hall. Figures 28 and 29 show the incident heat flux and temperature variation with time at different heights for column 1 face 1, respectively.

The incident heat flux on the columns has a similar shape to the total heat release rate. This is because the main heat flux induced on column surface is generate by the thermal radiation from

flame. Close to the initial ignition point of the column at a 2 m height, the heat flux was recorded as 21.2 kW/m^2 at 190 second at which point the surface temperature reaches 300°C . This value is greater than the critical heat flux of 13 kW/m^2 , which is the lowest heat flux required for the ignition of timber (Bartlett et al., 2019). Furthermore, column 1 was exposed to an incident heat flux greater than 13 kW/m^2 from floor level to around 4.5 m height igniting at different places on the surface. The good agreement with the literature values helps to validate FDS model results with the experimental parameters of timber at ignition.

It was observed that a maximum flame height of 5 m when the wood cribs were burning at the maximum HRR. Column surface height equal to the flame height, receives the maximum heat flux during the maximum HRR. Therefore, this region shows a higher heat flux throughout compared to the upper region of the column. Furthermore, with the decreasing HRR, the heat flux also decreases. After burning out of wood cribs, the burning area in column shows an increment in heat flux and then continue with a radiant feedback around 8 kW/m^2 due to the combustion flames in timber column.

In addition, the timber was exposed to maximum heat flux around 50 kW/m^2 and it agrees well with the assumed maximum heat flux range in previous section, when determining the values to use for the ignition temperature of timber and heat release rate of timber columns in combustion.

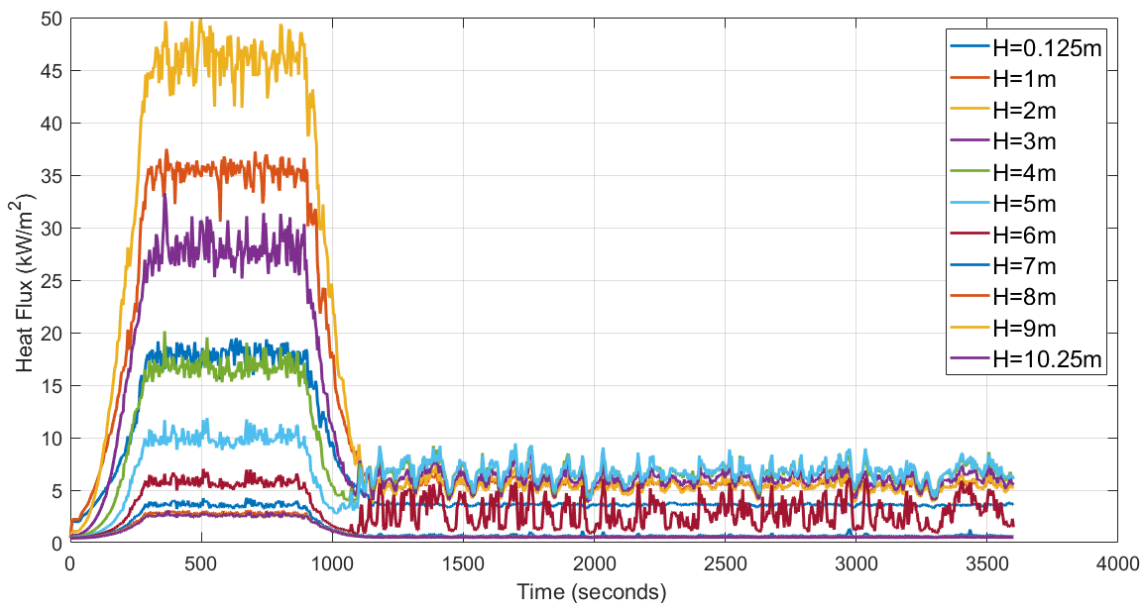


Figure 28: Incident heat flux change with height in Column1 face 1

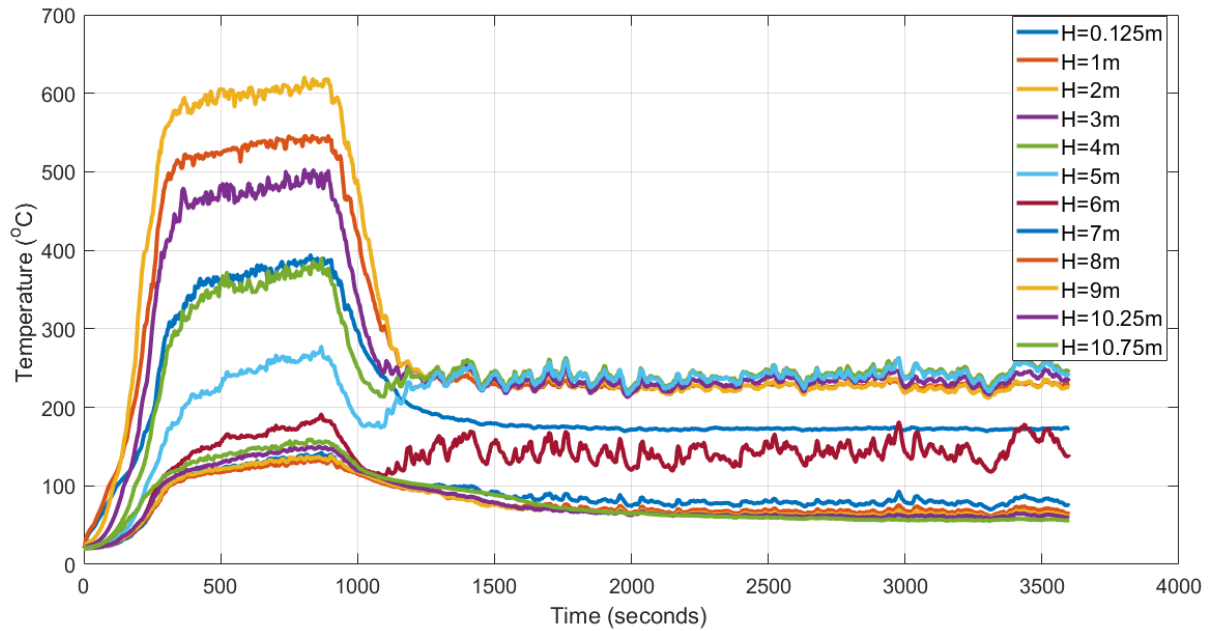


Figure 29: Surface temperature change with height in Column1 face 1

It can be seen that temperature curves are directly related to the irradiance heat flux at each height and follow a similar pattern as shown in Figure 29. From floor level to around 4.8 m height, the surface temperatures reach 300°C at different time intervals and it was visible in simulation when flaming combustion occurred. Maximum temperatures are visible when there is high radiative heat flux. The maximum recorded temperature in column surface is 610°C at 2 m height. When the heat flux from the fire starts to decrease, the surface temperatures also start to reduce following the same trend.

After the decay phase of the heat flux and the surface temperature it can be seen that those values at 5 m and 6 m come to a lower value and increase by small margin around 1200 second. The rise in temperature is due to the heat flux coming from burning column. However, the burning flame of column do not induce enough heat flux to reach surface temperature to 300°C to induce ignition at higher heights. Therefore, only the already ignited areas continue to burn at a steady rate and the fire spread is not clearly visible after the burnout of wood cribs.

Surface temperatures and incident heat flux values for heights from 7 m to ceiling level almost overlap along the height and shows very low values compared to the bottom part of the column. The reason for that is the top part of the column is heated by the heat transfer from the smoke layer unlike the lower level which is directly exposed to fire. Results show that the surface temperature of the column near the ceiling is a little higher above 10 m height compared to

temperature values between 8 m to 10 m. This is due to high smoke production from the burning of the wood cribs, which results in a visible smoke layer leading to a higher contact time for the smoke and timber surface near the ceiling. After the burnout of the wood cribs this changes since there is only smoke from the combustion of timber and it does not create clear steady smoke layer at ceiling.

Moreover, the maximum temperature recorded at any place in the smoke layer is around 300°C, which is during the maximum heat release rate as shown in Figure 30 and Figure 31. This clearly shows a big difference compared to the post flashover smoke temperatures in small compartments, which is around 1000°C as discussed in earlier chapter. The reason to have very low smoke temperatures in the Industrial Hall is because, there is high ventilation along with a large enclosure which has enough cold ambient air to regularly mix with plume to cool down the temperature. Furthermore, due to high ceiling height there is enough time for cold air to mix with plume to make smoke with lower temperatures at ceiling level.

From the results it is visible that exposure temperatures of timber in Industrial Hall is mainly governed by the radiative heat flux from the fire and effect of smoke layer is very low.

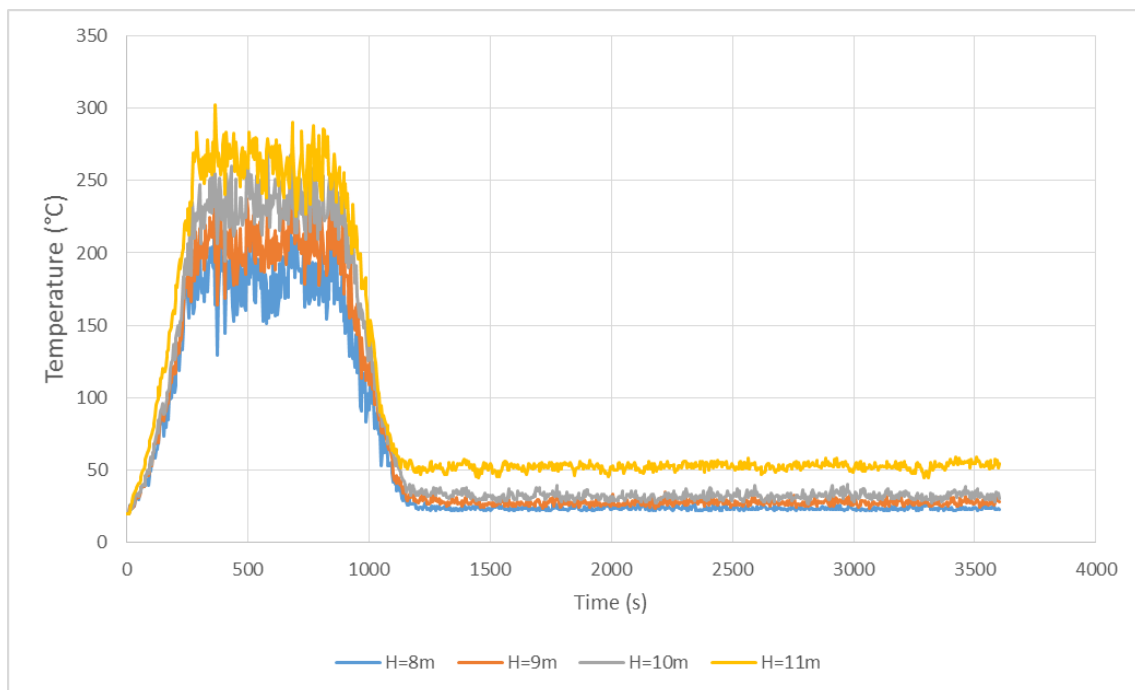


Figure 30: Smoke layer temperature change with height above the wood crib 1

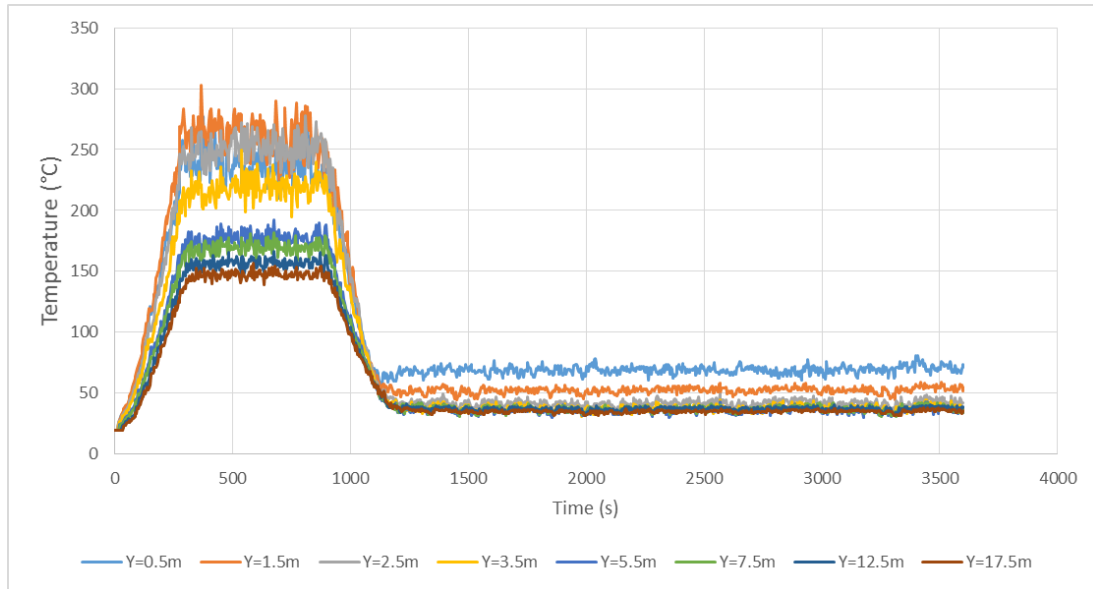


Figure 31: Smoke layer temperature change with horizontal distance from the column 1 surface 1 at 10.75 m height

It is important to understand the area of interest and limitations in a FDS model. A few suggestions are highlighted below to improve the pyrolysis model and charring of timber.

For ignition to occur in reality, gas phase pyrolysis has to mix with oxygen to create a flammable mixture and then this mixture has to reach the combustion reaction temperature. Rather than defining an ignition temperature, it is possible to use complex pyrolysis model in FDS. The complex pyrolysis model can define multiple solid phase reactions, including evaporation of moisture in timber, if it is required to simulate the combustion model in more detail.

Furthermore, it was recorded that surface temperatures in timber columns reaches more than 200°C, even though it doesn't reach the ignition temperature in many locations. In real scenario this temperature range can leads to slow charring of the timber even though there is no flaming ignition. This is really important since char layer protect the unburnt wood material. This effect was attempted to be considered in modelling, using the temperature dependent material properties to some extent. However, if it is required to model the char layer, it is possible to include the pyrolysis reaction in the FDS model. The complex pyrolysis model was not used in this study since it needs a deep understanding of the reactions that occur in solids during the ignition process. Since this study does not focus on the fundamental mechanisms of reactions, and there are a large set of data for timber material properties, the simple pyrolysis model was used.

4.6.3. Design Fire Curve

The design fire curves for the combustible timber columns were created using the adiabatic surface temperature (AST), since this temperature can be used to identify the maximum thermal heat energy that any surface location can receive during the fire. The adiabatic surface temperatures for surface 1 and surface 4 in column 1 has been plotted with respect to time and compared with ISO 834 as shown in Figures 32 and 33.

It was observed that exposure surface temperatures change as a function of height for all the surfaces and values depend on the heat transfer mode from the fire and smoke as discussed in previous sections under incident heat flux and surface temperature. The adiabatic surface temperatures follow a similar trend as surface temperature but values are slightly higher since the heat losses are neglected in the AST.

It was observed that the adiabatic surface temperatures in face 1 are generally lower than the ISO standard time temperature curve. However, AST at height 2 m has slightly higher values than the ISO curve at around 180 seconds. The maximum temperature difference in this time range was obtained as 60°C. Apart from that, all AST temperature values are below the ISO curve. After the wood cribs burn off, AST decrease furthermore while temperatures in standard curve increase. This makes a difference of around 700°C between both curves after 1200 seconds.

Furthermore, the adiabatic temperatures for the surface 4, which is not directly exposed to the fire, also has very low temperatures throughout the entire duration compared to the ISO standard fire curve. A comparison between both the curves shows a maximum difference of 600°C during the 60 minutes. On the other hand, surface 2 and 3 did not ignite having been exposed to a maximum adiabatic temperature around 180°C and significantly differ from the ISO fire curve, as shown in Appendix B.

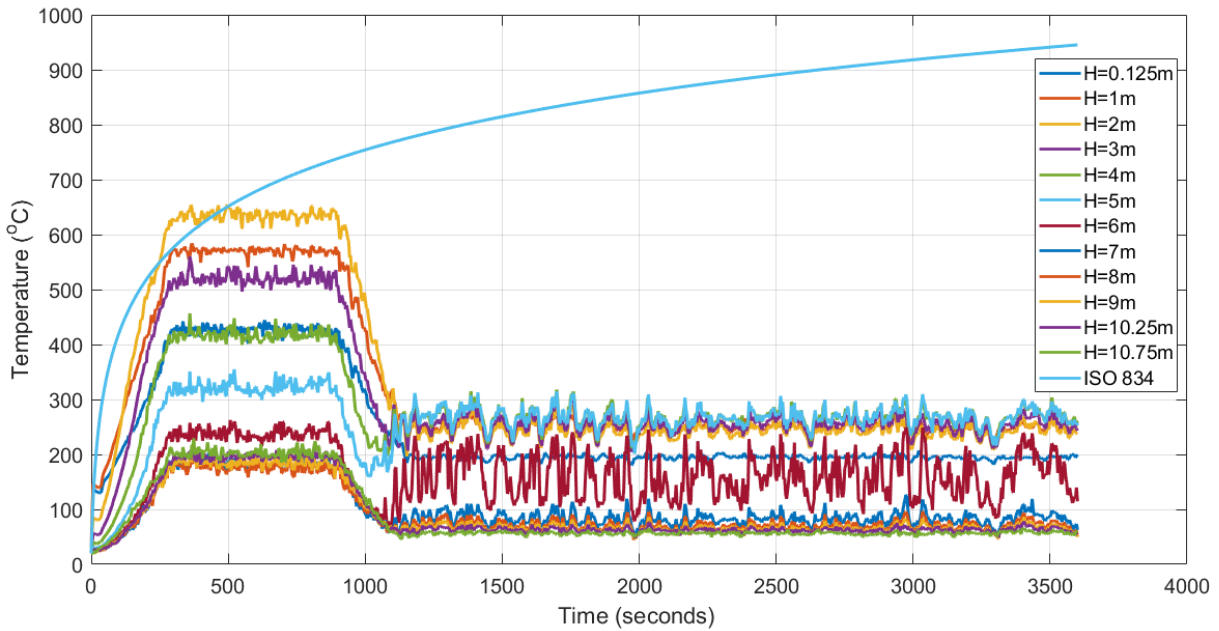


Figure 32: Adiabatic temperature change with time at different heights in column 1 face 1

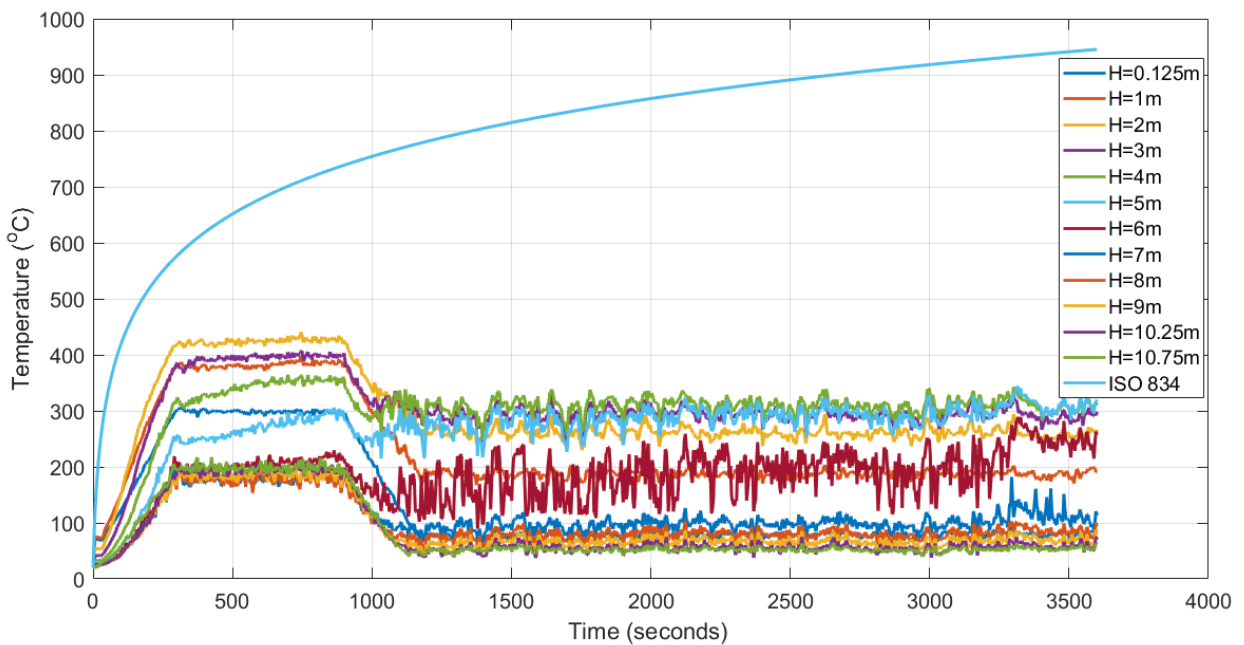


Figure 33: Adiabatic temperature change with time at different heights in column 1 face 4

In addition, another FDS simulation was modelled with non-combustible inert columns, without changing other parameters to compare the effect of additional fire load of timber columns. Figure 34 shows the adiabatic surface temperature comparison at 2 m and 3 m height for timber columns and inert columns. The temperature values show the similar trend for both types of columns during the burning of wood cribs. However, after the burnout of wood cribs,

timber columns continue to burn with higher temperatures around 250°C compared to the lower temperatures in inert columns induced by heated gas. The percentage difference of exposure temperatures after the 1200 seconds is around 330%. Furthermore, as shown in Figure 35, heat flux for timber column after 1200 second shows 123% percent difference compared to the heat flux received to inert columns.

To conclude, the results clearly show that the standard fire curves do not accurately represent exposure temperatures of columns and significantly overestimate the values compared to the temperature values from FDS simulation. It was discovered that, the burning timber columns have higher exposed temperatures when compared to columns with non-combustible surfaces. Therefore, the structural performance should be evaluated using the design fire curve and conservative results can be expected when using the standard fire curve. Underestimated results can be expected when using temperatures without considering combustibility of timber. Thus, the observed adiabatic surface temperature-time values for the four column 1 surfaces which are changing with height, were used for the thermal and mechanical analysis in the next chapters.

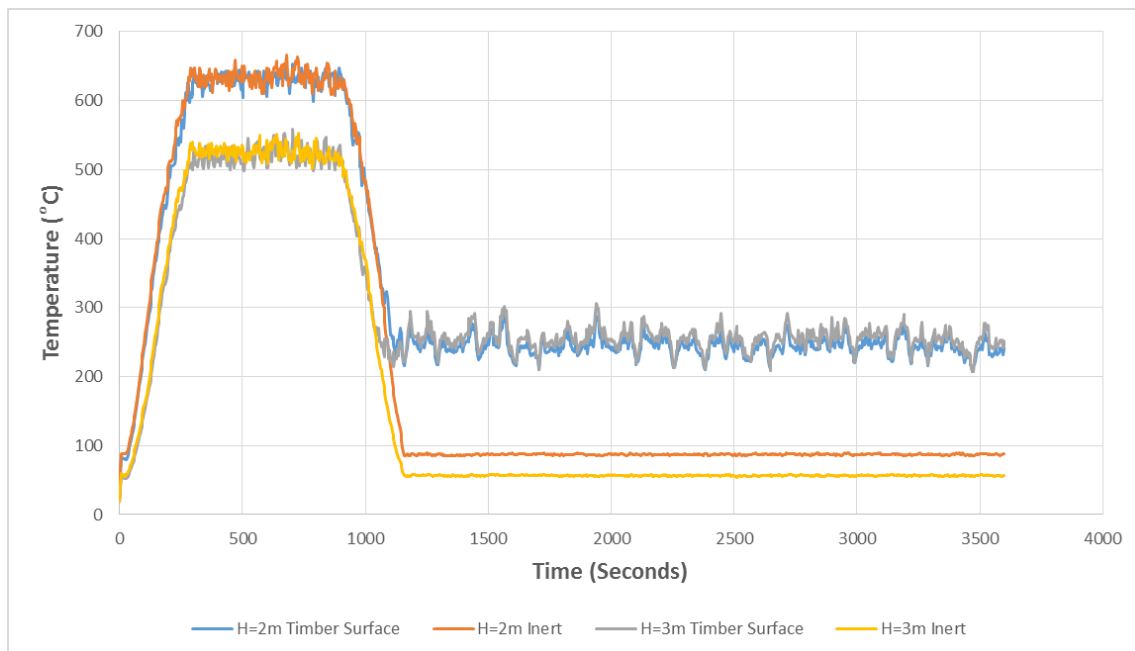


Figure 34: Adiabatic surface temperature comparison for inert and timber columns

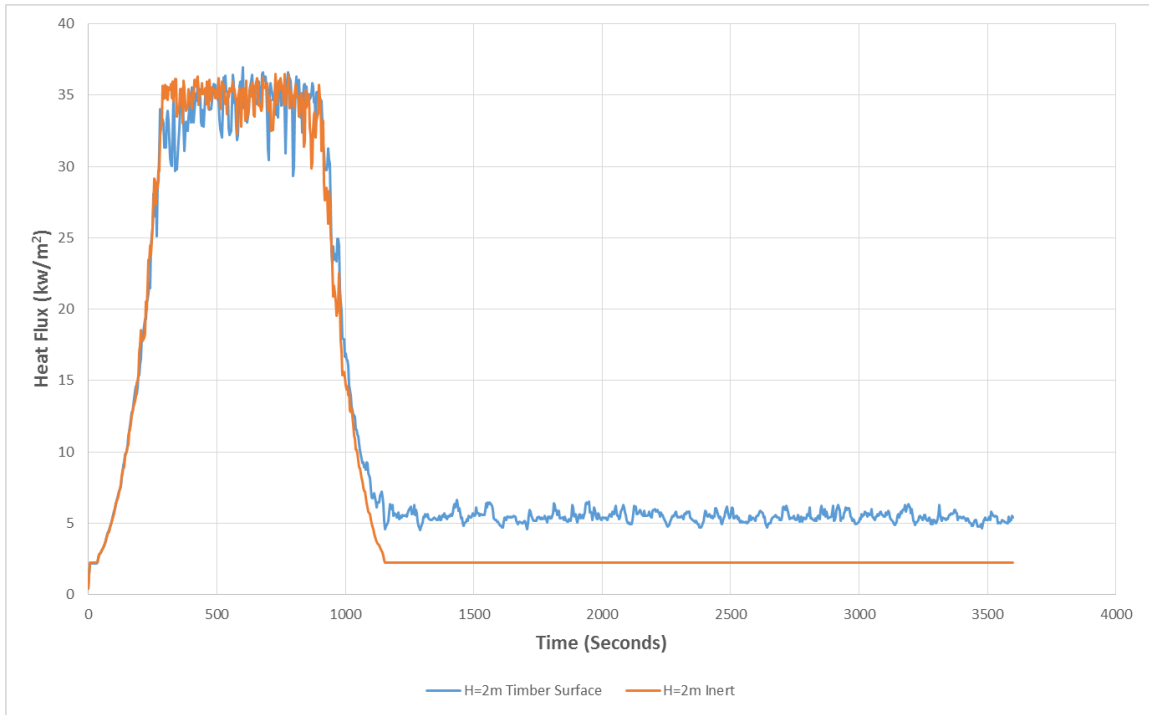


Figure 35: Heat Flux comparison for inert and timber columns

CHAPTER V

5. Thermal Analysis

The objective of the separate thermal model was to determine the temperature profiles inside the timber column section accurately when exposed to fire. Abaqus finite element software package was used to simulate two-dimensional heat transfer through the Glulam timber section.

5.1. Abaqus/Standard

Abaqus/Standard is a general purpose solver, which is ideal for linear and non-linear static, transient and steady state heat transfer and low speed dynamic problems. The solver uses the traditional implicit integration to solve the equations of finite element analysis. Abaqus/Standard has many control parameters for the accuracy of algorithms in integration and convergence scheme. These control parameters are automatically assigned with the default values to optimize the accuracy and efficiency of the simulation solution (Abaqus, 2014).

Since no high-speed dynamic events are expected in the thermal simulation associate with the fire, the commercially available finite element package Abaqus/Standard solver was used for both thermal analysis and mechanical analysis in the thesis study.

5.2. Abaqus Thermal Model

Uncoupled heat transfer analysis in Abaqus calculates the heat transfer in a solid without considering stress or deformation. Conduction is used as the dominant heat transfer mechanism within the structural element. On the other hand, Thermal boundary conditions for a structure can be defined with boundary convection and boundary radiation. Furthermore, it is possible to conduct transient heating or thermal steady state using the analysis.

As a baseline for the thermal numerical model, a timber material model for heat transfer was configured with the properties in Eurocode EN 1995-1-2 with ISO 834 exposure. Another model was created with similar model geometry and properties for the parametric, adiabatic temperature curves from the FDS analysis to see the temperature development inside the solid columns with time.

Transient heat transfer analysis step was used for the thermal simulations with pure conduction elements, which use the backward Euler method, also named as modified Crank-Nicholson operator for the time integration. This method has a very high stability for linear events

(Abaqus, 2014). Simulation time was set to 3600 seconds to compare results with the prescriptive design calculations.

A solid column geometry was modelled in Abaqus with a 300 mm x 220 mm section and 11 m height. Figure 36 shows the cross section of the finite element model (FEM) used to simulate thermal response of the timber column 1 in the Industrial Hall during a fire. In the 3D thermal model, the 2D heat transfer, which can be expected in a column during actual fire scenario was simulated. Considering that, the cross section of the column was meshed uniformly with a finer mesh with minimum element size of 4 mm. Previous studies show that cross section mesh size from 1 mm to 6 mm is acceptable for the thermal analysis in this kind of numerical modelling (O'Neill et al., 2014). A mesh sensitivity analysis was done with a mesh of 2.5 mm and results agreed well with the results from the 4 mm grid resolution. Since there is no heat flow occurring along the vertical direction (z-axis), a coarser mesh was used along this direction to reduce the computational cost with element size of 1 m (O'Neill et al., 2014).

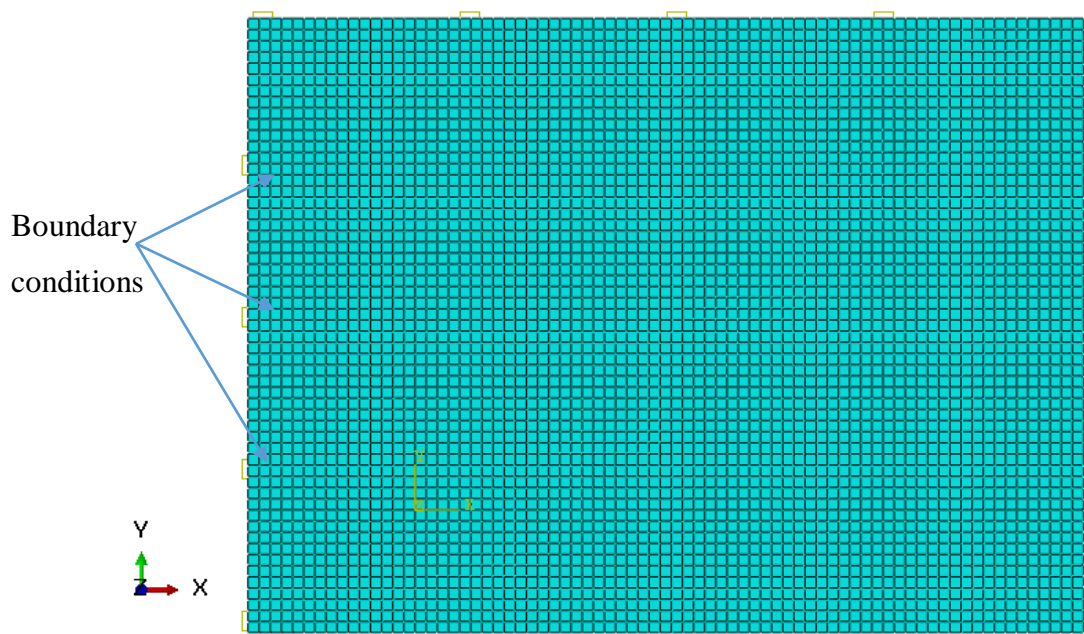


Figure 36: cross section of the thermal finite element model

The column was partitioned in 1m intervals to apply boundary conditions for 2D heat transfer. The entire columns geometry is required for the thermal model since later the geometry of the thermal analysis has to be imported and mapped with geometry of the mechanical model. The FEM for thermal analysis consisted of 129228 nodes and 116160 eight node linear heat transfer brick elements (DC3D8). Fully integrated first order elements were used since there is no structural response in thermal analysis and numerical instabilities are negligible.

Temperature-dependent material properties of the Glulam timber, which is based on many standard fire experiments, were used for density, conduction and specific heat capacity as mentioned in the previous section using Eurocode 1992-1-2.

Thermal boundary conditions for convection and radiation heat transfer were assigned using **surface film condition* and **surface radiation* keywords respectively. Heat transfer in both boundary conditions were calculated by the temperature curves given by **temperature amplitude*. The adiabatic surface temperature curves recorded from FDS analysis were used as the exposure temperatures in these boundary conditions.

The convective heat transfer coefficient used was 35 W/m²K. This value shows a reasonable agreement with previous studies for structural fire problems with longer exposure times (Atkinson et al., 1992) (Velloo et al., 2013).

Emissivity shows a significant variation with the temperatures and decreases with increasing temperature (López et al., 2013). In addition, different wood types show diverse emissivity values due to their appearance properties such as colour, texture and tone. However, for high temperatures it is possible to assume a uniform emissivity and value of 0.9 for soft wood, which was used for the radiation boundary condition in the Abaqus model (López et al., 2013) (Pitarma et al., 2019). Furthermore, the absolute zero temperature value of -273.15°C and the Stefan-Boltzmann constant of 5.67×10^{-8} were defined for the thermal model.

Initial temperature 20 °C was also defined with **predefined field* at the initial step of the simulation as a constant boundary condition throughout the mesh.

5.3. Results and Discussion

The thermal numerical model was validated by comparing standard fire exposure results with the prescriptive design calculations in Chapter 3. The Figure 37 shows the simulation results for the 300°C isotherm in timber cross section after 60 minutes of standard fire exposure. A similar temperature profile was observed along the height of the column at any given time.

The char layer was calculated as 42.5 mm and is similar to the Eurocode 5 char layer value of 42 mm for Glulam timber after 60 minutes standard fire exposure. It was observed that a uniform charring pattern occurs throughout the simulation in the column section with an average charring rate of 0.71 mm/min (Refer Appendix D) over the 60 minutes. The charring rate also shows a good agreement with the Eurocode charring rate value of 0.7 mm/min for

Glulam. Furthermore the corner roundings due to two-dimensional heat transfer, described in Eurocode, can also be observed. The excellent agreement with the Eurocode values indicates that the finite element model accurately represent charring of timber without any numerical instability for the standard fire exposure and the material properties in Eurocode 5.

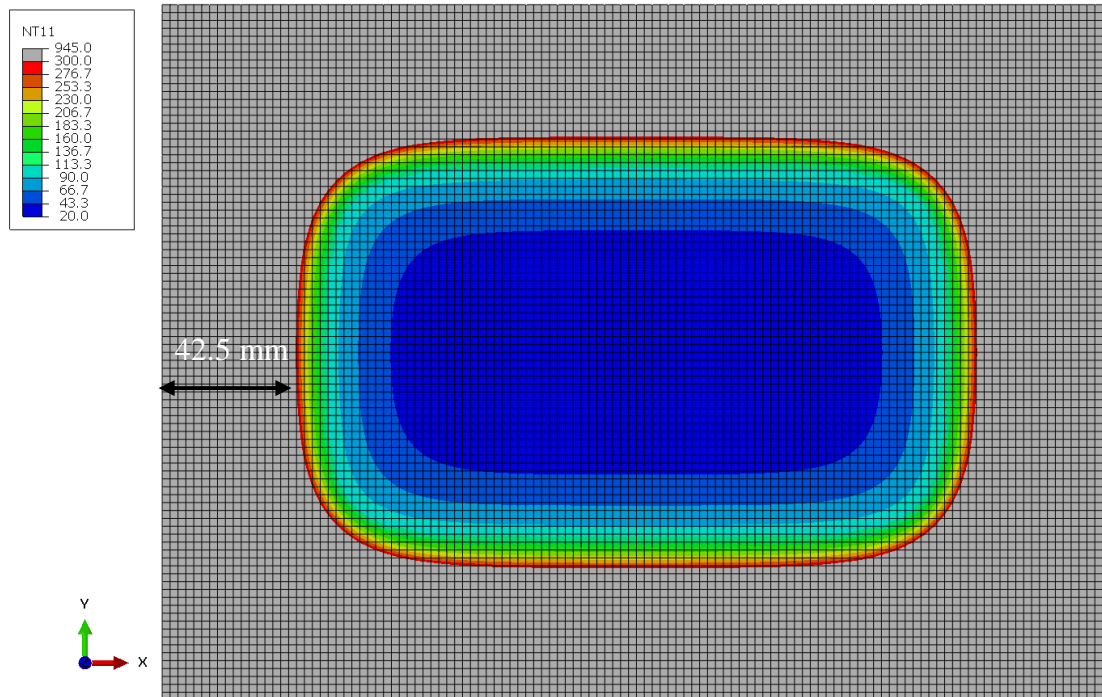


Figure 37: 300°C isotherm after 60 minutes standard fire exposure (From 2.5 mm mesh)

On the other hand, different temperature profiles were observed when exposed to the design fire curves. The cross-sectional temperatures varied along with the height of the column, unlike in ISO fire exposure. This is well explained by the adiabatic temperature curves generated in the previous section using FDS simulation which also changed with height. This shows that thermal distribution inside the solid follows a similar pattern. The maximum temperature values for every second was observed at the 2 m height of the column.

Figure 39 shows the temperature profile change with time in the timber cross section at 2 m height. It is clearly evident that solid wood shows high temperatures around the perimeter based on the heat flux received from the fire. Directly exposed surfaces to fire, transfer higher thermal energy across the cross section by the conduction compared to unexposed surfaces. Therefore, the temperatures inside the solid near to the directly exposed surfaces are increased rapidly. The contours in Figure 39 demonstrate this phenomena very well with the different temperature distributions from each surface.

Timber temperatures reached 300°C after 180 seconds at 2 metres height. This indicates that the ignition start time of the column observed in the FDS analysis, which was 190 seconds, is also reasonable. Furthermore, the maximum char layer observed from the simulation is around 9 mm as shown in figure 38. Only two surfaces, which were ignited in the FDS analysis showed charring in the thermal model. The charring behaviour exposed to the design fire is entirely different compared to the ISO exposure. The maximum charring depth has 79% difference between two methods and shows that ISO standard fire overestimates the charring layer for the columns in the Industrial Hall when designed with the prescriptive codes.

On the other hand, the maximum charring depth was recorded after 900 seconds in the simulation for design fire. Around this time, the decay phase of the exposed temperatures started. After that the temperatures near the outer surface started to decrease and char layer propagation gradually stopped since the temperature values became lower than 300°C. Even though the temperatures near the surfaces start to decrease, it was observed that the inner timber material still became heated from the incoming thermal energy from the conduction due to the temperature gradient. Since the different temperature profiles in solid leads to different structural performances, a coupled thermo-mechanical analysis was done to study the mechanical behaviour of the timber columns in the Industrial Hall when exposed to standard and design fire and it is discussed in the next chapter.

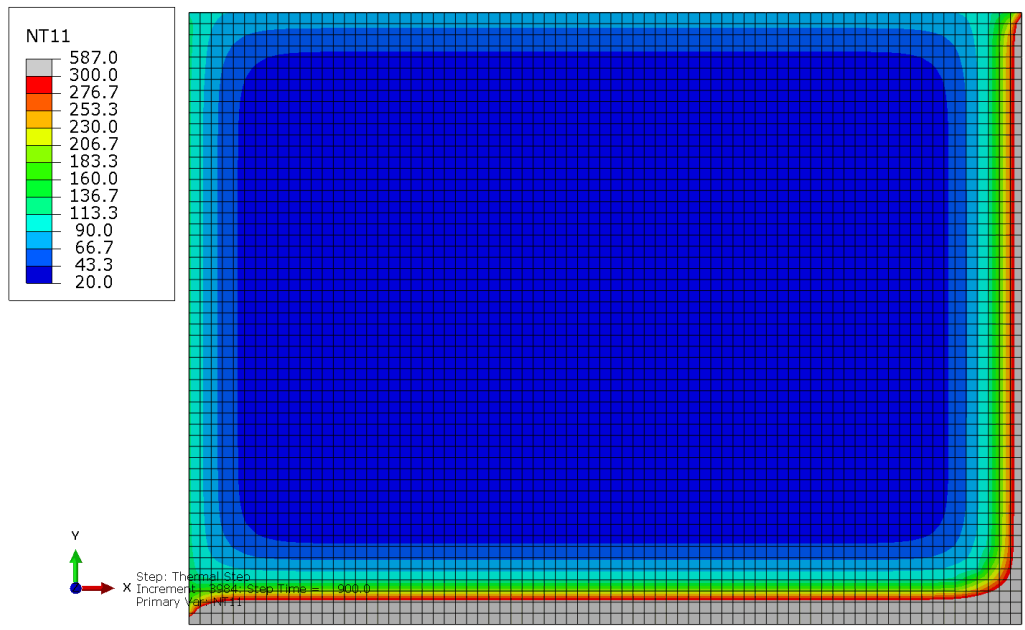
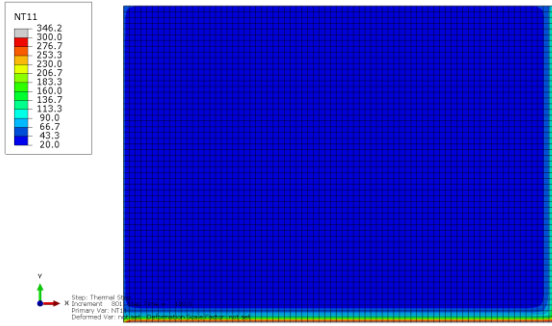
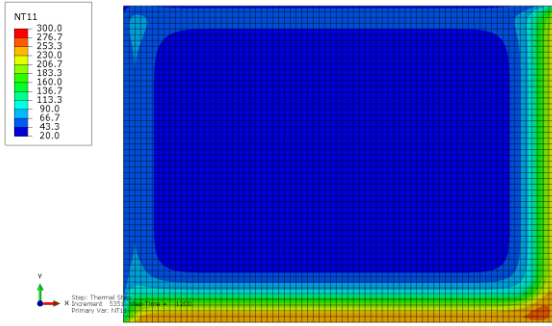


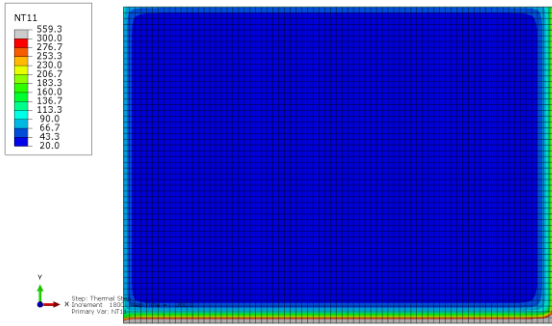
Figure 38: Maximum char layer observed at 2 m height after 900 seconds



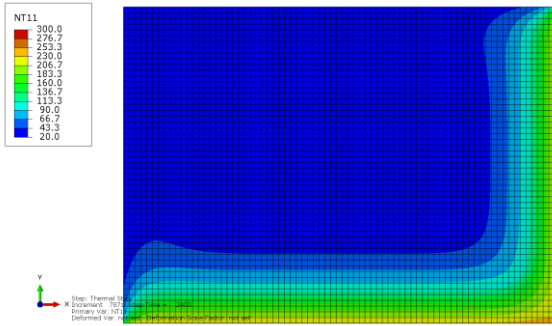
T = 180 s



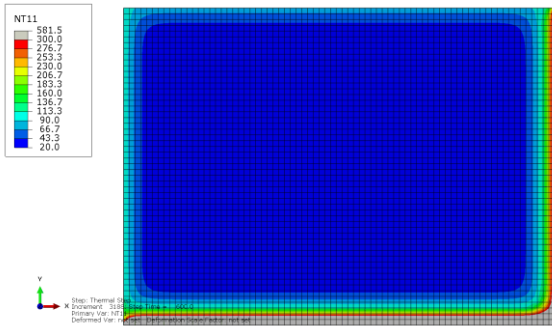
T = 1200 s



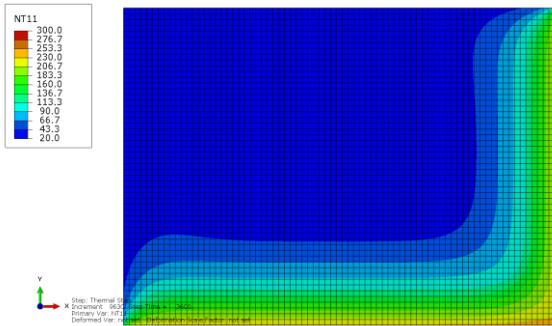
T = 300 s



T = 2400 s



T = 600 s



T = 3600 s

Figure 39: Temperature profile change with time in timber cross section at 2 m height during parametric fire exposure

CHAPTER VI

6. Thermo-Mechanical Analysis

6.1. Mechanical Model

The mechanical analysis was done to calculate the load-bearing capacity and buckling capacity of the timber column during fire exposure. The geometry of the mechanical numerical model was similar to the thermal finite element model. However, the mesh was defined differently in the mechanical model to account for the three-dimensional stress distribution. The finite element model consisted of 580800 C3D8R eight-node linear brick elements with reduced integration. The element size of 5 mm in the cross section and 50 mm along the vertical direction (z-axis) was used as described by O'Neill et al. (2014).

A reference node was added to the model to apply the fire limit state (FLS) load. Multi-Point Constraint (MPC) type Tie constraint was used to create interaction between the reference node and the top surface of the column. This constraint is able to uniformly distribute FLS load on the column top surface. As shown in the Figure 40, boundary conditions were applied to restrain vertical movement (along z-axis), out of plane bending (along x-axis) and displacement (along y-axis). Separate models were simulated to calculate structural response for 60 minutes ISO standard fire exposure and for 60 minutes design fire exposure.

The reduction of the timber mechanical properties, due to the exposure of elevated temperature, were accounted in the model by defining temperature dependent modulus of elasticity and compressive strength, as mentioned in Eurocode 5. In accordance with the Eurocode EN 1995-1-2, 2.4.1.4 and Annex B.9, thermal expansion of the timber material was not considered.

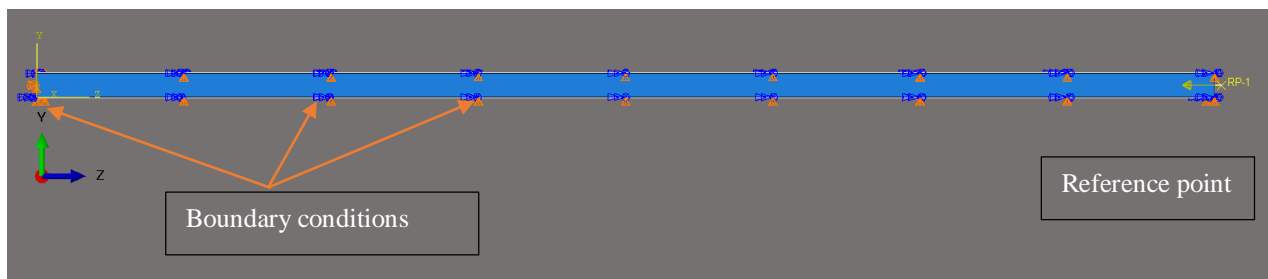


Figure 40: Mechanical finite element model

6.2. Load Bearing Capacity

Coupled thermo-mechanical stress analysis was used to simulate compressive stress change with time in the column due to the exposed temperature curves. Separate simulations were conducted for ISO standard fire exposure and design fire exposure to compare the maximum stress values in different fire conditions.

The output results file of the thermal analysis was imported to the model using **predefined field* with a mesh incompatible value of 0.0005. Specified loading conditions were applied at each increment of imported temperature profiles to generate the compressive stress variation for 60 minutes of fire exposure. The *Static-General* step was used to apply the FLS loading in the model.

The maximum stress value at each increment was compared with the maximum allowable compressive strength value corresponding to the element temperature, to see whether the element collapses or not.

6.3. Eigenvalue Buckling Analysis

The linear buckling analysis, also named as eigenvalue buckling analysis, in finite element analysis is used to identify the critical buckling load of a stiff structure with axial or membrane design loads (Ellobody, 2014). In Abaqus, the analysis follows the linear perturbation process. The Equation 17 shows the general eigenvalue buckling method, where the eigenvalues correspond to the failure buckling loads (Abaqus, 2014). The eigenvectors are the different theoretical buckling modes related to the eigenvalues. According to the linear buckling equation, buckling takes place after the resultant stiffness becomes zero due to the compressive load when the stress stiffness matrix equals the elastic stiffness.

$$(K_e + \lambda_i K_\Delta)v_i = 0 \quad (17)$$

Here, (I normally say ‘where’ rather than ‘here’ but ignore me (I’m just being picky))

K_e is the elastic stiffness matrix

K_Δ is the differential stress and load stiffness matrix due to incremental loading

λ_i is the eigenvalues

v_i is the eigenvectors representing different buckled mode shapes

The eigenvalue buckling analysis can predict a large number of modes. Even though the structural response right before the failure is nonlinear, general linear buckling analysis provides good estimation for collapse critical loads and mode shapes (Abaqus, 2014). In addition, the first mode with a positive buckling load factor is the most important for the static loading condition. Several first modes can be useful for the modal analysis due to seismic loading.

6.3.1. Buckling Model

The Abaqus model used for the buckling analysis has a similar geometry, mesh and material properties as used for the compression finite element model discussed in the previous section. The buckling step in the numerical model is created using **linear perturbation Buckle* requesting three eigenvalues by an incremental loading pattern. A unit load was applied because the load is scaled by load multipliers in eigenvalue analysis, and therefore the magnitude of the applied loading is not important. Furthermore, The Subspace eigensolver is used considering the speed for analyses with few eigenmodes.

Separate buckling analyses were conducted for FLS loading during the 60 minutes of standard and parametric design fire exposure. The output result file of the thermal analysis was imported as explained in the previous section.

Results and Discussion

Compressive stress analysis

Figures 41 and 42 show the compressive stress profile along the vertical direction (z-axis) in the timber section after exposure to an ISO standard fire and design fire, respectively. The stress profiles follow similar contours to the temperature profiles observed inside the column. It was evident that there were low-stress values near to the outer surface, which exposed the column to high temperatures and high stresses in the middle and in the regions with low temperatures. This is due to the reduction of mechanical properties with the time. Results showed that compression values to be increasing with the time for both fire exposures. The maximum compressive stress was observed at the 3600 s in both cases.

The timber cross section exposed to standard fire showed a maximum of 10.6 compressive stress MPa along the z-direction. The stresses in the other two directions were very low, as expected. There was no stress change with the height in the column for a given time step during the ISO fire exposure.

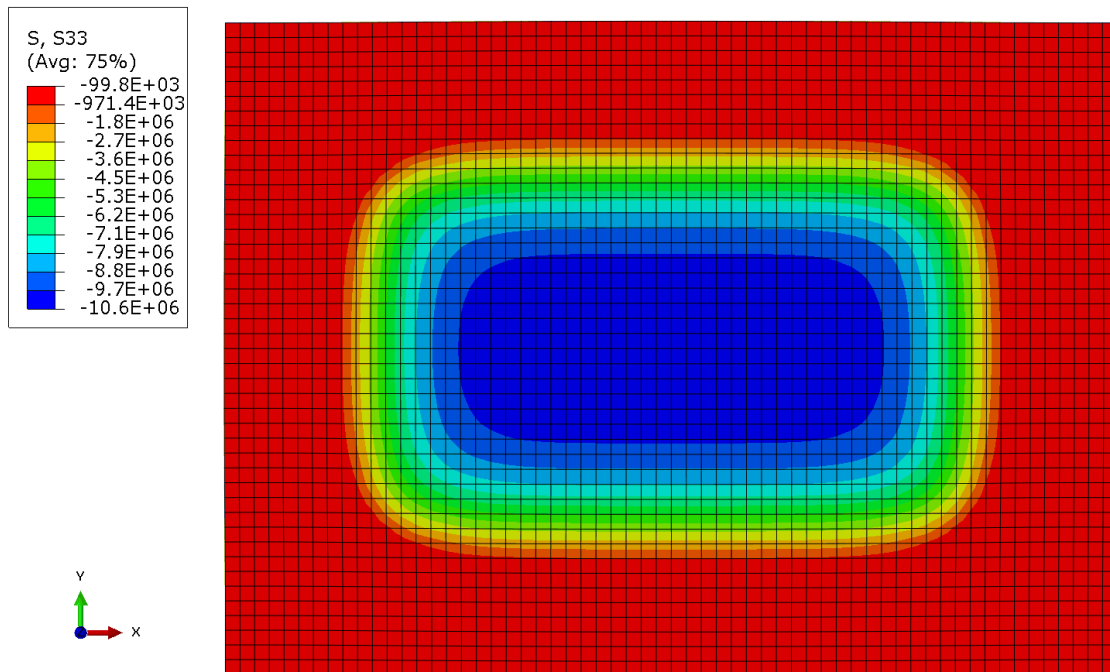


Figure 41: Compressive stress profile along the vertical direction in timber section exposed to ISO standard fire

Maximum compressive stress value of 4.6 MPa was observed for the timber section exposed to the design fire. A similar maximum value was evident along the height of the column. Nevertheless, it was noticed that the area of maximum stress in the cross section was higher in the lower part of the column compared to the top part of the column. This can be explained with the temperature profiles in different heights of the section. The lower part of the column, which was exposed to a higher heat flux was shown to have a smaller region with low temperatures compared to the top part of the column. Thus, high stresses tends to concentrate on this region in the lower part of the column. On the other hand, in the top part of the column, there is a bigger area with lower temperatures. Therefore, stress has a higher area to distribute, and the area with the maximum temperature is like to be lower.

In addition, it was observed that there were high compressive stress values in the y direction in the timber section for design fire exposure, unlike in the standard fire exposure. A maximum value of 1.8 MPa was recorded for transverse compressive stress. This can be explained with the bending of the timber column during the design fire exposure, as shown in the Figure 43. Even though the axial load was applied on the column, the non-uniform stress distribution, which was resulted from the non-uniform temperature profiles, creates an eccentricity leading to bending. Since the out of plane direction restrained by the boundary condition, only the bending about the strong axis of the cross section was observed.

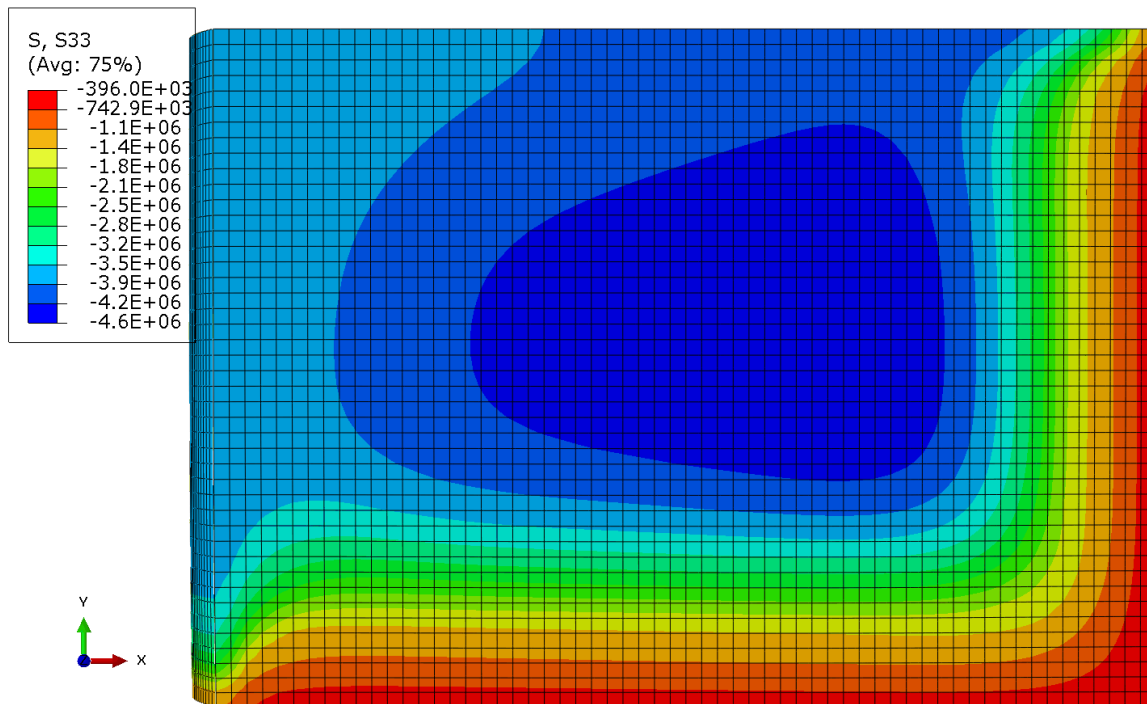


Figure 42: Compressive stress profile along the vertical direction in timber section exposed design fire

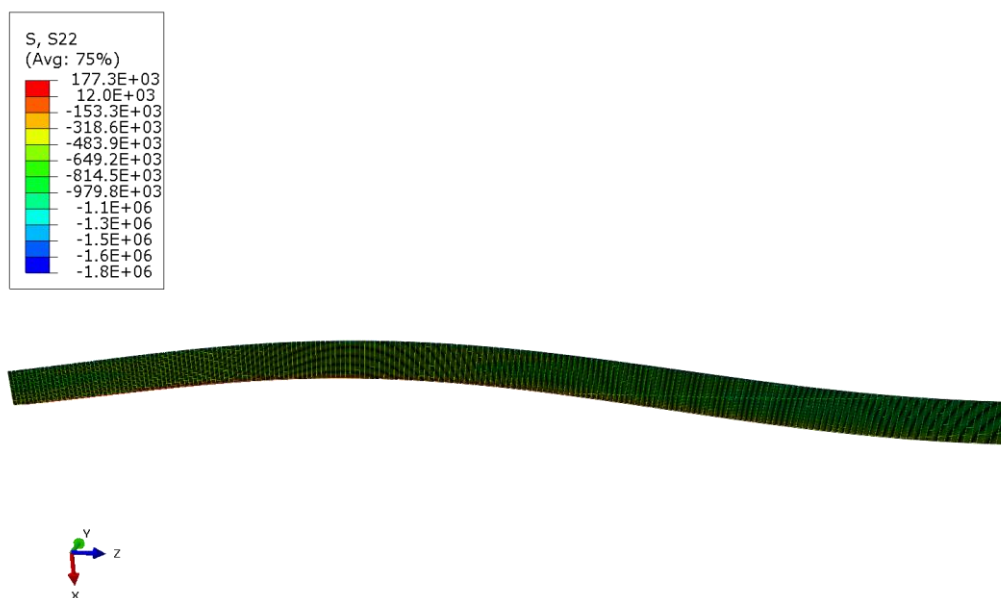


Figure 43: Bending deformation of the timber column exposed to design fire

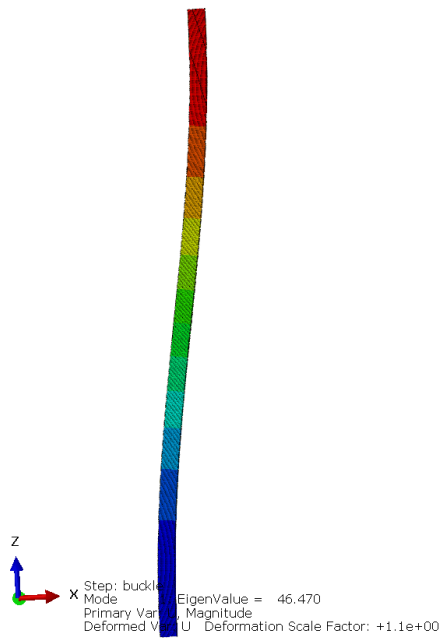
To conclude, the maximum stresses resulted in the column were smaller than the design compressive strength parallel to grain in fire value of 18.5 MPa, during the standard fire exposure and design fire exposure. Therefore, the column can be assumed to be safe from the compressive failure. It should be noted that due to the bending, the stresses occurs in the other

directions which have a lower strength in timber which can leads to failure. Therefore, a special attention should be given to these areas.

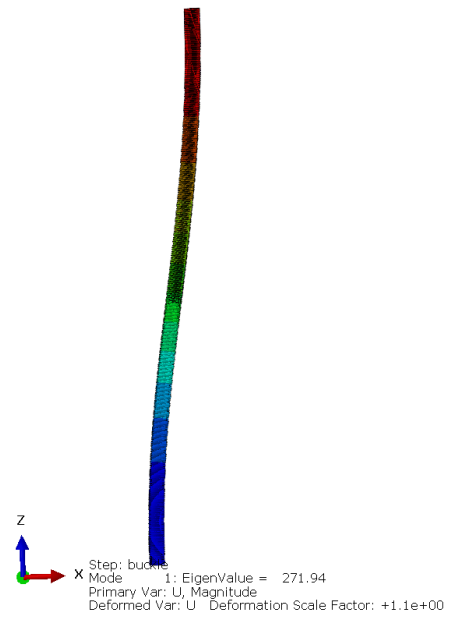
Critical buckling load analysis

It was observed that there was a critical buckling load of 46.5 kN for the standard fire exposure and 271.94 kN for the design fire exposure from the buckling analysis as shown in the Figure 44. The critical buckling at standard fire exposure shows 82.9% percent difference compared to the critical buckling load for design parametric fire exposure. The observed critical value for the standard fire is smaller than the applied fire limit loading, which is 209.2 kN. Therefore, the column will fail due to buckling during standard fire exposure. On the other hand, the critical buckling load during 60 minutes of design fire exposure is greater than the applied FLS loading. Thus, the column can withstand the FLS loading without collapsing.

In the Abaqus linear buckling analysis, from the imported temperatures, only one increment can be used in a perturbation step. Therefore, the temperature values of the column at each minute were imported separately, and the FLS load was applied to determine the critical buckling load during 60 minutes of fire exposure. This method is applicable only when there is no material or geometry nonlinearity and when no transverse forces are acting on members to create lateral sway for the second-order elastic buckling. On the other hand, it was visible that bending of the column during the design fire exposure. This can result high deflections in the structure. In some scenarios, the deflections can lead to geometric non-linear effects on the structure (Loh, 2006). Since the linear buckling analysis does not capture this behaviour it is recommended to do a second-order analysis to see the structural response in timber columns. The study in this thesis focused on developing a method to analyse thermo-mechanical structural performance when exposed to a real fire in a large compartments. Therefore, only the elastic region behaviour for the compressive members were considered to compare with the prescriptive fire codes. The effect due to the above factors in time history data was not considered.



(a) Standard fire exposure



(b) Design fire exposure

Figure 44: (a)-(b): Critical buckling mode and loads for different fire exposure in the timber column

CHAPTER VII

7. Conclusion

This thesis focussed on a performance-based approach by developing a numerical technique to analyse the thermo-mechanical response of timber columns in a large Industrial Hall, when exposed to a real fire. The building had an existing steel structure and the requirement was to replace it with engineered timber elements.

In the first part of the thesis, design calculations were carried out to determine equivalent Glulam timber column cross section for adequate load bearing capacity at the ambient conditions using the Eurocode 5 (EN 1995-1-2, 2004). The design calculations were performed to determine the load bearing capacity of the timber columns exposed to the ISO 834 (ISO 834-1:1999, 1999) standard fire curve for 60 minutes. It was determined by the calculation that the timber columns have adequate compressive strength but fail due to buckling under these conditions.

A summary of the work carried out and the conclusions are presented under the following subsections.

Fire Modelling Method for a Combustible Structure

An attempt was made to develop fire modelling techniques for large enclosure fires, whilst accounting for burning of the timber elements. Fire Dynamic Simulator (FDS), which solves simplified forms of Navier-Stokes equations numerically for thermally driven fluid flow and smoke flow was used for simulating the fire scenario. The pre-processing and the post processing were done using the graphical interface in PyroSim software.

A detailed study was presented on selecting the key parameters and boundary conditions. The ignition and the burning properties of the timber were taken from the literature considering the exposed heat fluxes. The initial assumptions based on heat fluxes when selecting the timber properties, were confirmed with the simulation results.

Adiabatic surface temperature values were used as the timber column exposure temperature due to the solid heat transfer model limitations in FDS software. It was observed from the simulation results that the standard fire curves do not accurately represent exposure

temperatures of columns and significantly overestimate the values compared to the exposure temperature values expected from real fire exposure.

A simulation was also conducted with inert timber columns without combustion to determine the effect of the extra fuel load from the combustible columns. It was discovered that, the burning timber columns have higher exposed temperatures when compared to columns with non-combustible surfaces.

Simulation of Temperature Profiles in Solid

A detail study of temperature profiles inside the solid timber section was presented for ISO standard and design fire exposure using the uncoupled heat transfer analysis in Abaqus. The temperature profile in the solid was determined by defining the exposed temperature values as the convective and radiation boundary conditions. The ISO 834 temperature-time curve and adiabatic surface temperatures from FDS modelling were used for the boundary conditions.

The thermal numerical model was validated by comparing standard fire exposure results with the prescriptive design calculations in Chapter 3. The charring depth and the charring rate comparison had a good agreement between finite element model results and Eurocode 5 results, indicating the accurate representation of timber charring using numerical model for the given Glulam material properties in Eurocode. The temperature contours inside the column section were uniform along the vertical axis of column for any time increment in ISO fire exposure.

The predicted solid cross section temperature values for the design fire exposure showed high temperatures near to the burning surfaces and lower values in the other regions. The lower part of the column showed high temperatures due to high exposed heat flux compared to the top part of the column. The time taken for the timber temperature to reach 300°C reasonably matched the column ignition time in the FDS simulation.

A comparison of the timber solid section temperature profiles in the Industrial Hall for the design fire exposure and ISO standard fire exposure has shown that, the ISO standard fire curve over-estimates the maximum charring depth by 79%.

Mechanical Analysis of Columns

An analysis of structural performance of the timber columns when exposed to fire exposure was carried out using a coupled thermo-mechanical stress analysis. Adequacy of the load bearing capacity and the buckling capacity of the section for Fire Limit State (FLS) loading

during the 60 minutes fire exposure was predicted using the Abaqus simulation. In the simulation, temperature result file from previous analysis was imported and FLS loading was applied at each increment to see the structural response.

The columns showed an adequate load bearing capacity for both, standard and parametric design fire exposures. The critical buckling load was observed to be smaller than the applied FLS loading in the standard fire exposure. The resulting failure of the column member is similar to the design calculation in Eurocode 5. On the other hand, the column showed an adequate buckling capacity during 60 minutes for design fire exposure.

Overall, the real fire exposure should be accounted for in the structural timber designs. When simulating the fire scenarios, combustion of the timber columns has a considerable impact. The fire simulation technique discussed in this research can be used to model the fire and heat transfer to structural timber elements, considering the combustion of the timber.

To conclude, the design calculations prescribed in Eurocode 5 and based on ISO standard fire exposure, largely over-estimate the structural performance of the timber columns when compared to exposure to real fires in large enclosures. The coupled thermo-mechanical analysis simulation technique in this thesis can be used to perform an accurate structural fire analysis using the exposure temperatures as boundary conditions.

7.1. Limitations and the potential future work

With the limitations discussed earlier in this thesis, potential areas have been identified for further investigation and some recommendations have been put forward next.

The pyrolysis model of timber used in FDS model based on experimental results, can be further improve to model the char layer using a complex pyrolysis model. A deep study on the fundamental principles of combustion reactions should be done prior to the modelling.

The material properties of the walls and floor in the current study were limited to inert conditions. The effect of the properties of wall materials should also be investigated to see the influence of radiative heat feedback mechanism effect on heat fluxes.

A sensitivity analysis can be done to see the effect of the fire size, fire duration and distance to the fire source from the timber elements to see the change of exposed timber temperatures with the time.

This thesis mainly focused on the structural fire behaviour of the timber column elements. A structure will resist the fire as a combination of the fire performance of its structural elements. Therefore, the robustness of a structure during a fire should be studied in detail on an individual element level to get more understanding of the overall structural behaviour for a given fire exposure.

A second-order buckling analysis can be used to investigate buckling behaviour when exposed to design fires. The study can be extended to check different failure criteria on the structural timber elements including geometry and material nonlinearity.

Coupling the FDS fire model and Abaqus thermo-mechanical model together can be used to simulate fire performance and structural performance at each time step. This could lead to a more realistic representation of the real-world scenario.

Acknowledgement

First and foremost, I would like to convey gratitude to my thesis supervisors, Professor Bart Merci and Professor Andrea Frangi, for continuous guidance and support throughout the research work.

Many thanks to Juan Blond for helping me from the start of the thesis topic selection to the very end. Discussions with you about the thesis work always I found to be interesting and important.

I am thankful to Fahrni Reto and other members in the Timber Structures group at ETH Zurich for hosting me during the thesis work and supporting always without any hesitation.

A great thanks goes to Jost Peter and Basler & Hofmann Company for making my stay in Switzerland a comfortable while always looking after my requirements.

I would like to thank my friends from undergraduate studies, Vajira Lasantha and Varakini Sanmugadas for your insights and comments about my thesis work. My extended thanks goes to Fearghal Gill, Bobby Bray and other IMFSE colleagues for the interesting and helpful conversations.

Another special person to thank is my fiancé Manju, for always helping me and having my back at difficult times. Your encouragement always had a big impact. Also I would like to thank my mother, Chandrika, my father, Damitha and my sister Tharushika, who were continuously supporting me to achieve everything.

Finally, I want to thank the IMFSE team for creating a very interesting program and also the sponsoring companies, for the continued financial support during the two years of incredible journey in the fire safety world.

.

References

- Rein, G. (2013). 9/11 World Trade Center Attacks: Lessons in Fire Safety Engineering After the Collapse of the Towers. *Fire Technology*, 49(3), 583–585. <https://doi.org/10.1007/s10694-013-0337-6>
- EN 1995-1-2. (2004). *Eurocode 5: Design of timber structures - Part 1-2: General - Structural fire design*.
- Rehm, R. G., Pitts, W. M., Baum, H. R., Evans, D. D., Prasad, K., McGrattan, K. B., & Forney, G. P. (2003). Initial model for fires in the World Trade Center towers. *Fire Safety Science*, January, 25–40. <https://doi.org/10.3801/IAFSS.FSS.7-25>
- ISO 834-1:1999. (1999). *Fire-resistance tests - Elements of building construction - Part 1: General requirements*. International Organization for Standardization, Geneva, Switzerland.
- Marty Ahrens. (2007). High-Rise Building Fires. In *Journal of Disaster Research* (Vol. 2, Issue 4). <https://doi.org/10.20965/jdr.2007.p0236>
- Mohamed, I. F., Edwards, D. J., Mateo-Garcia, M., Costin, G., & Thwala, W. D. D. (2019). An investigation into the construction industry's view on fire prevention in high-rise buildings post Grenfell. *International Journal of Building Pathology and Adaptation*, December. <https://doi.org/10.1108/IJBPA-05-2019-0048>
- Schmid, J., Fahrni, R., Frangi, A., & Zurich, E. T. H. (2019). *Determination of design fires in compartment-ments with combustible structure – modification of existing design equations*.
- O'Neill, J., Abu, A., Carradine, D., Moss, P., & Buchanan, A. (2014). Modelling the fire performance of structural timber-concrete composite floors. *Journal of Structural Fire Engineering*, 5(2), 113–123. <https://doi.org/10.1260/2040-2317.5.2.113>
- Kuzman, M. K., Oblak, L., & Vratuša, S. (2010). Glued laminated timber in architecture. *Drvna Industrija*, 61(3), 197–204.
- Anshari, B., Guan, Z. W., Kitamori, A., Jung, K., & Komatsu, K. (2012). Structural behaviour of glued laminated timber beams pre-stressed by compressed wood. *Construction and Building Materials*, 29(November 2017), 24–32. <https://doi.org/10.1016/j.conbuildmat.2011.10.002>

- Lowden, L., & Hull, T. (2013). Flammability behaviour of wood and a review of the methods for its reduction. *Fire Science Reviews*, 2(1), 4. <https://doi.org/10.1186/2193-0414-2-4>
- Yang, T. H., Wang, S. Y., Tsai, M. J., & Lin, C. Y. (2009). The charring depth and charring rate of glued laminated timber after a standard fire exposure test. *Building and Environment*. <https://doi.org/10.1016/j.buildenv.2008.02.010>
- Werther, N., Neill, J. W. O., Spellman, P. M., Abu, A. K., Moss, P. J., Buchanan, A. H., & Winter, S. (2012). Parametric Study of Modelling Structural Timber in Fire With Different Software Packages. *7th International Conference on Structures in Fire*.
- Gillie, M. (2009). Analysis of heated structures: Nature and modelling benchmarks. *Fire Safety Journal*, 44(5), 673–680. <https://doi.org/10.1016/j.firesaf.2009.01.003>
- Basler & Hofmann. (2017). *Performance-based project , the Swiss experience :*
- Bailey, C. (2004). Structural fire design: Core or specialist subject? *Structural Engineer*, 82(9), 32–38.
- Arora, H. (2014). *Exploring Potential Problems Causing the Final Implemented Design to Deviate in a Performance Based Fire Safety Design Approach*. Lund University, Sweden.
- Nour, M. (2018). *Fire Safety Design System between Performance-Based vs Prescriptive Design-Tools and Challenges Fire Safety Design System between Performance-Based vs Prescriptive Design – Tools and Challenges* (Issue April).
- Ronchi, E., & Nilsson, D. (2013). Fire evacuation in high-rise buildings: a review of human behaviour and modelling research. *Fire Science Reviews*, 2(1), 7. <https://doi.org/10.1186/2193-0414-2-7>
- Buchanan, A. H. (1999). Implementation of performance-based fire codes. *Fire Safety Journal*, 32(4), 377–383. [https://doi.org/10.1016/S0379-7112\(99\)00002-8](https://doi.org/10.1016/S0379-7112(99)00002-8)
- Hurley, M. J. ., & Rosenbaum, E. R. (2015). *Performance-Based Design in SFPE Handbook of Fire Protection Engineering* (5 th). New York: Springer.
- Drysdale, D. (2011). *An Introduction to Fire Dynamics* (3rd ed.). John Wiley & Sons, Ltd, Chichester.
- Buchanan, Andrew H., & Abu, A. K. (2017). Structural Design for Fire Safety. In *Structural Design for Fire Safety*. John Wiley & Sons, Ltd. <https://doi.org/10.1002/9781118700402>

- Law, M. (1983). A basis for the design of fire protection of building structures. *The Structural Engineer*, 61A.
- Butcher, E. G., Chitty, T. B., & Ashton, L. A. (1966). *The Temperature Attained by Steel in Building Fires*. Fire Research Technical Paper No. 15.H.M. Stationery Office, London.
- Thomas, P. H., & Heselden, A. J. . (1972). *Fully Developed Fires in Single Compartments*. CIB Report No 20, Fire Research Note 923. Fire Research Station, London.
- Magnusson, S. E., & Thelandersson, S. (1970). Temperature-time curves of complete process of fire development; theoretical study of wood fuel fires in enclosed spaces. *Acta Polytechnica Scandinavica. Civil Engineering and Building Construction Series 65*.
- Kirby, B. R., Wainman, D. E., Tomlinson, L. N., Kay, T. R., & Peacock, B. N. (1999). Natural Fires in Large Scale Compartments. *International Journal on Engineering Performance-Based Fire Codes*, 1(2), 43–58.
- Ingberg, S. . (1928). Tests of the severity of building fires. *National Fire Protection Quarterly*, 22(1), 43–61.
- Law, M. (1971). *A Relationship Between Fire Grading and Building Design and Contents*. Fire Research Note No. 877. Fire Research Station, London.
- Frangi, A., Fontana, M., Hugi, E., & Jübstl, R. (2009). Experimental analysis of cross-laminated timber panels in fire. *Fire Safety Journal*, 44(8), 1078–1087. <https://doi.org/10.1016/j.firesaf.2009.07.007>
- Klippel, M., & Frangi, A. (2017). Fire safety of glued-laminated timber beams in bending. *Journal of Structural Engineering (United States)*, 143(7), 1–10. [https://doi.org/10.1061/\(ASCE\)ST.1943-541X.0001781](https://doi.org/10.1061/(ASCE)ST.1943-541X.0001781)
- Laplanche, K., Dhima, D., & Racher, P. (2006). Thermo-mechanical analysis of the timber connection under fire using 3D finite element model. *9th World Conference on Timber Engineering 2006, WCTE 2006*, 1(February), 279–286.
- Thi, V. D., Khelifa, M., Oudjene, M., Ganaoui, M. El, & Rogaume, Y. (2017). Finite element analysis of heat transfer through timber elements exposed to fire. *Engineering Structures*, 143, 11–21. <https://doi.org/10.1016/j.engstruct.2017.04.014>
- Fragiacomo, M., Menis, A., Clemente, I., Bochicchio, G., & Ceccotti, A. (2013). Fire resistance

- of cross-laminated timber panels loaded out of plane. *Journal of Structural Engineering (United States)*, 139(12), 1–11. [https://doi.org/10.1061/\(ASCE\)ST.1943-541X.0000787](https://doi.org/10.1061/(ASCE)ST.1943-541X.0000787)
- Schmid, J., Klippel, M., Just, A., Frangi, A., & Tiso, M. (2018). Simulation of the Fire Resistance of Cross-laminated Timber (CLT). *Fire Technology*, 54(5), 1113–1148. <https://doi.org/10.1007/s10694-018-0728-9>
- Brandon, D., Kagiya, K., & Hakkarainen, T. (2018). *Performance based design for mass timber structures in fire – a design example*. COST Action FP1404, Zürich, Switzerland. <https://doi.org/10.3929/ethz>
- Brandon, D. (2018). *Engineering methods for structural fire design of wood buildings – structural integrity during a full natural fire*.
- McGrattan, K., Hostikka, S., McDermott, R., Floyd, J., Weinschenk, C., & Overhold, K. (2016). Sixth Edition Fire Dynamics Simulator User 's Guide (FDS). In *NIST Special Publication 1019: Vol. Sixth Edit*. <https://doi.org/10.6028/NIST.SP.1019>
- Wickström, U., Duthinh, D., & McGrattan, K. (2007). Adiabatic Surface Temperature for Calculating Heat Transfer To Fire Introduction. *Interflam 2007*, 2, 943–953.
- Pluto, M. (2018). *Tank Shell Design According to Eurocodes and Evaluation of Calculation Methods*. Karlstads universitet.
- Lantsoght, E. O. L., Van Der Veen, C., & Walraven, J. C. (2014). Shear in one-way slabs under concentrated load close to support. *ACI Structural Journal*, 111(1), 223.
- Shoukry, M. E., Mahmoud, Z. I., Hashem, T. M., & Mohamed, G. A. (2018). Flexural analysis of RC rectangular slabs subjected to patch load. *Alexandria Engineering Journal*, 57(4), 3273–3279. <https://doi.org/10.1016/j.aej.2017.12.005>
- EN 1991-1-1. (2002). *Eurocode 1: Actions on structures - Part 1-1: General actions - Densities, self-weight, imposed loads for buildings*.
- EN 1990:2002+A1. (2005). *Eurocode 0- Basis of structural design*.
- EN 1995-1-1. (2004). *Eurocode 5: Design of timber structures - Part 1-1: General - Common rules and rules for buildings*.
- EN 1194:1999. (1999). *Timber structures-Glued laminated timber-Strength classes and determination of characteristic values*.

- Ryder, N. L., Sutula, J. A., Schemel, C. F., Hamer, A. J., & Brunt, V. Van. (2004). Consequence modeling using the fire dynamics simulator. *Journal of Hazardous Materials*, 115(1-3 SPEC. ISS.), 149–154. <https://doi.org/10.1016/j.jhazmat.2004.06.018>
- Luketa-Hanlin, A. (2006). A review of large-scale LNG spills: Experiments and modeling. *Journal of Hazardous Materials*, 132(2–3), 119–140. <https://doi.org/10.1016/j.jhazmat.2005.10.008>
- Busini, V. (1895). Atmospheric dispersion. In *Nature* (Vol. 51, Issue 1321). Elsevier Inc. <https://doi.org/10.1201/b13691-15>
- SFPE Handbook. (2016). *SFPE Handbook of Fire Protection Engineering* (Third Edit).
- Anderson, J., Sjostrom, J., Alastair, T., Dai, X., Welch, S., & Rush, D. (2019). FDS simulations and modelling efforts of travelling fires in a large elongated compartment. *15th International Conference and Exhibition on Fire Science and Engineering, November*, 2085–2094.
- Degler, J., Eliasson, A., Anderson, J., Lange, D., & Rush, D. (2015). A-priori modelling of the Tisova Fire Test as input to the experimental work. *The First International Conference on Structural Safety under Fire & Blast, September*, 429–438.
- López, G., Basterra, L. A., Acuña, L., & Casado, M. (2013). Determination of the emissivity of wood for inspection by infrared thermography. *Journal of Nondestructive Evaluation*, 32(2), 172–176. <https://doi.org/10.1007/s10921-013-0170-3>
- Babrauskas, V. (2002). Journal of Fire Protection Ignition of Wood : A Review of. *Journal of Fire Protection Engineering*, 12(August), 81–88. <https://doi.org/10.1106/104239102028711>
- Bartlett, A. I., Hadden, R. M., & Bisby, L. A. (2019). A Review of Factors Affecting the Burning Behaviour of Wood for Application to Tall Timber Construction. *Fire Technology*, 55(1), 1–49. <https://doi.org/10.1007/s10694-018-0787-y>
- Fangrat, J., Hasemi, Y., Yoshida, M., & Hirata, T. (1996). Surface temperature at ignition of wooden based slabs. *Fire Safety Journal*, 27(3), 249–259. [https://doi.org/10.1016/S0379-7112\(96\)00046-X](https://doi.org/10.1016/S0379-7112(96)00046-X)
- Li, Y. (1992). Measurement Of The Ignition Temperature Of Wood. *Fire Safety Science*, 1(4), 380–385.

- Atreya, A. (1983). Pyrolysis, ignition and fire spread on horizontal surfaces of wood. In *Pyrolysis, Ignition and Fire Spread on Horizontal Surfaces of Wood* (Issue September). <http://www.scopus.com/inward/record.url?eid=2-s2.0-0003600043&partnerID=tZOtx3y1>
- Di Ha Le, T., & Tsai, M. T. (2019). Experimental assessment of the fire resistance mechanisms of timber-steel composites. *Materials*, *12*(23). <https://doi.org/10.3390/ma12234003>
- Tran, H. C., & White, R. H. (1992). Burning rate of solid wood measured in a heat release rate calorimeter. *Fire and Materials*, *16*(4), 197–206. <https://doi.org/10.1002/fam.810160406>
- Fonseca, E. M. M., & Barreira, L. M. S. (2009). Charring rate determination of wood pine profiles submitted to high temperatures. *WIT Transactions on the Built Environment*, *108*, 449–457. <https://doi.org/10.2495/SAFE090421>
- Zadeh, S. E., Beji, T., & Merci, B. (2015). Validation of the Pyrolysis Model of Fds 6 for a Large-Scale Ethanol Pool Fire. *Ninth Mediterranean Combustion Symposium, Proceedings*.
- He, Y., Jamieson, C., Jeary, A., & Wang, J. (2008). Effect of computation domain on simulation of small compartment fires. *Fire Safety Science*, 1365–1376. <https://doi.org/10.3801/IAFSS.FSS.9-1365>
- Zhang, X., Yang, M., Wang, J., & He, Y. (2010). Effects of computational domain on numerical simulation of building fires. *Journal of Fire Protection Engineering*, *20*(4), 225–251. <https://doi.org/10.1177/1042391510367349>
- Yuen, A. C. Y., Yeoh, G. H., Yuen, R. K. K., & Lo, S. M. (2016). Numerical study on small-scale fire whirl using large eddy simulation. *International Conference on Fluid Flow, Heat and Mass Transfer*, *165*, 1–8. <https://doi.org/10.11159/ffhmt16.165>
- Zhang, W., Hamer, A., Klassen, M., Carpenter, D., & Roby, R. (2002). Turbulence statistics in a fire room model by large eddy simulation. *Fire Safety Journal*, *37*(8), 721–752. [https://doi.org/10.1016/S0379-7112\(02\)00030-9](https://doi.org/10.1016/S0379-7112(02)00030-9)
- McGrattan, K., Hostikka, S., McDermott, R., Floyd, J., Weinschenk, C., & Overholt, K. (2015). Sixth edition fire dynamics simulator technical reference guide volume 1 : mathematical model. In *NIST Special Publication 1018* (Vol. 1). <https://doi.org/10.6028/NIST.SP.1018-1>

- Salley, M. H., & Kassawara, R. P. (2007). *Verification and Validation of Selected Fire Models for Nuclear Power Plant Applications*.
<http://scholar.google.com/scholar?hl=en&btnG=Search&q=intitle:Verification+and+Validation+of+Selected+Fire+Models+for+Nuclear+Power+Plant+Applications#0>
- Abaqus, Analysis User's Guide*. (2014). Dassault Systemes Simulia Corp., Providence, Rhode Island.
- Atkinson, G. T., & Drysdale, D. D. (1992). Convective heat transfer from fire gases. *Fire Safety Journal*, 19(2–3), 217–245. [https://doi.org/10.1016/0379-7112\(92\)90034-A](https://doi.org/10.1016/0379-7112(92)90034-A)
- Veloo, P. S., & Quintiere, J. G. (2013). Convective heat transfer coefficient in compartment fires. *Journal of Fire Sciences*, 31(5), 410–423. <https://doi.org/10.1177/0734904113479001>
- Pitarma, R., & Crisóstomo, J. (2019). An approach method to evaluate wood emissivity. *Journal of Engineering (United Kingdom)*, 2019. <https://doi.org/10.1155/2019/4925056>
- Ellobody, E. (2014). Finite Element Analysis of Steel and Steel-Concrete Composite Bridges. In *Finite Element Analysis and Design of Steel and Steel-Concrete Composite Bridges*. Elsevier Inc. <https://doi.org/10.1016/b978-0-12-417247-0.00005-3>
- Loh, A. (2006). *A Simple Procedure for Performing Second Order Analysis Using a Linear Structural Analysis Program*.

Appendices

Appendix A - Drawings of Industrial Hall

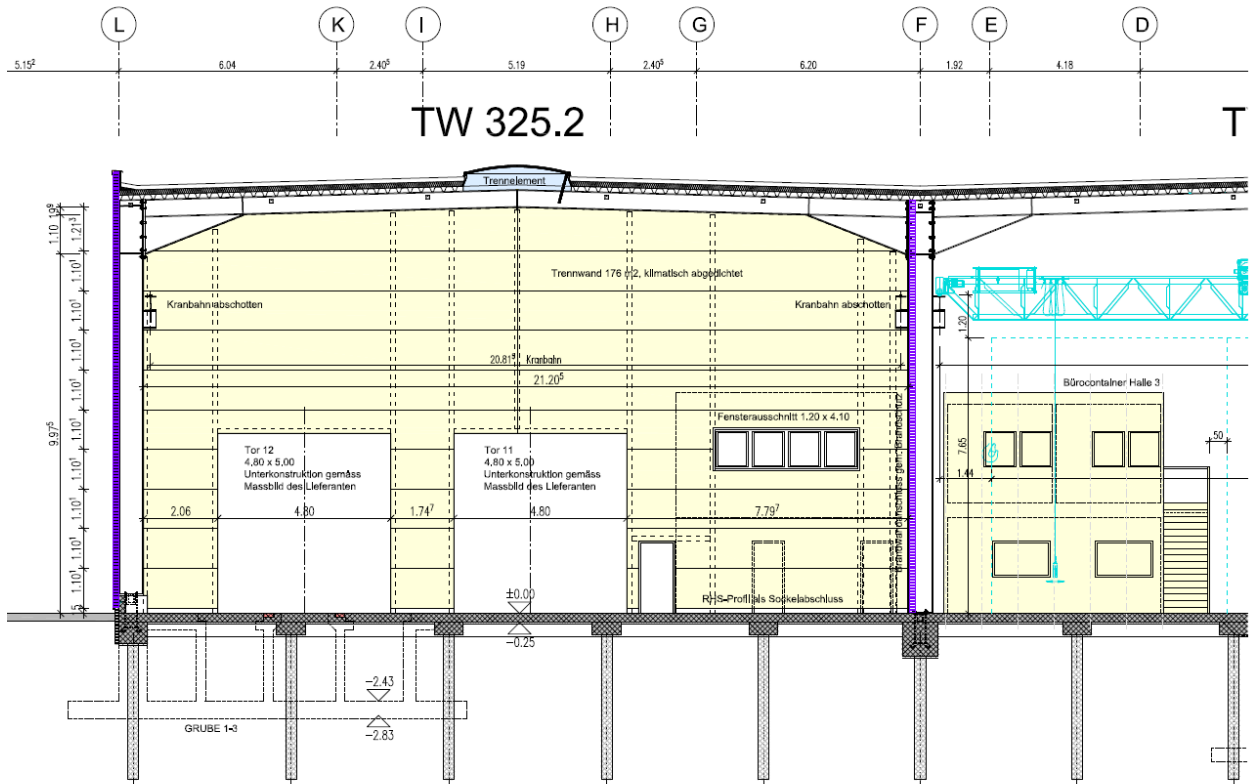


Figure 45: Side view of the Industrial hall

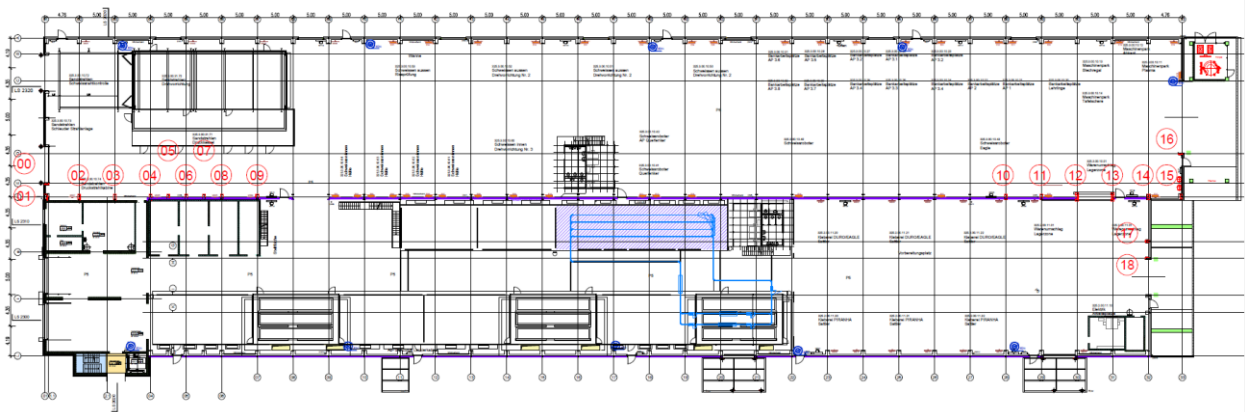


Figure 46: Existing column grid of the Industrial hall

Appendix B- FDS Results

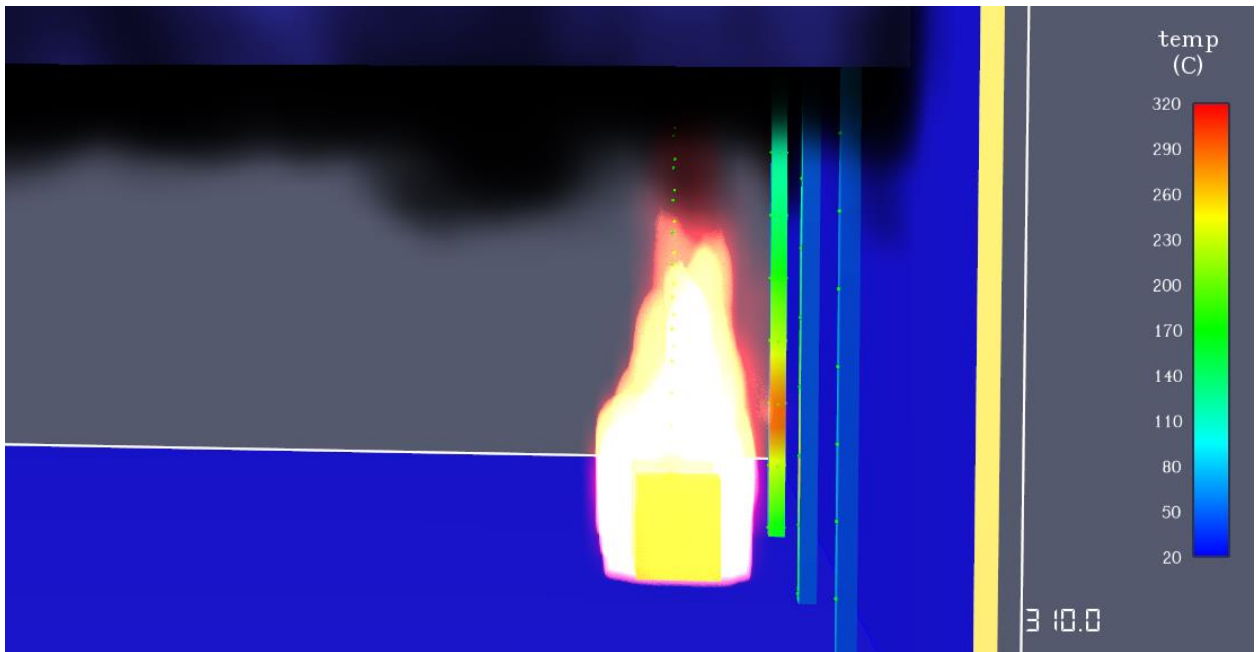


Figure 47: Ignition point of Column 1 face 4 (T=310s)

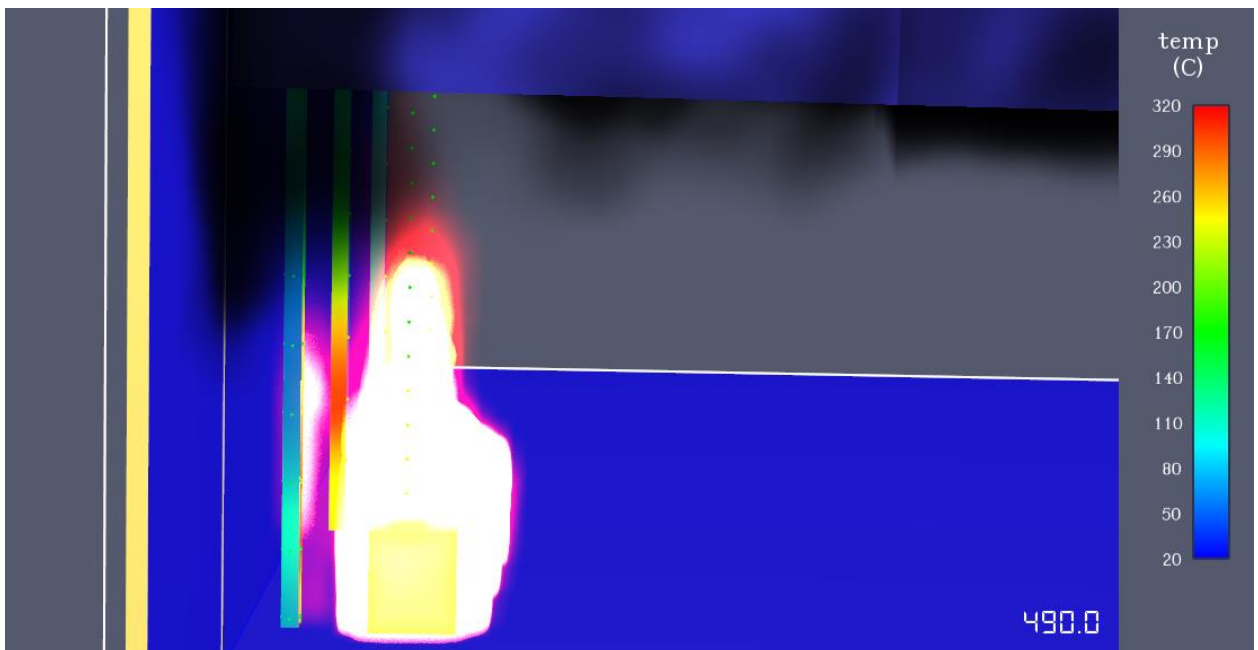


Figure 48: Ignition point of Column 2 face 2 (T=490s)

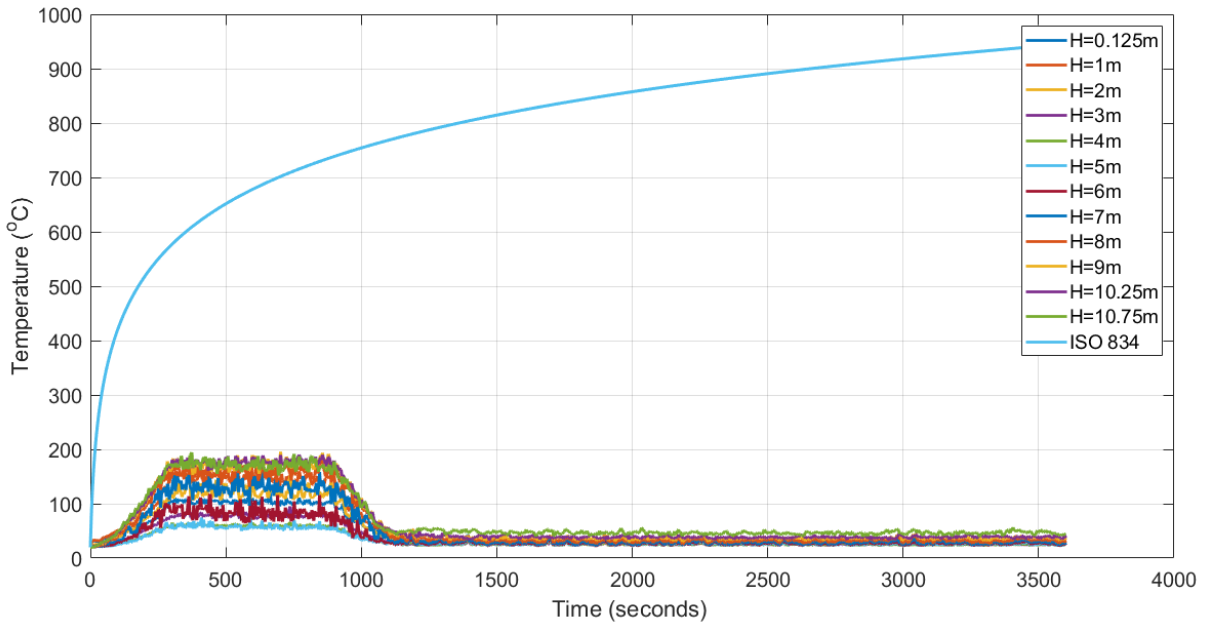


Figure 49: Adiabatic temperature change with time at different heights in column 1 face 2

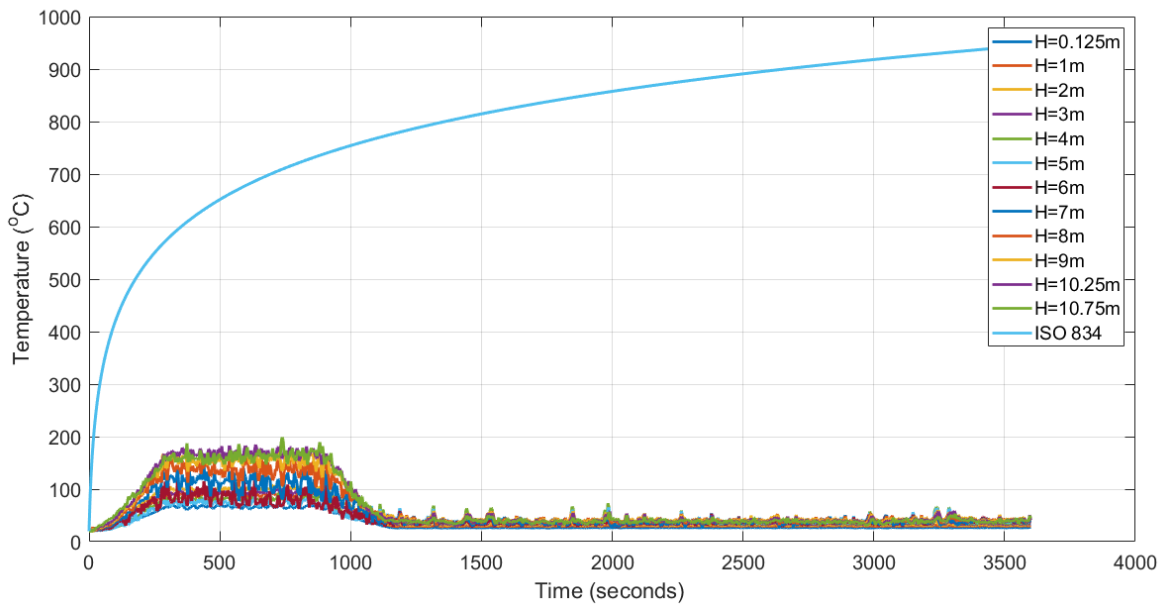


Figure 50: Adiabatic temperature change with time at different heights in column 1 face 3

Appendix C - Temperature dependent material properties for softwood timber (EN 1995-1-2)

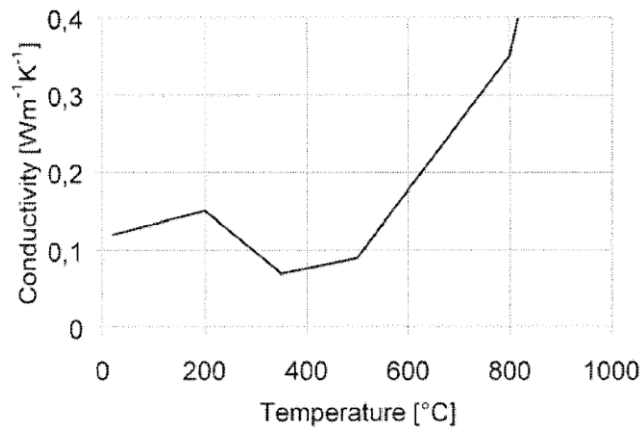


Figure B1 – Temperature-thermal conductivity relationship for wood and the char layer

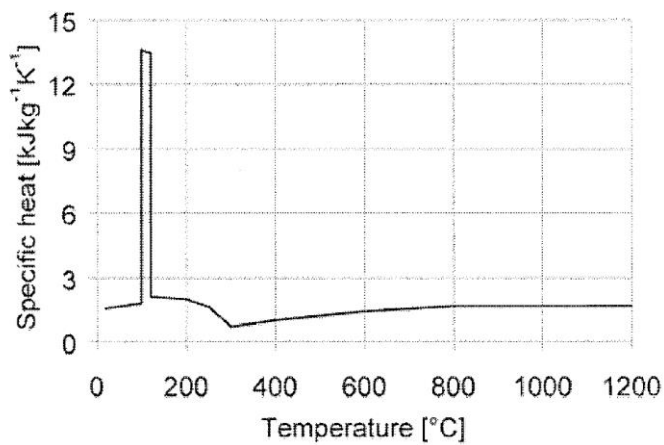


Figure B2 – Temperature-specific heat relationship for wood and charcoal

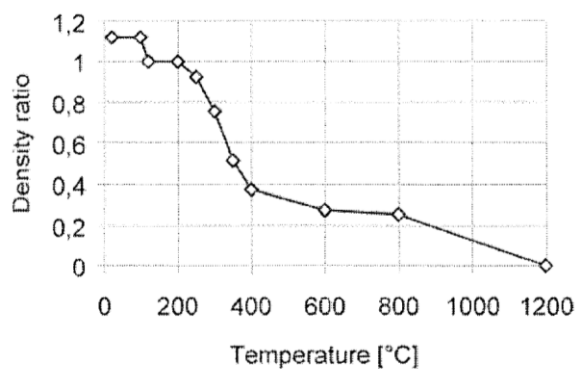


Figure B3 – Temperature-density ratio relationship for softwood with an initial moisture content of 12 %

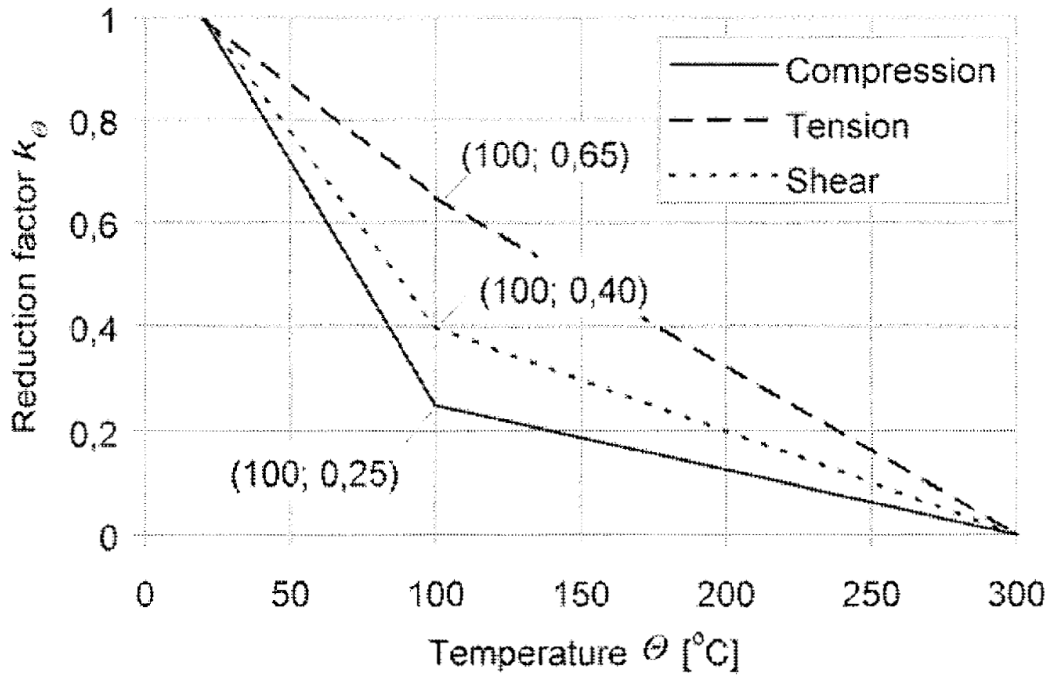


Figure B4 – Reduction factor for strength parallel to grain of softwood

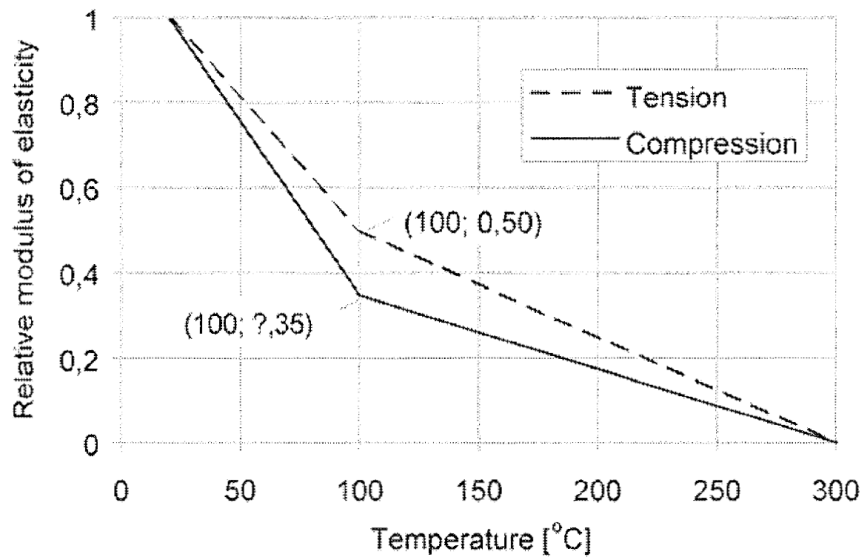
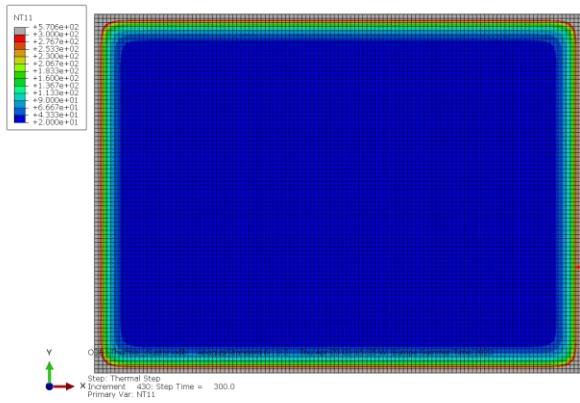


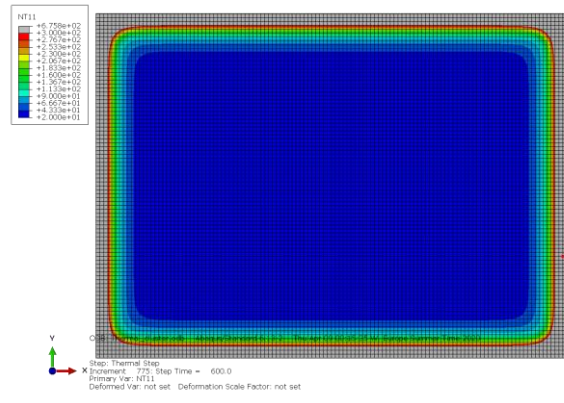
Figure B5 – Effect of temperature on modulus of elasticity parallel to grain of softwood

Figure 51: Temperature dependent material properties for softwood timber (EN 1995-1-2)

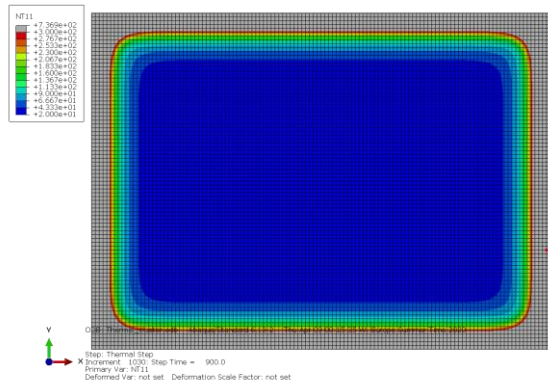
Appendix D - Thermal Analysis Results



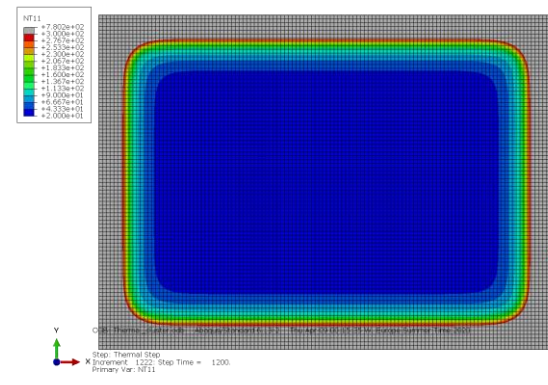
T= 300 s



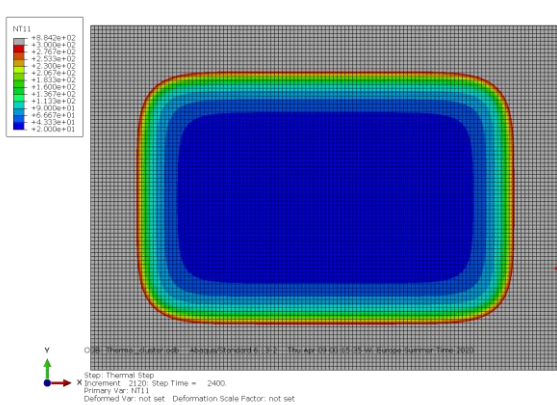
T=600 s



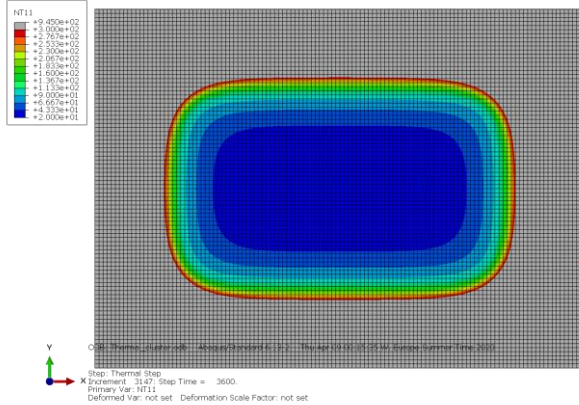
T= 900 s



T=1200 s



T= 2400 s



T=3600 s

Figure 52: Char layer development with time for standard fire exposure

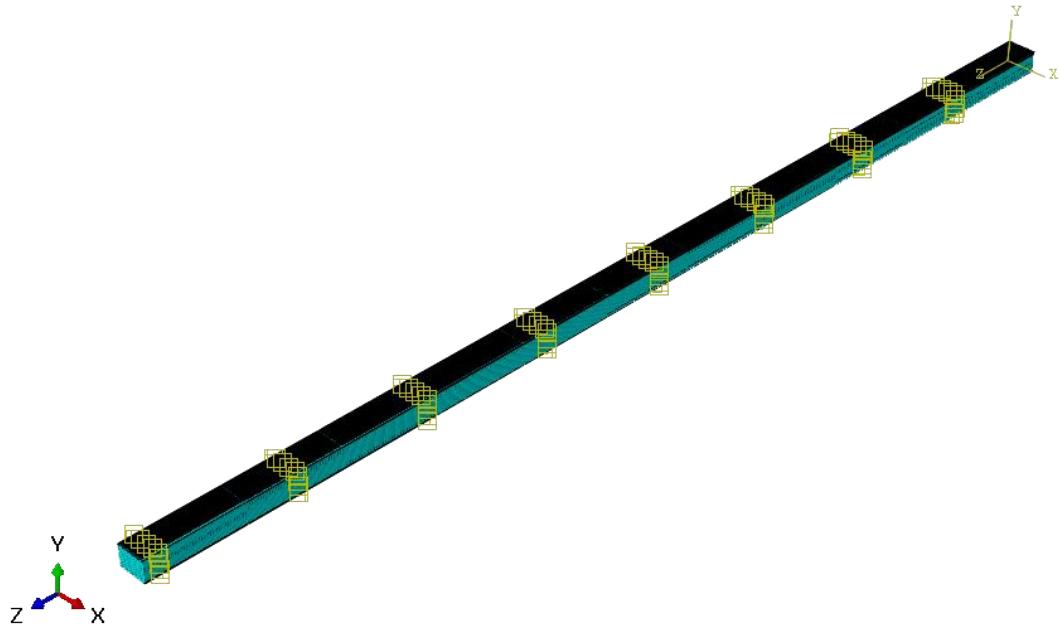


Figure 53: Thermal finite element model

7.2. Appendix E – FDS Input File

Radiation1000_Msh_250.fds

Generated by PyroSim - Version 2019.3.1204

17-Apr-2020 00:55:00

-----User Section (not generated by PyroSim)-----

&PROP ID='props', EMISSIVITY=0.8, HEAT_TRANSFER_COEFFICIENT=25.0/

&DEVC ID='C1INWLDevice01F', DEPTH=0.025, QUANTITY='INSIDE WALL TEMPERATURE',
XYZ=7.625,23.25,2.125, IOR=-2/

&DEVC ID='C1INWLDevice02F', DEPTH=0.1, QUANTITY='INSIDE WALL TEMPERATURE',
XYZ=7.625,23.25,2.125, IOR=-2/

&DEVC ID='C1INWLDevice03F', DEPTH=0.2, QUANTITY='INSIDE WALL TEMPERATURE',
XYZ=7.625,23.25,2.125, IOR=-2/

&DEVC ID='C1INWLDevice04F', DEPTH=0.25, QUANTITY='INSIDE WALL TEMPERATURE',
XYZ=7.625,23.25,2.125, IOR=-2/

&DEVC ID='C1INWLDevice01B', DEPTH=0.0, QUANTITY='INSIDE WALL TEMPERATURE',
XYZ=7.625,23.25,2.125, IOR=-2/

&DEVC ID='C1INWLDevice02B', DEPTH=-0.1, QUANTITY='INSIDE WALL TEMPERATURE',
XYZ=7.625,23.25,2.125, IOR=-2/

&DEVC ID='C1INWLDevice03B', DEPTH=-0.2, QUANTITY='INSIDE WALL TEMPERATURE',
XYZ=7.625,23.25,2.125, IOR=-2/

&DEVC ID='C1INWLDevice04B', DEPTH=-0.22, QUANTITY='INSIDE WALL TEMPERATURE',
XYZ=7.625,23.25,2.125, IOR=-2/

&DEVC ID='C1INWLDevice05B', DEPTH=-0.25, QUANTITY='INSIDE WALL TEMPERATURE',
XYZ=7.625,23.25,2.125, IOR=-2/

&DEVC ID='C1INWLDENSITY01', DEPTH=0.025, QUANTITY='SOLID DENSITY', MATL_ID='wood',
XYZ=7.625,23.25,2.125, IOR=-2/

&DEVC ID='C1INWLDENSITY02', DEPTH=0.1, QUANTITY='SOLID DENSITY', MATL_ID='wood',
XYZ=7.625,23.25,2.125, IOR=-2/

&DEVC ID='C1INWLCOND01', DEPTH=0.025, QUANTITY='SOLID CONDUCTIVITY', MATL_ID='wood',
XYZ=7.625,23.25,2.125, IOR=-2/

&DEVC ID='C1INWLCOND02', DEPTH=0.1, QUANTITY='SOLID CONDUCTIVITY', MATL_ID='wood',
XYZ=7.625,23.25,2.125, IOR=-2/

&DEVC ID='C1INWLSHC01', DEPTH=0.025, QUANTITY='SOLID SPECIFIC HEAT', MATL_ID='wood',
XYZ=7.625,23.25,2.125, IOR=-2/

&DEVC ID='C1INWLSHC02', DEPTH=0.1, QUANTITY='SOLID SPECIFIC HEAT', MATL_ID='wood',
XYZ=7.625,23.25,2.125, IOR=-2/

-----PyroSim-generated Section-----

&HEAD CHID='Radiation1000_Msh_250/'

```

&TIME T_END=3600.0/
&DUMP DT_RESTART=300.0, DT_SL3D=0.25/
&RADI NUMBER_RADIATION_ANGLES=1000/

&MESH ID='MESH-fire-nearfield-b', IJK=30,38,60, XB=5.5,13.0,15.0,24.5,0.0,15.0, MPI_PROCESS=0, N_THREADS=8/
&MESH ID='MESH-fire-nearfield-a', IJK=22,38,60, XB=0.0,5.5,15.0,24.5,0.0,15.0, MPI_PROCESS=1, N_THREADS=4/
&MESH ID='MESH-fire-nearfield-b', IJK=48,38,60, XB=13.0,25.0,15.0,24.5,0.0,15.0, MPI_PROCESS=2,
N_THREADS=4/
&MESH ID='MESH-far-room-Coarse-b-a', IJK=50,60,30, XB=0.0,12.5,0.0,15.0,7.5,15.0, MPI_PROCESS=3,
N_THREADS=3/
&MESH ID='MESH-far-room-Coarse-b-b', IJK=50,60,30, XB=12.5,25.0,0.0,15.0,7.5,15.0, MPI_PROCESS=4,
N_THREADS=3/
&MESH ID='MESH-far-room-Coarse-a-a', IJK=50,60,30, XB=0.0,12.5,0.0,15.0,0.0,7.5, MPI_PROCESS=5,
N_THREADS=3/
&MESH ID='MESH-far-room-Coarse-a-b', IJK=50,60,30, XB=12.5,25.0,0.0,15.0,0.0,7.5, MPI_PROCESS=6,
N_THREADS=3/

&REAC ID='WOOD_OAK',
  FYI='SFPE Handbook, 3rd Ed',
  FUEL='REAC_FUEL',
  C=1.0,
  H=1.7,
  O=0.72,
  N=1.0E-3,
  AUTO_IGNITION_TEMPERATURE=0.0,
  CO_YIELD=4.0E-3,
  SOOT_YIELD=0.015,
  HEAT_OF_COMBUSTION=1.42E4,
  RADIATIVE_FRACTION=0.35/

&DEVC ID='C1-ADT Temp 01', QUANTITY='ADIABATIC SURFACE TEMPERATURE', XYZ=7.625,23.25,0.125,
IOR=-2/
&DEVC ID='C1-ADT Temp 02', QUANTITY='ADIABATIC SURFACE TEMPERATURE', XYZ=7.625,23.25,1.125,
IOR=-2/
&DEVC ID='C1-ADT Temp 03', QUANTITY='ADIABATIC SURFACE TEMPERATURE', XYZ=7.625,23.25,2.125,
IOR=-2/
&DEVC ID='C1-ADT Temp 04', QUANTITY='ADIABATIC SURFACE TEMPERATURE', XYZ=7.625,23.25,3.125,
IOR=-2/
&DEVC ID='C1-ADT Temp 05', QUANTITY='ADIABATIC SURFACE TEMPERATURE', XYZ=7.625,23.25,4.125,
IOR=-2/
&DEVC ID='C1-ADT Temp 06', QUANTITY='ADIABATIC SURFACE TEMPERATURE', XYZ=7.625,23.25,5.125,
IOR=-2/

```

&DEVC ID='C1-ADT Temp 07', QUANTITY='ADIABATIC SURFACE TEMPERATURE', XYZ=7.625,23.25,6.125, IOR=-2/

&DEVC ID='C1-ADT Temp 08', QUANTITY='ADIABATIC SURFACE TEMPERATURE', XYZ=7.625,23.25,7.125, IOR=-2/

&DEVC ID='C1-ADT Temp 09', QUANTITY='ADIABATIC SURFACE TEMPERATURE', XYZ=7.625,23.25,8.125, IOR=-2/

&DEVC ID='C1-ADT Temp 10', QUANTITY='ADIABATIC SURFACE TEMPERATURE', XYZ=7.625,23.25,9.125, IOR=-2/

&DEVC ID='C1-ADT Temp 11', QUANTITY='ADIABATIC SURFACE TEMPERATURE', XYZ=7.625,23.25,10.125, IOR=-2/

&DEVC ID='C1-ADT Temp 12', QUANTITY='ADIABATIC SURFACE TEMPERATURE', XYZ=7.625,23.25,10.75, IOR=-2/

&DEVC ID='C1-IHF Temp 01', QUANTITY='INCIDENT HEAT FLUX', XYZ=7.625,23.25,0.125, IOR=-2/

&DEVC ID='C1-IHF Temp 02', QUANTITY='INCIDENT HEAT FLUX', XYZ=7.625,23.25,1.125, IOR=-2/

&DEVC ID='C1-IHF Temp 03', QUANTITY='INCIDENT HEAT FLUX', XYZ=7.625,23.25,2.125, IOR=-2/

&DEVC ID='C1-IHF Temp 04', QUANTITY='INCIDENT HEAT FLUX', XYZ=7.625,23.25,3.125, IOR=-2/

&DEVC ID='C1-IHF Temp 05', QUANTITY='INCIDENT HEAT FLUX', XYZ=7.625,23.25,4.125, IOR=-2/

&DEVC ID='C1-IHF Temp 06', QUANTITY='INCIDENT HEAT FLUX', XYZ=7.625,23.25,5.125, IOR=-2/

&DEVC ID='C1-IHF Temp 07', QUANTITY='INCIDENT HEAT FLUX', XYZ=7.625,23.25,6.125, IOR=-2/

&DEVC ID='C1-IHF Temp 08', QUANTITY='INCIDENT HEAT FLUX', XYZ=7.625,23.25,7.125, IOR=-2/

&DEVC ID='C1-IHF Temp 09', QUANTITY='INCIDENT HEAT FLUX', XYZ=7.625,23.25,8.125, IOR=-2/

&DEVC ID='C1-IHF Temp 10', QUANTITY='INCIDENT HEAT FLUX', XYZ=7.625,23.25,9.125, IOR=-2/

&DEVC ID='C1-IHF Temp 11', QUANTITY='INCIDENT HEAT FLUX', XYZ=7.625,23.25,10.125, IOR=-2/

&DEVC ID='C1-NHF Temp 01', QUANTITY='NET HEAT FLUX', XYZ=7.625,23.25,0.125, IOR=-2/

&DEVC ID='C1-NHF Temp 02', QUANTITY='NET HEAT FLUX', XYZ=7.625,23.25,1.125, IOR=-2/

&DEVC ID='C1-NHF Temp 03', QUANTITY='NET HEAT FLUX', XYZ=7.625,23.25,2.125, IOR=-2/

&DEVC ID='C1-NHF Temp 04', QUANTITY='NET HEAT FLUX', XYZ=7.625,23.25,3.125, IOR=-2/

&DEVC ID='C1-NHF Temp 05', QUANTITY='NET HEAT FLUX', XYZ=7.625,23.25,4.125, IOR=-2/

&DEVC ID='C1-NHF Temp 06', QUANTITY='NET HEAT FLUX', XYZ=7.625,23.25,5.125, IOR=-2/

&DEVC ID='C1-NHF Temp 07', QUANTITY='NET HEAT FLUX', XYZ=7.625,23.25,6.125, IOR=-2/

&DEVC ID='C1-NHF Temp 08', QUANTITY='NET HEAT FLUX', XYZ=7.625,23.25,7.125, IOR=-2/

&DEVC ID='C1-NHF Temp 09', QUANTITY='NET HEAT FLUX', XYZ=7.625,23.25,8.125, IOR=-2/

&DEVC ID='C1-NHF Temp 10', QUANTITY='NET HEAT FLUX', XYZ=7.625,23.25,9.125, IOR=-2/

&DEVC ID='C1-NHF Temp 11', QUANTITY='NET HEAT FLUX', XYZ=7.625,23.25,10.125, IOR=-2/

&DEVC ID='C1-NHF Temp 12', QUANTITY='NET HEAT FLUX', XYZ=7.625,23.25,10.75, IOR=-2/

&DEVC ID='C1-Wall Temp 01', QUANTITY='WALL TEMPERATURE', XYZ=7.625,23.25,0.125, IOR=-2/

&DEVC ID='C1-Wall Temp 02', QUANTITY='WALL TEMPERATURE', XYZ=7.625,23.25,1.125, IOR=-2/

&DEVC ID='C1-Wall Temp 03', QUANTITY='WALL TEMPERATURE', XYZ=7.625,23.25,2.125, IOR=-2/

&DEVC ID='C1-Wall Temp 04', QUANTITY='WALL TEMPERATURE', XYZ=7.625,23.25,3.125, IOR=-2/

&DEVC ID='C1-Wall Temp 05', QUANTITY='WALL TEMPERATURE', XYZ=7.625,23.25,4.125, IOR=-2/

&DEVC ID='C1-Wall Temp 06', QUANTITY='WALL TEMPERATURE', XYZ=7.625,23.25,5.125, IOR=-2/

&DEVC ID='C1-Wall Temp 07', QUANTITY='WALL TEMPERATURE', XYZ=7.625,23.25,6.125, IOR=-2/
&DEVC ID='C1-Wall Temp 08', QUANTITY='WALL TEMPERATURE', XYZ=7.625,23.25,7.125, IOR=-2/
&DEVC ID='C1-Wall Temp 09', QUANTITY='WALL TEMPERATURE', XYZ=7.625,23.25,8.125, IOR=-2/
&DEVC ID='C1-Wall Temp 10', QUANTITY='WALL TEMPERATURE', XYZ=7.625,23.25,9.125, IOR=-2/
&DEVC ID='C1-Wall Temp 11', QUANTITY='WALL TEMPERATURE', XYZ=7.625,23.25,10.125, IOR=-2/
&DEVC ID='C1-Wall Temp 12', QUANTITY='WALL TEMPERATURE', XYZ=7.625,23.25,10.75, IOR=-2/
&DEVC ID='C1-Back Temp 01', QUANTITY='BACK WALL TEMPERATURE', XYZ=7.625,23.25,0.125, IOR=-2/
&DEVC ID='C1-Back Temp 02', QUANTITY='BACK WALL TEMPERATURE', XYZ=7.625,23.25,1.125, IOR=-2/
&DEVC ID='C1-Back Temp 03', QUANTITY='BACK WALL TEMPERATURE', XYZ=7.625,23.25,2.125, IOR=-2/
&DEVC ID='C1-Back Temp 04', QUANTITY='BACK WALL TEMPERATURE', XYZ=7.625,23.25,3.125, IOR=-2/
&DEVC ID='C1-Back Temp 05', QUANTITY='BACK WALL TEMPERATURE', XYZ=7.625,23.25,4.125, IOR=-2/
&DEVC ID='C1-Back Temp 06', QUANTITY='BACK WALL TEMPERATURE', XYZ=7.625,23.25,5.125, IOR=-2/
&DEVC ID='C1-Back Temp 07', QUANTITY='BACK WALL TEMPERATURE', XYZ=7.625,23.25,6.125, IOR=-2/
&DEVC ID='C1-Back Temp 08', QUANTITY='BACK WALL TEMPERATURE', XYZ=7.625,23.25,7.125, IOR=-2/
&DEVC ID='C1-Back Temp 09', QUANTITY='BACK WALL TEMPERATURE', XYZ=7.625,23.25,8.125, IOR=-2/
&DEVC ID='C1-Back Temp 10', QUANTITY='BACK WALL TEMPERATURE', XYZ=7.625,23.25,9.125, IOR=-2/
&DEVC ID='C1-Back Temp 11', QUANTITY='BACK WALL TEMPERATURE', XYZ=7.625,23.25,10.125, IOR=-2/
&DEVC ID='C1-Back Temp 12', QUANTITY='BACK WALL TEMPERATURE', XYZ=7.625,23.25,10.75, IOR=-2/
&DEVC ID='C1-Gas Temp 01', QUANTITY='GAS TEMPERATURE', XYZ=7.625,23.25,0.125, IOR=-2/
&DEVC ID='C1-Gas Temp 02', QUANTITY='GAS TEMPERATURE', XYZ=7.625,23.25,1.125, IOR=-2/
&DEVC ID='C1-Gas Temp 03', QUANTITY='GAS TEMPERATURE', XYZ=7.625,23.25,2.125, IOR=-2/
&DEVC ID='C1-Gas Temp 04', QUANTITY='GAS TEMPERATURE', XYZ=7.625,23.25,3.125, IOR=-2/
&DEVC ID='C1-Gas Temp 05', QUANTITY='GAS TEMPERATURE', XYZ=7.625,23.25,4.125, IOR=-2/
&DEVC ID='C1-Gas Temp 06', QUANTITY='GAS TEMPERATURE', XYZ=7.625,23.25,5.125, IOR=-2/
&DEVC ID='C1-Gas Temp 07', QUANTITY='GAS TEMPERATURE', XYZ=7.625,23.25,6.125, IOR=-2/
&DEVC ID='C1-Gas Temp 08', QUANTITY='GAS TEMPERATURE', XYZ=7.625,23.25,7.125, IOR=-2/
&DEVC ID='C1-Gas Temp 09', QUANTITY='GAS TEMPERATURE', XYZ=7.625,23.25,8.125, IOR=-2/
&DEVC ID='C1-Gas Temp 10', QUANTITY='GAS TEMPERATURE', XYZ=7.625,23.25,9.125, IOR=-2/
&DEVC ID='C1-Gas Temp 11', QUANTITY='GAS TEMPERATURE', XYZ=7.625,23.25,10.125, IOR=-2/
&DEVC ID='C1-Gas Temp 12', QUANTITY='GAS TEMPERATURE', XYZ=7.625,23.25,10.75, IOR=-2/
&DEVC ID='C1_F2S-ADT Temp 01', QUANTITY='ADIABATIC SURFACE TEMPERATURE', XYZ=7.5,23.375,0.125, IOR=-1/
&DEVC ID='C1_F2S-ADT Temp 02', QUANTITY='ADIABATIC SURFACE TEMPERATURE', XYZ=7.5,23.375,1.125, IOR=-1/
&DEVC ID='C1_F2S-ADT Temp 03', QUANTITY='ADIABATIC SURFACE TEMPERATURE', XYZ=7.5,23.375,2.125, IOR=-1/
&DEVC ID='C1_F2S-ADT Temp 04', QUANTITY='ADIABATIC SURFACE TEMPERATURE', XYZ=7.5,23.375,3.125, IOR=-1/
&DEVC ID='C1_F2S-ADT Temp 05', QUANTITY='ADIABATIC SURFACE TEMPERATURE', XYZ=7.5,23.375,4.125, IOR=-1/

&DEVC ID='C1_F2S-ADT Temp 06', QUANTITY='ADIABATIC SURFACE TEMPERATURE', XYZ=7.5,23.375,5.125, IOR=-1/
&DEVC ID='C1_F2S-ADT Temp 07', QUANTITY='ADIABATIC SURFACE TEMPERATURE', XYZ=7.5,23.375,6.125, IOR=-1/
&DEVC ID='C1_F2S-ADT Temp 08', QUANTITY='ADIABATIC SURFACE TEMPERATURE', XYZ=7.5,23.375,7.125, IOR=-1/
&DEVC ID='C1_F2S-ADT Temp 09', QUANTITY='ADIABATIC SURFACE TEMPERATURE', XYZ=7.5,23.375,8.125, IOR=-1/
&DEVC ID='C1_F2S-ADT Temp 10', QUANTITY='ADIABATIC SURFACE TEMPERATURE', XYZ=7.5,23.375,9.125, IOR=-1/
&DEVC ID='C1_F2S-ADT Temp 11', QUANTITY='ADIABATIC SURFACE TEMPERATURE', XYZ=7.5,23.375,10.125, IOR=-1/
&DEVC ID='C1_F2S-ADT Temp 12', QUANTITY='ADIABATIC SURFACE TEMPERATURE', XYZ=7.5,23.375,10.75, IOR=-1/
&DEVC ID='C1_F2S-Wall Temp 01', QUANTITY='ADIABATIC SURFACE TEMPERATURE', XYZ=7.5,23.375,0.125, IOR=-1/
&DEVC ID='C1_F2S-Wall Temp 02', QUANTITY='WALL TEMPERATURE', XYZ=7.5,23.375,1.125, IOR=-1/
&DEVC ID='C1_F2S-Wall Temp 03', QUANTITY='WALL TEMPERATURE', XYZ=7.5,23.375,2.125, IOR=-1/
&DEVC ID='C1_F2S-Wall Temp 04', QUANTITY='WALL TEMPERATURE', XYZ=7.5,23.375,3.125, IOR=-1/
&DEVC ID='C1_F2S-Wall Temp 05', QUANTITY='WALL TEMPERATURE', XYZ=7.5,23.375,4.125, IOR=-1/
&DEVC ID='C1_F2S-Wall Temp 06', QUANTITY='WALL TEMPERATURE', XYZ=7.5,23.375,5.125, IOR=-1/
&DEVC ID='C1_F2S-Wall Temp 07', QUANTITY='WALL TEMPERATURE', XYZ=7.5,23.375,6.125, IOR=-1/
&DEVC ID='C1_F2S-Wall Temp 08', QUANTITY='WALL TEMPERATURE', XYZ=7.5,23.375,7.125, IOR=-1/
&DEVC ID='C1_F2S-Wall Temp 09', QUANTITY='WALL TEMPERATURE', XYZ=7.5,23.375,8.125, IOR=-1/
&DEVC ID='C1_F2S-Wall Temp 10', QUANTITY='WALL TEMPERATURE', XYZ=7.5,23.375,9.125, IOR=-1/
&DEVC ID='C1_F2S-Wall Temp 11', QUANTITY='WALL TEMPERATURE', XYZ=7.5,23.375,10.125, IOR=-1/
&DEVC ID='C1_F2S-Wall Temp 12', QUANTITY='WALL TEMPERATURE', XYZ=7.5,23.375,10.75, IOR=-1/
&DEVC ID='C1_F4S-ADT Temp 01', QUANTITY='ADIABATIC SURFACE TEMPERATURE', XYZ=7.75,23.375,0.125, IOR=1/
&DEVC ID='C1_F4S-ADT Temp 02', QUANTITY='ADIABATIC SURFACE TEMPERATURE', XYZ=7.75,23.375,1.125, IOR=1/
&DEVC ID='C1_F4S-ADT Temp 03', QUANTITY='ADIABATIC SURFACE TEMPERATURE', XYZ=7.75,23.375,2.125, IOR=1/
&DEVC ID='C1_F4S-ADT Temp 04', QUANTITY='ADIABATIC SURFACE TEMPERATURE', XYZ=7.75,23.375,3.125, IOR=1/
&DEVC ID='C1_F4S-ADT Temp 05', QUANTITY='ADIABATIC SURFACE TEMPERATURE', XYZ=7.75,23.375,4.125, IOR=1/
&DEVC ID='C1_F4S-ADT Temp 06', QUANTITY='ADIABATIC SURFACE TEMPERATURE', XYZ=7.75,23.375,5.125, IOR=1/
&DEVC ID='C1_F4S-ADT Temp 07', QUANTITY='ADIABATIC SURFACE TEMPERATURE', XYZ=7.75,23.375,6.125, IOR=1/
&DEVC ID='C1_F4S-ADT Temp 08', QUANTITY='ADIABATIC SURFACE TEMPERATURE', XYZ=7.75,23.375,7.125, IOR=1/
&DEVC ID='C1_F4S-ADT Temp 09', QUANTITY='ADIABATIC SURFACE TEMPERATURE', XYZ=7.75,23.375,8.125, IOR=1/

&DEVC ID='C1_F4S-ADT Temp 10', QUANTITY='ADIABATIC SURFACE TEMPERATURE', XYZ=7.75,23.375,9.125, IOR=1/

&DEVC ID='C1_F4S-ADT Temp 11', QUANTITY='ADIABATIC SURFACE TEMPERATURE', XYZ=7.75,23.375,10.125, IOR=1/

&DEVC ID='C1_F4S-ADT Temp 12', QUANTITY='ADIABATIC SURFACE TEMPERATURE', XYZ=7.75,23.375,10.75, IOR=1/

&DEVC ID='C1_F4S-Wall Temp 01', QUANTITY='WALL TEMPERATURE', XYZ=7.75,23.375,0.125, IOR=1/

&DEVC ID='C1_F4S-Wall Temp 02', QUANTITY='WALL TEMPERATURE', XYZ=7.75,23.375,1.125, IOR=1/

&DEVC ID='C1_F4S-Wall Temp 03', QUANTITY='WALL TEMPERATURE', XYZ=7.75,23.375,2.125, IOR=1/

&DEVC ID='C1_F4S-Wall Temp 04', QUANTITY='WALL TEMPERATURE', XYZ=7.75,23.375,3.125, IOR=1/

&DEVC ID='C1_F4S-Wall Temp 05', QUANTITY='WALL TEMPERATURE', XYZ=7.75,23.375,4.125, IOR=1/

&DEVC ID='C1_F4S-Wall Temp 06', QUANTITY='WALL TEMPERATURE', XYZ=7.75,23.375,5.125, IOR=1/

&DEVC ID='C1_F4S-Wall Temp 07', QUANTITY='WALL TEMPERATURE', XYZ=7.75,23.375,6.125, IOR=1/

&DEVC ID='C1_F4S-Wall Temp 08', QUANTITY='WALL TEMPERATURE', XYZ=7.75,23.375,7.125, IOR=1/

&DEVC ID='C1_F4S-Wall Temp 09', QUANTITY='WALL TEMPERATURE', XYZ=7.75,23.375,8.125, IOR=1/

&DEVC ID='C1_F4S-Wall Temp 10', QUANTITY='WALL TEMPERATURE', XYZ=7.75,23.375,9.125, IOR=1/

&DEVC ID='C1_F4S-Wall Temp 11', QUANTITY='WALL TEMPERATURE', XYZ=7.75,23.375,10.125, IOR=1/

&DEVC ID='C1_F4S-Wall Temp 12', QUANTITY='WALL TEMPERATURE', XYZ=7.75,23.375,10.75, IOR=1/

&DEVC ID='C1_F3B-Wall Temp 01', QUANTITY='WALL TEMPERATURE', XYZ=7.625,23.5,0.125, IOR=2/

&DEVC ID='C1_F3B-Wall Temp 02', QUANTITY='WALL TEMPERATURE', XYZ=7.625,23.5,1.125, IOR=2/

&DEVC ID='C1_F3B-Wall Temp 03', QUANTITY='WALL TEMPERATURE', XYZ=7.625,23.5,2.125, IOR=2/

&DEVC ID='C1_F3B-Wall Temp 04', QUANTITY='WALL TEMPERATURE', XYZ=7.625,23.5,3.125, IOR=2/

&DEVC ID='C1_F3B-Wall Temp 05', QUANTITY='WALL TEMPERATURE', XYZ=7.625,23.5,4.125, IOR=2/

&DEVC ID='C1_F3B-Wall Temp 06', QUANTITY='WALL TEMPERATURE', XYZ=7.625,23.5,5.125, IOR=2/

&DEVC ID='C1_F3B-Wall Temp 07', QUANTITY='WALL TEMPERATURE', XYZ=7.625,23.5,6.125, IOR=2/

&DEVC ID='C1_F3B-Wall Temp 08', QUANTITY='WALL TEMPERATURE', XYZ=7.625,23.5,7.125, IOR=2/

&DEVC ID='C1_F3B-Wall Temp 09', QUANTITY='WALL TEMPERATURE', XYZ=7.625,23.5,8.125, IOR=2/

&DEVC ID='C1_F3B-Wall Temp 10', QUANTITY='WALL TEMPERATURE', XYZ=7.625,23.5,9.125, IOR=2/

&DEVC ID='C1_F3B-Wall Temp 11', QUANTITY='WALL TEMPERATURE', XYZ=7.625,23.5,10.125, IOR=2/

&DEVC ID='C1_F3B-Wall Temp 12', QUANTITY='WALL TEMPERATURE', XYZ=7.625,23.5,10.75, IOR=2/

&DEVC ID='C1_F3B-ADTI Temp 01', QUANTITY='ADIABATIC SURFACE TEMPERATURE', XYZ=7.625,23.5,0.125, IOR=2/

&DEVC ID='C1_F3B-ADTI Temp 02', QUANTITY='ADIABATIC SURFACE TEMPERATURE', XYZ=7.625,23.5,1.125, IOR=2/

&DEVC ID='C1_F3B-ADTI Temp 03', QUANTITY='ADIABATIC SURFACE TEMPERATURE', XYZ=7.625,23.5,2.125, IOR=2/

&DEVC ID='C1_F3B-ADTI Temp 04', QUANTITY='ADIABATIC SURFACE TEMPERATURE', XYZ=7.625,23.5,3.125, IOR=2/

&DEVC ID='C1_F3B-ADTI Temp 05', QUANTITY='ADIABATIC SURFACE TEMPERATURE', XYZ=7.625,23.5,4.125, IOR=2/

&DEVC ID='C1_F3B-ADTI Temp 06', QUANTITY='ADIABATIC SURFACE TEMPERATURE', XYZ=7.625,23.5,5.125, IOR=2/

&DEVC ID='C1_F3B-ADTI Temp 07', QUANTITY='ADIABATIC SURFACE TEMPERATURE', XYZ=7.625,23.5,6.125, IOR=-2/

&DEVC ID='C1_F3B-ADTI Temp 08', QUANTITY='ADIABATIC SURFACE TEMPERATURE', XYZ=7.625,23.5,7.125, IOR=-2/

&DEVC ID='C1_F3B-ADTI Temp 09', QUANTITY='ADIABATIC SURFACE TEMPERATURE', XYZ=7.625,23.5,8.125, IOR=-2/

&DEVC ID='C1_F3B-ADTI Temp 10', QUANTITY='ADIABATIC SURFACE TEMPERATURE', XYZ=7.625,23.5,9.125, IOR=-2/

&DEVC ID='C1_F3B-ADTI Temp 11', QUANTITY='ADIABATIC SURFACE TEMPERATURE', XYZ=7.625,23.5,10.125, IOR=-2/

&DEVC ID='C1_F3B-ADTI Temp 12', QUANTITY='ADIABATIC SURFACE TEMPERATURE', XYZ=7.625,23.5,10.75, IOR=-2/

&DEVC ID='C2-Gas Temp 01', QUANTITY='GAS TEMPERATURE', XYZ=12.875,23.25,0.125, IOR=-2/

&DEVC ID='C2-Gas Temp 02', QUANTITY='GAS TEMPERATURE', XYZ=12.875,23.25,1.125, IOR=-2/

&DEVC ID='C2-Gas Temp 03', QUANTITY='GAS TEMPERATURE', XYZ=12.875,23.25,2.125, IOR=-2/

&DEVC ID='C2-Gas Temp 04', QUANTITY='GAS TEMPERATURE', XYZ=12.875,23.25,3.125, IOR=-2/

&DEVC ID='C2-Gas Temp 05', QUANTITY='GAS TEMPERATURE', XYZ=12.875,23.25,4.125, IOR=-2/

&DEVC ID='C2-Gas Temp 06', QUANTITY='GAS TEMPERATURE', XYZ=12.875,23.25,5.125, IOR=-2/

&DEVC ID='C2-Gas Temp 07', QUANTITY='GAS TEMPERATURE', XYZ=12.875,23.25,6.125, IOR=-2/

&DEVC ID='C2-Gas Temp 08', QUANTITY='GAS TEMPERATURE', XYZ=12.875,23.25,7.125, IOR=-2/

&DEVC ID='C2-Gas Temp 09', QUANTITY='GAS TEMPERATURE', XYZ=12.875,23.25,8.125, IOR=-2/

&DEVC ID='C2-Gas Temp 10', QUANTITY='GAS TEMPERATURE', XYZ=12.875,23.25,9.125, IOR=-2/

&DEVC ID='C2-Gas Temp 11', QUANTITY='GAS TEMPERATURE', XYZ=12.875,23.25,10.125, IOR=-2/

&DEVC ID='C2-Gas Temp 12', QUANTITY='GAS TEMPERATURE', XYZ=12.875,23.25,10.75, IOR=-2/

&DEVC ID='C2-Wall Temp 01', QUANTITY='WALL TEMPERATURE', XYZ=12.875,23.25,0.125, IOR=-2/

&DEVC ID='C2-Wall Temp 02', QUANTITY='WALL TEMPERATURE', XYZ=12.875,23.25,1.125, IOR=-2/

&DEVC ID='C2-Wall Temp 03', QUANTITY='WALL TEMPERATURE', XYZ=12.875,23.25,2.125, IOR=-2/

&DEVC ID='C2-Wall Temp 04', QUANTITY='WALL TEMPERATURE', XYZ=12.875,23.25,3.125, IOR=-2/

&DEVC ID='C2-Wall Temp 05', QUANTITY='WALL TEMPERATURE', XYZ=12.875,23.25,4.125, IOR=-2/

&DEVC ID='C2-Wall Temp 06', QUANTITY='WALL TEMPERATURE', XYZ=12.875,23.25,5.125, IOR=-2/

&DEVC ID='C2-Wall Temp 07', QUANTITY='WALL TEMPERATURE', XYZ=12.875,23.25,6.125, IOR=-2/

&DEVC ID='C2-Wall Temp 08', QUANTITY='WALL TEMPERATURE', XYZ=12.875,23.25,7.125, IOR=-2/

&DEVC ID='C2-Wall Temp 09', QUANTITY='WALL TEMPERATURE', XYZ=12.875,23.25,8.125, IOR=-2/

&DEVC ID='C2-Wall Temp 10', QUANTITY='WALL TEMPERATURE', XYZ=12.875,23.25,9.125, IOR=-2/

&DEVC ID='C2-Wall Temp 11', QUANTITY='WALL TEMPERATURE', XYZ=12.875,23.25,10.125, IOR=-2/

&DEVC ID='C2-Wall Temp 12', QUANTITY='WALL TEMPERATURE', XYZ=12.875,23.25,10.75, IOR=-2/

&DEVC ID='C2-ADT Temp 01', QUANTITY='ADIABATIC SURFACE TEMPERATURE', XYZ=12.875,23.25,0.125, IOR=-2/

&DEVC ID='C2-ADT Temp 02', QUANTITY='ADIABATIC SURFACE TEMPERATURE', XYZ=12.875,23.25,1.125, IOR=-2/

&DEVC ID='C2-ADT Temp 03', QUANTITY='ADIABATIC SURFACE TEMPERATURE', XYZ=12.875,23.25,2.125, IOR=-2/

&DEVC ID='C2-ADT Temp 04', QUANTITY='ADIABATIC SURFACE TEMPERATURE', XYZ=12.875,23.25,3.125, IOR=-2/
&DEVC ID='C2-ADT Temp 05', QUANTITY='ADIABATIC SURFACE TEMPERATURE', XYZ=12.875,23.25,4.125, IOR=-2/
&DEVC ID='C2-ADT Temp 06', QUANTITY='ADIABATIC SURFACE TEMPERATURE', XYZ=12.875,23.25,5.125, IOR=-2/
&DEVC ID='C2-ADT Temp 07', QUANTITY='ADIABATIC SURFACE TEMPERATURE', XYZ=12.875,23.25,6.125, IOR=-2/
&DEVC ID='C2-ADT Temp 08', QUANTITY='ADIABATIC SURFACE TEMPERATURE', XYZ=12.875,23.25,7.125, IOR=-2/
&DEVC ID='C2-ADT Temp 09', QUANTITY='ADIABATIC SURFACE TEMPERATURE', XYZ=12.875,23.25,8.125, IOR=-2/
&DEVC ID='C2-ADT Temp 10', QUANTITY='ADIABATIC SURFACE TEMPERATURE', XYZ=12.875,23.25,9.125, IOR=-2/
&DEVC ID='C2-ADT Temp 11', QUANTITY='ADIABATIC SURFACE TEMPERATURE', XYZ=12.875,23.25,10.125, IOR=-2/
&DEVC ID='C2-ADT Temp 12', QUANTITY='ADIABATIC SURFACE TEMPERATURE', XYZ=12.875,23.25,10.75, IOR=-2/
&DEVC ID='C3-Wall Temp 01', QUANTITY='WALL TEMPERATURE', XYZ=18.125,23.25,0.125, IOR=-2/
&DEVC ID='C3-Wall Temp 02', QUANTITY='WALL TEMPERATURE', XYZ=18.125,23.25,1.125, IOR=-2/
&DEVC ID='C3-Wall Temp 03', QUANTITY='WALL TEMPERATURE', XYZ=18.125,23.25,2.125, IOR=-2/
&DEVC ID='C3-Wall Temp 04', QUANTITY='WALL TEMPERATURE', XYZ=18.125,23.25,3.125, IOR=-2/
&DEVC ID='C3-Wall Temp 05', QUANTITY='WALL TEMPERATURE', XYZ=18.125,23.25,4.125, IOR=-2/
&DEVC ID='C3-Wall Temp 06', QUANTITY='WALL TEMPERATURE', XYZ=18.125,23.25,5.125, IOR=-2/
&DEVC ID='C3-Wall Temp 07', QUANTITY='WALL TEMPERATURE', XYZ=18.125,23.25,6.125, IOR=-2/
&DEVC ID='C3-Wall Temp 08', QUANTITY='WALL TEMPERATURE', XYZ=18.125,23.25,7.125, IOR=-2/
&DEVC ID='C3-Wall Temp 09', QUANTITY='WALL TEMPERATURE', XYZ=18.125,23.25,8.125, IOR=-2/
&DEVC ID='C3-Wall Temp 10', QUANTITY='WALL TEMPERATURE', XYZ=18.125,23.25,9.125, IOR=-2/
&DEVC ID='C3-Wall Temp 11', QUANTITY='WALL TEMPERATURE', XYZ=18.125,23.25,10.125, IOR=-2/
&DEVC ID='C3-Wall Temp 12', QUANTITY='WALL TEMPERATURE', XYZ=18.125,23.25,10.75, IOR=-2/
&DEVC ID='C3-ADT Temp 01', QUANTITY='ADIABATIC SURFACE TEMPERATURE', XYZ=18.125,23.25,0.125, IOR=-2/
&DEVC ID='C3-ADT Temp 02', QUANTITY='ADIABATIC SURFACE TEMPERATURE', XYZ=18.125,23.25,1.125, IOR=-2/
&DEVC ID='C3-ADT Temp 03', QUANTITY='ADIABATIC SURFACE TEMPERATURE', XYZ=18.125,23.25,2.125, IOR=-2/
&DEVC ID='C3-ADT Temp 04', QUANTITY='ADIABATIC SURFACE TEMPERATURE', XYZ=18.125,23.25,3.125, IOR=-2/
&DEVC ID='C3-ADT Temp 05', QUANTITY='ADIABATIC SURFACE TEMPERATURE', XYZ=18.125,23.25,4.125, IOR=-2/
&DEVC ID='C3-ADT Temp 06', QUANTITY='ADIABATIC SURFACE TEMPERATURE', XYZ=18.125,23.25,5.125, IOR=-2/
&DEVC ID='C3-ADT Temp 07', QUANTITY='ADIABATIC SURFACE TEMPERATURE', XYZ=18.125,23.25,6.125, IOR=-2/

&DEVC ID='C3-ADT Temp 08', QUANTITY='ADIABATIC SURFACE TEMPERATURE', XYZ=18.125,23.25,7.125,
IOR=-2/

&DEVC ID='C3-ADT Temp 09', QUANTITY='ADIABATIC SURFACE TEMPERATURE', XYZ=18.125,23.25,8.125,
IOR=-2/

&DEVC ID='C3-ADT Temp 10', QUANTITY='ADIABATIC SURFACE TEMPERATURE', XYZ=18.125,23.25,9.125,
IOR=-2/

&DEVC ID='C3-ADT Temp 11', QUANTITY='ADIABATIC SURFACE TEMPERATURE', XYZ=18.125,23.25,10.125,
IOR=-2/

&DEVC ID='C3-ADT Temp 12', QUANTITY='ADIABATIC SURFACE TEMPERATURE', XYZ=18.125,23.25,10.75,
IOR=-2/

&DEVC ID='WC1-GAS 01', QUANTITY='TEMPERATURE', XYZ=7.5,21.75,1.55/

&DEVC ID='WC1-GAS 02', QUANTITY='TEMPERATURE', XYZ=7.5,21.75,2.0/

&DEVC ID='WC1-GAS 03', QUANTITY='TEMPERATURE', XYZ=7.5,21.75,2.5/

&DEVC ID='WC1-GAS 04', QUANTITY='TEMPERATURE', XYZ=7.5,21.75,3.0/

&DEVC ID='WC1-GAS 05', QUANTITY='TEMPERATURE', XYZ=7.5,21.75,3.5/

&DEVC ID='WC1-GAS 06', QUANTITY='TEMPERATURE', XYZ=7.5,21.75,4.0/

&DEVC ID='WC1-GAS 07', QUANTITY='TEMPERATURE', XYZ=7.5,21.75,4.5/

&DEVC ID='WC1-GAS 08', QUANTITY='TEMPERATURE', XYZ=7.5,21.75,5.0/

&DEVC ID='WC1-GAS 09', QUANTITY='TEMPERATURE', XYZ=7.5,21.75,5.5/

&DEVC ID='WC1-GAS 10', QUANTITY='TEMPERATURE', XYZ=7.5,21.75,6.0/

&DEVC ID='WC1-GAS 11', QUANTITY='TEMPERATURE', XYZ=7.5,21.75,6.5/

&DEVC ID='WC1-GAS 12', QUANTITY='TEMPERATURE', XYZ=7.5,21.75,7.0/

&DEVC ID='WC1-GAS 13', QUANTITY='TEMPERATURE', XYZ=7.5,21.75,7.5/

&DEVC ID='WC1-GAS 14', QUANTITY='TEMPERATURE', XYZ=7.5,21.75,8.0/

&DEVC ID='WC1-GAS 15', QUANTITY='TEMPERATURE', XYZ=7.5,21.75,8.5/

&DEVC ID='WC1-GAS 16', QUANTITY='TEMPERATURE', XYZ=7.5,21.75,9.0/

&DEVC ID='WC1-GAS 17', QUANTITY='TEMPERATURE', XYZ=7.5,21.75,9.5/

&DEVC ID='WC1-GAS 18', QUANTITY='TEMPERATURE', XYZ=7.5,21.75,10.0/

&DEVC ID='WC1-GAS 19', QUANTITY='TEMPERATURE', XYZ=7.5,21.75,10.5/

&DEVC ID='WC1-GAS 20', QUANTITY='TEMPERATURE', XYZ=7.5,21.75,10.75/

&DEVC ID='WC2-GAS 01', QUANTITY='TEMPERATURE', XYZ=9.375,21.625,1.55/

&DEVC ID='WC2-GAS 02', QUANTITY='TEMPERATURE', XYZ=9.375,21.625,2.0/

&DEVC ID='WC2-GAS 03', QUANTITY='TEMPERATURE', XYZ=9.375,21.625,2.5/

&DEVC ID='WC2-GAS 04', QUANTITY='TEMPERATURE', XYZ=9.375,21.625,3.0/

&DEVC ID='WC2-GAS 05', QUANTITY='TEMPERATURE', XYZ=9.375,21.625,3.5/

&DEVC ID='WC2-GAS 06', QUANTITY='TEMPERATURE', XYZ=9.375,21.625,4.0/

&DEVC ID='WC2-GAS 07', QUANTITY='TEMPERATURE', XYZ=9.375,21.625,4.5/

&DEVC ID='WC2-GAS 08', QUANTITY='TEMPERATURE', XYZ=9.375,21.625,5.0/

&DEVC ID='WC2-GAS 09', QUANTITY='TEMPERATURE', XYZ=9.375,21.625,5.5/

&DEVC ID='WC2-GAS 10', QUANTITY='TEMPERATURE', XYZ=9.375,21.625,6.0/

&DEVC ID='WC2-GAS 11', QUANTITY='TEMPERATURE', XYZ=9.375,21.625,6.5/
&DEVC ID='WC2-GAS 12', QUANTITY='TEMPERATURE', XYZ=9.375,21.625,7.0/
&DEVC ID='WC2-GAS 13', QUANTITY='TEMPERATURE', XYZ=9.375,21.625,7.5/
&DEVC ID='WC2-GAS 14', QUANTITY='TEMPERATURE', XYZ=9.375,21.625,8.0/
&DEVC ID='WC2-GAS 15', QUANTITY='TEMPERATURE', XYZ=9.375,21.625,8.5/
&DEVC ID='WC2-GAS 16', QUANTITY='TEMPERATURE', XYZ=9.375,21.625,9.0/
&DEVC ID='WC2-GAS 17', QUANTITY='TEMPERATURE', XYZ=9.375,21.625,9.5/
&DEVC ID='WC2-GAS 18', QUANTITY='TEMPERATURE', XYZ=9.375,21.625,10.0/
&DEVC ID='WC2-GAS 19', QUANTITY='TEMPERATURE', XYZ=9.375,21.625,10.5/
&DEVC ID='WC2-GAS 20', QUANTITY='TEMPERATURE', XYZ=9.375,21.625,10.75/
&DEVC ID='LayGASC1 01', QUANTITY='TEMPERATURE', XYZ=7.625,23.25,10.75, ORIENTATION=0.0,-1.0,0.0/
&DEVC ID='LayGASC1 02', QUANTITY='TEMPERATURE', XYZ=7.625,22.75,10.75, ORIENTATION=0.0,-1.0,0.0/
&DEVC ID='LayGASC1 03', QUANTITY='TEMPERATURE', XYZ=7.625,22.25,10.75, ORIENTATION=0.0,-1.0,0.0/
&DEVC ID='LayGASC1 Z 03', QUANTITY='TEMPERATURE', XYZ=7.625,22.25,10.75/
&DEVC ID='LayGASC1 04', QUANTITY='TEMPERATURE', XYZ=7.625,21.75,10.75, ORIENTATION=0.0,-1.0,0.0/
&DEVC ID='LayGASC1 05', QUANTITY='TEMPERATURE', XYZ=7.625,21.25,10.75, ORIENTATION=0.0,-1.0,0.0/
&DEVC ID='LayGASC1 06', QUANTITY='TEMPERATURE', XYZ=7.625,20.75,10.75, ORIENTATION=0.0,-1.0,0.0/
&DEVC ID='LayGASC1 07', QUANTITY='TEMPERATURE', XYZ=7.625,20.25,10.75, ORIENTATION=0.0,-1.0,0.0/
&DEVC ID='LayGASC1 08', QUANTITY='TEMPERATURE', XYZ=7.625,19.75,10.75, ORIENTATION=0.0,-1.0,0.0/
&DEVC ID='LayGASC1 09', QUANTITY='TEMPERATURE', XYZ=7.625,19.25,10.75, ORIENTATION=0.0,-1.0,0.0/
&DEVC ID='LayGASC1 10', QUANTITY='TEMPERATURE', XYZ=7.625,16.0,10.75, ORIENTATION=0.0,-1.0,0.0/
&DEVC ID='LayGASC1 11', QUANTITY='TEMPERATURE', XYZ=7.625,15.0,10.75, ORIENTATION=0.0,-1.0,0.0/
&DEVC ID='LayGASC1 12', QUANTITY='TEMPERATURE', XYZ=7.625,14.0,10.75, ORIENTATION=0.0,-1.0,0.0/
&DEVC ID='LayGASC1 13', QUANTITY='TEMPERATURE', XYZ=7.625,9.0,10.75, ORIENTATION=0.0,-1.0,0.0/
&DEVC ID='LayGASC1 14', QUANTITY='TEMPERATURE', XYZ=7.625,4.0,10.75, ORIENTATION=0.0,-1.0,0.0/
&DEVC ID='LayGASC2 01', QUANTITY='TEMPERATURE', XYZ=13.125,23.25,10.75, ORIENTATION=0.0,-1.0,0.0/
&DEVC ID='LayGASC2 02', QUANTITY='TEMPERATURE', XYZ=13.125,22.75,10.75, ORIENTATION=0.0,-1.0,0.0/
&DEVC ID='LayGASC2 03', QUANTITY='TEMPERATURE', XYZ=13.125,22.25,10.75, ORIENTATION=0.0,-1.0,0.0/
&DEVC ID='LayGASC2 04', QUANTITY='TEMPERATURE', XYZ=13.125,21.75,10.75, ORIENTATION=0.0,-1.0,0.0/
&DEVC ID='LayGASC2 05', QUANTITY='TEMPERATURE', XYZ=13.125,21.25,10.75, ORIENTATION=0.0,-1.0,0.0/
&DEVC ID='LayGASC2 06', QUANTITY='TEMPERATURE', XYZ=13.125,20.75,10.75, ORIENTATION=0.0,-1.0,0.0/
&DEVC ID='LayGASC2 07', QUANTITY='TEMPERATURE', XYZ=13.125,20.25,10.75, ORIENTATION=0.0,-1.0,0.0/
&DEVC ID='LayGASC2 08', QUANTITY='TEMPERATURE', XYZ=13.125,19.75,10.75, ORIENTATION=0.0,-1.0,0.0/
&DEVC ID='LayGASC2 09', QUANTITY='TEMPERATURE', XYZ=13.125,19.25,10.75, ORIENTATION=0.0,-1.0,0.0/
&DEVC ID='LayGASC2 10', QUANTITY='TEMPERATURE', XYZ=13.125,16.0,10.75, ORIENTATION=0.0,-1.0,0.0/
&DEVC ID='LayGASC2 11', QUANTITY='TEMPERATURE', XYZ=13.125,15.0,10.75, ORIENTATION=0.0,-1.0,0.0/
&DEVC ID='LayGASC2 12', QUANTITY='TEMPERATURE', XYZ=13.125,14.0,10.75, ORIENTATION=0.0,-1.0,0.0/
&DEVC ID='LayGASC2 13', QUANTITY='TEMPERATURE', XYZ=13.125,9.0,10.75, ORIENTATION=0.0,-1.0,0.0/

&DEVC ID='LayGASC2 14', QUANTITY='TEMPERATURE', XYZ=13.125,4.0,10.75, ORIENTATION=0.0,-1.0,0.0/

&MATL ID='wood',

SPECIFIC_HEAT_RAMP='wood_SPECIFIC_HEAT_RAMP',
CONDUCTIVITY_RAMP='wood_CONDUCTIVITY_RAMP',
DENSITY=380.0,
EMISSIVITY=0.8,
HEAT_OF_COMBUSTION=1.42E4/

&RAMP ID='wood_SPECIFIC_HEAT_RAMP', T=20.0, F=1.53/

&RAMP ID='wood_SPECIFIC_HEAT_RAMP', T=98.0, F=1.77/

&RAMP ID='wood_SPECIFIC_HEAT_RAMP', T=99.0, F=13.6/

&RAMP ID='wood_SPECIFIC_HEAT_RAMP', T=119.0, F=13.5/

&RAMP ID='wood_SPECIFIC_HEAT_RAMP', T=120.0, F=2.12/

&RAMP ID='wood_SPECIFIC_HEAT_RAMP', T=200.0, F=2.0/

&RAMP ID='wood_SPECIFIC_HEAT_RAMP', T=250.0, F=1.62/

&RAMP ID='wood_SPECIFIC_HEAT_RAMP', T=300.0, F=0.71/

&RAMP ID='wood_SPECIFIC_HEAT_RAMP', T=350.0, F=0.85/

&RAMP ID='wood_SPECIFIC_HEAT_RAMP', T=400.0, F=1.0/

&RAMP ID='wood_SPECIFIC_HEAT_RAMP', T=600.0, F=1.4/

&RAMP ID='wood_SPECIFIC_HEAT_RAMP', T=800.0, F=1.65/

&RAMP ID='wood_SPECIFIC_HEAT_RAMP', T=1200.0, F=1.65/

&RAMP ID='wood_CONDUCTIVITY_RAMP', T=20.0, F=0.12/

&RAMP ID='wood_CONDUCTIVITY_RAMP', T=200.0, F=0.15/

&RAMP ID='wood_CONDUCTIVITY_RAMP', T=350.0, F=0.07/

&RAMP ID='wood_CONDUCTIVITY_RAMP', T=500.0, F=0.09/

&RAMP ID='wood_CONDUCTIVITY_RAMP', T=800.0, F=0.35/

&RAMP ID='wood_CONDUCTIVITY_RAMP', T=1200.0, F=1.5/

&SURF ID='Surface220cm',

RGB=19,240,32,

HRRPUA=100.0,

IGNITION_TEMPERATURE=300.0,

MATL_ID(1,1)='wood',

MATL_MASS_FRACTION(1,1)=1.0,

THICKNESS(1)=0.22/

&SURF ID='Surface300cm',

RGB=96,63,198,

HRRPUA=100.0,

IGNITION_TEMPERATURE=300.0,
MATL_ID(1,1)='wood',
MATL_MASS_FRACTION(1,1)=1.0,
THICKNESS(1)=0.25/
&SURF ID='Woodcrib',
COLOR='RED',
HRRPUA=1.0,
RAMP_Q='Woodcrib_RAMP_Q',
TMP_FRONT=300.0/
&RAMP ID='Woodcrib_RAMP_Q', T=0.0, F=0.0/
&RAMP ID='Woodcrib_RAMP_Q', T=5.0, F=0.167857/
&RAMP ID='Woodcrib_RAMP_Q', T=10.0, F=0.671429/
&RAMP ID='Woodcrib_RAMP_Q', T=15.0, F=1.510714/
&RAMP ID='Woodcrib_RAMP_Q', T=20.0, F=2.685714/
&RAMP ID='Woodcrib_RAMP_Q', T=25.0, F=4.196429/
&RAMP ID='Woodcrib_RAMP_Q', T=30.0, F=6.042857/
&RAMP ID='Woodcrib_RAMP_Q', T=35.0, F=8.225/
&RAMP ID='Woodcrib_RAMP_Q', T=40.0, F=10.742857/
&RAMP ID='Woodcrib_RAMP_Q', T=45.0, F=13.596429/
&RAMP ID='Woodcrib_RAMP_Q', T=50.0, F=16.785714/
&RAMP ID='Woodcrib_RAMP_Q', T=55.0, F=20.310714/
&RAMP ID='Woodcrib_RAMP_Q', T=60.0, F=24.171429/
&RAMP ID='Woodcrib_RAMP_Q', T=65.0, F=28.367857/
&RAMP ID='Woodcrib_RAMP_Q', T=70.0, F=32.9/
&RAMP ID='Woodcrib_RAMP_Q', T=75.0, F=37.767857/
&RAMP ID='Woodcrib_RAMP_Q', T=80.0, F=42.971429/
&RAMP ID='Woodcrib_RAMP_Q', T=85.0, F=48.510714/
&RAMP ID='Woodcrib_RAMP_Q', T=90.0, F=54.385714/
&RAMP ID='Woodcrib_RAMP_Q', T=95.0, F=60.596429/
&RAMP ID='Woodcrib_RAMP_Q', T=100.0, F=67.142857/
&RAMP ID='Woodcrib_RAMP_Q', T=105.0, F=74.025/
&RAMP ID='Woodcrib_RAMP_Q', T=110.0, F=81.242857/
&RAMP ID='Woodcrib_RAMP_Q', T=115.0, F=88.796429/
&RAMP ID='Woodcrib_RAMP_Q', T=120.0, F=96.685714/
&RAMP ID='Woodcrib_RAMP_Q', T=125.0, F=104.910714/
&RAMP ID='Woodcrib_RAMP_Q', T=130.0, F=113.471429/
&RAMP ID='Woodcrib_RAMP_Q', T=135.0, F=122.367857/
&RAMP ID='Woodcrib_RAMP_Q', T=140.0, F=131.6/

&RAMP ID='Woodcrib_RAMP_Q', T=145.0, F=141.167857/
&RAMP ID='Woodcrib_RAMP_Q', T=150.0, F=151.071429/
&RAMP ID='Woodcrib_RAMP_Q', T=155.0, F=161.310714/
&RAMP ID='Woodcrib_RAMP_Q', T=160.0, F=171.885714/
&RAMP ID='Woodcrib_RAMP_Q', T=165.0, F=182.796429/
&RAMP ID='Woodcrib_RAMP_Q', T=170.0, F=194.042857/
&RAMP ID='Woodcrib_RAMP_Q', T=175.0, F=205.625/
&RAMP ID='Woodcrib_RAMP_Q', T=180.0, F=217.542857/
&RAMP ID='Woodcrib_RAMP_Q', T=185.0, F=229.796429/
&RAMP ID='Woodcrib_RAMP_Q', T=190.0, F=242.385714/
&RAMP ID='Woodcrib_RAMP_Q', T=195.0, F=255.310714/
&RAMP ID='Woodcrib_RAMP_Q', T=200.0, F=268.571429/
&RAMP ID='Woodcrib_RAMP_Q', T=205.0, F=282.167857/
&RAMP ID='Woodcrib_RAMP_Q', T=210.0, F=296.1/
&RAMP ID='Woodcrib_RAMP_Q', T=215.0, F=310.367857/
&RAMP ID='Woodcrib_RAMP_Q', T=220.0, F=324.971429/
&RAMP ID='Woodcrib_RAMP_Q', T=225.0, F=339.910714/
&RAMP ID='Woodcrib_RAMP_Q', T=230.0, F=355.185714/
&RAMP ID='Woodcrib_RAMP_Q', T=235.0, F=370.796429/
&RAMP ID='Woodcrib_RAMP_Q', T=240.0, F=386.742857/
&RAMP ID='Woodcrib_RAMP_Q', T=245.0, F=403.025/
&RAMP ID='Woodcrib_RAMP_Q', T=250.0, F=419.642857/
&RAMP ID='Woodcrib_RAMP_Q', T=255.0, F=436.596429/
&RAMP ID='Woodcrib_RAMP_Q', T=260.0, F=453.885714/
&RAMP ID='Woodcrib_RAMP_Q', T=265.0, F=471.510714/
&RAMP ID='Woodcrib_RAMP_Q', T=270.0, F=489.471429/
&RAMP ID='Woodcrib_RAMP_Q', T=275.0, F=507.767857/
&RAMP ID='Woodcrib_RAMP_Q', T=280.0, F=526.4/
&RAMP ID='Woodcrib_RAMP_Q', T=285.0, F=545.367857/
&RAMP ID='Woodcrib_RAMP_Q', T=290.0, F=564.671429/
&RAMP ID='Woodcrib_RAMP_Q', T=295.0, F=571.428571/
&RAMP ID='Woodcrib_RAMP_Q', T=300.0, F=571.428571/
&RAMP ID='Woodcrib_RAMP_Q', T=305.0, F=571.428571/
&RAMP ID='Woodcrib_RAMP_Q', T=310.0, F=571.428571/
&RAMP ID='Woodcrib_RAMP_Q', T=315.0, F=571.428571/
&RAMP ID='Woodcrib_RAMP_Q', T=320.0, F=571.428571/
&RAMP ID='Woodcrib_RAMP_Q', T=325.0, F=571.428571/
&RAMP ID='Woodcrib_RAMP_Q', T=330.0, F=571.428571/

&RAMP ID='Woodcrib_RAMP_Q', T=715.0, F=571.428571/
&RAMP ID='Woodcrib_RAMP_Q', T=720.0, F=571.428571/
&RAMP ID='Woodcrib_RAMP_Q', T=725.0, F=571.428571/
&RAMP ID='Woodcrib_RAMP_Q', T=730.0, F=571.428571/
&RAMP ID='Woodcrib_RAMP_Q', T=735.0, F=571.428571/
&RAMP ID='Woodcrib_RAMP_Q', T=740.0, F=571.428571/
&RAMP ID='Woodcrib_RAMP_Q', T=745.0, F=571.428571/
&RAMP ID='Woodcrib_RAMP_Q', T=750.0, F=571.428571/
&RAMP ID='Woodcrib_RAMP_Q', T=755.0, F=571.428571/
&RAMP ID='Woodcrib_RAMP_Q', T=760.0, F=571.428571/
&RAMP ID='Woodcrib_RAMP_Q', T=765.0, F=571.428571/
&RAMP ID='Woodcrib_RAMP_Q', T=770.0, F=571.428571/
&RAMP ID='Woodcrib_RAMP_Q', T=775.0, F=571.428571/
&RAMP ID='Woodcrib_RAMP_Q', T=780.0, F=571.428571/
&RAMP ID='Woodcrib_RAMP_Q', T=785.0, F=571.428571/
&RAMP ID='Woodcrib_RAMP_Q', T=790.0, F=571.428571/
&RAMP ID='Woodcrib_RAMP_Q', T=795.0, F=571.428571/
&RAMP ID='Woodcrib_RAMP_Q', T=800.0, F=571.428571/
&RAMP ID='Woodcrib_RAMP_Q', T=805.0, F=571.428571/
&RAMP ID='Woodcrib_RAMP_Q', T=810.0, F=571.428571/
&RAMP ID='Woodcrib_RAMP_Q', T=815.0, F=571.428571/
&RAMP ID='Woodcrib_RAMP_Q', T=820.0, F=571.428571/
&RAMP ID='Woodcrib_RAMP_Q', T=825.0, F=571.428571/
&RAMP ID='Woodcrib_RAMP_Q', T=830.0, F=571.428571/
&RAMP ID='Woodcrib_RAMP_Q', T=835.0, F=571.428571/
&RAMP ID='Woodcrib_RAMP_Q', T=840.0, F=571.428571/
&RAMP ID='Woodcrib_RAMP_Q', T=845.0, F=571.428571/
&RAMP ID='Woodcrib_RAMP_Q', T=850.0, F=571.428571/
&RAMP ID='Woodcrib_RAMP_Q', T=855.0, F=571.428571/
&RAMP ID='Woodcrib_RAMP_Q', T=860.0, F=571.428571/
&RAMP ID='Woodcrib_RAMP_Q', T=865.0, F=571.428571/
&RAMP ID='Woodcrib_RAMP_Q', T=870.0, F=571.428571/
&RAMP ID='Woodcrib_RAMP_Q', T=875.0, F=571.428571/
&RAMP ID='Woodcrib_RAMP_Q', T=880.0, F=571.428571/
&RAMP ID='Woodcrib_RAMP_Q', T=885.0, F=571.428571/
&RAMP ID='Woodcrib_RAMP_Q', T=890.0, F=571.428571/
&RAMP ID='Woodcrib_RAMP_Q', T=895.0, F=564.671429/
&RAMP ID='Woodcrib_RAMP_Q', T=900.0, F=545.367857/

&RAMP ID='Woodcrib_RAMP_Q', T=905.0, F=526.4/
&RAMP ID='Woodcrib_RAMP_Q', T=910.0, F=507.767857/
&RAMP ID='Woodcrib_RAMP_Q', T=915.0, F=489.471429/
&RAMP ID='Woodcrib_RAMP_Q', T=920.0, F=471.510714/
&RAMP ID='Woodcrib_RAMP_Q', T=925.0, F=453.885714/
&RAMP ID='Woodcrib_RAMP_Q', T=930.0, F=436.596429/
&RAMP ID='Woodcrib_RAMP_Q', T=935.0, F=419.642857/
&RAMP ID='Woodcrib_RAMP_Q', T=940.0, F=403.025/
&RAMP ID='Woodcrib_RAMP_Q', T=945.0, F=386.742857/
&RAMP ID='Woodcrib_RAMP_Q', T=950.0, F=370.796429/
&RAMP ID='Woodcrib_RAMP_Q', T=955.0, F=355.185714/
&RAMP ID='Woodcrib_RAMP_Q', T=960.0, F=339.910714/
&RAMP ID='Woodcrib_RAMP_Q', T=965.0, F=324.971429/
&RAMP ID='Woodcrib_RAMP_Q', T=970.0, F=310.367857/
&RAMP ID='Woodcrib_RAMP_Q', T=975.0, F=296.1/
&RAMP ID='Woodcrib_RAMP_Q', T=980.0, F=282.167857/
&RAMP ID='Woodcrib_RAMP_Q', T=985.0, F=268.571429/
&RAMP ID='Woodcrib_RAMP_Q', T=990.0, F=255.310714/
&RAMP ID='Woodcrib_RAMP_Q', T=995.0, F=242.385714/
&RAMP ID='Woodcrib_RAMP_Q', T=1000.0, F=229.796429/
&RAMP ID='Woodcrib_RAMP_Q', T=1005.0, F=217.542857/
&RAMP ID='Woodcrib_RAMP_Q', T=1010.0, F=205.625/
&RAMP ID='Woodcrib_RAMP_Q', T=1015.0, F=194.042857/
&RAMP ID='Woodcrib_RAMP_Q', T=1020.0, F=182.796429/
&RAMP ID='Woodcrib_RAMP_Q', T=1025.0, F=171.885714/
&RAMP ID='Woodcrib_RAMP_Q', T=1030.0, F=161.310714/
&RAMP ID='Woodcrib_RAMP_Q', T=1035.0, F=151.071429/
&RAMP ID='Woodcrib_RAMP_Q', T=1040.0, F=141.167857/
&RAMP ID='Woodcrib_RAMP_Q', T=1045.0, F=131.6/
&RAMP ID='Woodcrib_RAMP_Q', T=1050.0, F=122.367857/
&RAMP ID='Woodcrib_RAMP_Q', T=1055.0, F=113.471429/
&RAMP ID='Woodcrib_RAMP_Q', T=1060.0, F=104.910714/
&RAMP ID='Woodcrib_RAMP_Q', T=1065.0, F=96.685714/
&RAMP ID='Woodcrib_RAMP_Q', T=1070.0, F=88.796429/
&RAMP ID='Woodcrib_RAMP_Q', T=1075.0, F=81.242857/
&RAMP ID='Woodcrib_RAMP_Q', T=1080.0, F=74.025/
&RAMP ID='Woodcrib_RAMP_Q', T=1085.0, F=67.142857/
&RAMP ID='Woodcrib_RAMP_Q', T=1090.0, F=60.596429/

&RAMP ID='Woodcrib_RAMP_Q', T=1095.0, F=54.385714/
 &RAMP ID='Woodcrib_RAMP_Q', T=1100.0, F=48.510714/
 &RAMP ID='Woodcrib_RAMP_Q', T=1105.0, F=42.971429/
 &RAMP ID='Woodcrib_RAMP_Q', T=1110.0, F=37.767857/
 &RAMP ID='Woodcrib_RAMP_Q', T=1115.0, F=32.9/
 &RAMP ID='Woodcrib_RAMP_Q', T=1120.0, F=28.367857/
 &RAMP ID='Woodcrib_RAMP_Q', T=1125.0, F=24.171429/
 &RAMP ID='Woodcrib_RAMP_Q', T=1130.0, F=20.310714/
 &RAMP ID='Woodcrib_RAMP_Q', T=1135.0, F=16.785714/
 &RAMP ID='Woodcrib_RAMP_Q', T=1140.0, F=13.596429/
 &RAMP ID='Woodcrib_RAMP_Q', T=1145.0, F=10.742857/
 &RAMP ID='Woodcrib_RAMP_Q', T=1150.0, F=8.225/
 &RAMP ID='Woodcrib_RAMP_Q', T=1155.0, F=6.042857/
 &RAMP ID='Woodcrib_RAMP_Q', T=1160.0, F=4.196429/
 &RAMP ID='Woodcrib_RAMP_Q', T=1165.0, F=2.685714/
 &RAMP ID='Woodcrib_RAMP_Q', T=1170.0, F=1.510714/
 &RAMP ID='Woodcrib_RAMP_Q', T=1175.0, F=0.671429/
 &RAMP ID='Woodcrib_RAMP_Q', T=1180.0, F=0.167857/
 &RAMP ID='Woodcrib_RAMP_Q', T=1185.0, F=0.0/
 &RAMP ID='Woodcrib_RAMP_Q', T=1190.0, F=0.0/
 &RAMP ID='Woodcrib_RAMP_Q', T=1195.0, F=0.0/
 &RAMP ID='Woodcrib_RAMP_Q', T=1200.0, F=0.0/

&OBST ID='Obstruction', XB=7.5,7.75,23.25,23.5,0.0,11.0,
 SURF_ID6='Surface220cm','Surface220cm','Surface300cm','Surface300cm','Surface300cm','Surface300cm'/

&OBST ID='Obstruction', XB=12.75,13.0,23.25,23.5,0.0,11.0,
 SURF_ID6='Surface220cm','Surface220cm','Surface300cm','Surface300cm','Surface300cm','Surface300cm'/

&OBST ID='Obstruction', XB=18.0,18.25,23.25,23.5,0.0,11.0,
 SURF_ID6='Surface220cm','Surface220cm','Surface300cm','Surface300cm','Surface300cm','Surface300cm'/

&OBST ID='Obstruction', XB=0.0,25.0,24.0,24.25,0.0,11.0, SURF_ID='INERT'/

&OBST ID='Obstruction', XB=0.0,25.0,0.75,1.0,0.0,11.0, SURF_ID='INERT'/

&OBST ID='Obstruction', XB=6.0,6.25,1.0,24.0,8.0,11.0, SURF_ID='INERT'/

&OBST ID='Obstruction', XB=18.75,19.0,1.0,24.0,8.0,11.0, SURF_ID='INERT'/

&OBST ID='Obstruction', XB=6.0,19.0,0.75,24.25,11.0,11.25, SURF_ID='INERT'/

&OBST ID='Wood Crib 01', XB=7.25,8.0,21.0,22.25,0.0,1.5, SURF_ID='INERT'/

&OBST ID='Wood Crib 02', XB=9.0,9.75,21.0,22.25,0.0,1.5, SURF_ID='INERT'/

&OBST ID='Wood Crib 03', XB=10.75,11.5,21.0,22.25,0.0,1.5, SURF_ID='INERT'/

&VENT ID='Mesh Vent: MESH-fire-nearfield-b [YMAX]', SURF_ID='OPEN', XB=5.5,13.0,24.5,24.5,0.0,15.0/

&VENT ID='Mesh Vent: MESH-fire-nearfield-b [ZMAX]', SURF_ID='OPEN', XB=5.5,13.0,15.0,24.5,15.0,15.0/
 &VENT ID='Mesh Vent: MESH-fire-nearfield-a [XMIN]', SURF_ID='OPEN', XB=0.0,0.0,15.0,24.5,0.0,15.0/
 &VENT ID='Mesh Vent: MESH-fire-nearfield-a [YMAX]', SURF_ID='OPEN', XB=0.0,5.5,24.5,24.5,0.0,15.0/
 &VENT ID='Mesh Vent: MESH-fire-nearfield-a [ZMAX]', SURF_ID='OPEN', XB=0.0,5.5,15.0,24.5,15.0,15.0/
 &VENT ID='Mesh Vent: MESH-fire-nearfield-b [XMAX]', SURF_ID='OPEN', XB=25.0,25.0,15.0,24.5,0.0,15.0/
 &VENT ID='Mesh Vent: MESH-fire-nearfield-b [YMAX]', SURF_ID='OPEN', XB=13.0,25.0,24.5,24.5,0.0,15.0/
 &VENT ID='Mesh Vent: MESH-fire-nearfield-b [ZMAX]', SURF_ID='OPEN', XB=13.0,25.0,15.0,24.5,15.0,15.0/
 &VENT ID='Mesh Vent: MESH-far-room-Coarse-b-a [XMIN]', SURF_ID='OPEN', XB=0.0,0.0,0.0,15.0,7.5,15.0/
 &VENT ID='Mesh Vent: MESH-far-room-Coarse-b-a [YMIN]', SURF_ID='OPEN', XB=0.0,12.5,0.0,0.0,7.5,15.0/
 &VENT ID='Mesh Vent: MESH-far-room-Coarse-b-a [ZMAX]', SURF_ID='OPEN', XB=0.0,12.5,0.0,15.0,15.0,15.0/
 &VENT ID='Mesh Vent: MESH-far-room-Coarse-b-b [XMAX]', SURF_ID='OPEN', XB=25.0,25.0,0.0,15.0,7.5,15.0/
 &VENT ID='Mesh Vent: MESH-far-room-Coarse-b-b [YMIN]', SURF_ID='OPEN', XB=12.5,25.0,0.0,0.0,7.5,15.0/
 &VENT ID='Mesh Vent: MESH-far-room-Coarse-b-b [ZMAX]', SURF_ID='OPEN', XB=12.5,25.0,0.0,15.0,15.0,15.0/
 &VENT ID='Mesh Vent: MESH-far-room-Coarse-a-a [XMIN]', SURF_ID='OPEN', XB=0.0,0.0,0.0,15.0,0.0,7.5/
 &VENT ID='Mesh Vent: MESH-far-room-Coarse-a-a [YMIN]', SURF_ID='OPEN', XB=0.0,12.5,0.0,0.0,0.0,7.5/
 &VENT ID='Mesh Vent: MESH-far-room-Coarse-a-b [XMAX]', SURF_ID='OPEN', XB=25.0,25.0,0.0,15.0,0.0,7.5/
 &VENT ID='Mesh Vent: MESH-far-room-Coarse-a-b [YMIN]', SURF_ID='OPEN', XB=12.5,25.0,0.0,0.0,0.0,7.5/
 &VENT ID='WC1 Vent01', SURF_ID='Woodcrib', XB=7.25,7.25,21.0,22.25,0.0,1.5/
 &VENT ID='WC1 Vent02', SURF_ID='Woodcrib', XB=7.25,8.0,21.0,21.0,0.0,1.5/
 &VENT ID='WC1 Vent03', SURF_ID='Woodcrib', XB=8.0,8.0,21.0,22.25,0.0,1.5/
 &VENT ID='WC1 Vent04', SURF_ID='Woodcrib', XB=7.25,8.0,22.25,22.25,0.0,1.5/
 &VENT ID='WC1 Vent05', SURF_ID='Woodcrib', XB=7.25,8.0,21.0,22.25,1.5,1.5/
 &VENT ID='WC2 Vent01', SURF_ID='Woodcrib', XB=9.0,9.0,21.0,22.25,0.0,1.5/
 &VENT ID='WC2 Vent02', SURF_ID='Woodcrib', XB=9.0,9.75,21.0,21.0,0.0,1.5/
 &VENT ID='WC2 Vent03', SURF_ID='Woodcrib', XB=9.75,9.75,21.0,22.25,0.0,1.5/
 &VENT ID='WC2 Vent04', SURF_ID='Woodcrib', XB=9.0,9.75,22.25,22.25,0.0,1.5/
 &VENT ID='WC2 Vent05', SURF_ID='Woodcrib', XB=9.0,9.75,21.0,22.25,1.5,1.5/
 &VENT ID='WC3 Vent01', SURF_ID='Woodcrib', XB=10.75,10.75,21.0,22.25,0.0,1.5/
 &VENT ID='WC3 Vent02', SURF_ID='Woodcrib', XB=10.75,11.5,21.0,21.0,0.0,1.5/
 &VENT ID='WC3 Vent03', SURF_ID='Woodcrib', XB=11.5,11.5,21.0,22.25,0.0,1.5/
 &VENT ID='WC3 Vent04', SURF_ID='Woodcrib', XB=10.75,11.5,22.25,22.25,0.0,1.5/
 &VENT ID='WC3 Vent05', SURF_ID='Woodcrib', XB=10.75,11.5,21.0,22.25,1.5,1.5/

&BNDF QUANTITY='BURNING RATE'/

&BNDF QUANTITY='WALL TEMPERATURE'/

&SLCF QUANTITY='TEMPERATURE', VECTOR=.TRUE., CELL_CENTERED=.TRUE., PBX=9.375/

&SLCF QUANTITY='TEMPERATURE', VECTOR=.TRUE., CELL_CENTERED=.TRUE., PBY=23.25/

&SLCF QUANTITY='HRRPUV', VECTOR=.TRUE., CELL_CENTERED=.TRUE., PBX=9.375/
&SLCF QUANTITY='HRRPUV', VECTOR=.TRUE., CELL_CENTERED=.TRUE., PBY=23.25/

&TAIL /